Eur. Phys. J. C (2020) 80:43
https://doi.org/10.1140/epjc/s10052-019-7585-7

THE EUROPEAN PHYSICAL JOURNAL C

Regular Article - Experimental Physics

Measurement of electroweak production of a W boson in association with two jets in proton–proton collisions at $\sqrt{s} = 13\,\text{TeV}$

CMS Collaboration*

CERN, 1211 Geneva 23, Switzerland

Received: 10 March 2019 / Accepted: 22 December 2019

Abstract A measurement is presented of electroweak (EW) production of a W boson in association with two jets in proton–proton collisions at $\sqrt{s} = 13\,\text{TeV}$. The data sample was recorded by the CMS Collaboration at the LHC and corresponds to an integrated luminosity of $35.9\,\text{fb}^{-1}$. The measurement is performed for the $\ell\nu$jj final state (with $\ell\nu$ indicating a lepton–neutrino pair, and j representing the quarks produced in the hard interaction) in a kinematic region defined by invariant mass $m_{\text{jj}} > 120\,\text{GeV}$ and transverse momenta $p_{\text{Tj}} > 25\,\text{GeV}$. The cross section of the process is measured in the electron and muon channels yielding $\sigma_{\text{EW}}(\text{Wjj}) = 6.23 \pm 0.12\,(\text{stat}) \pm 0.61\,(\text{syst})\,\text{pb}$ per channel, in agreement with leading-order standard model predictions. The additional hadronic activity of events in a signal-enriched region is studied, and the measurements are compared with predictions. The final state is also used to perform a search for anomalous trilinear gauge couplings. Limits on anomalous trilinear gauge couplings associated with dimension-six operators are given in the framework of an effective field theory. The corresponding 95% confidence level intervals are $-2.3 < c_{\text{WWW}}/\Lambda^2 < 2.5\,\text{TeV}^{-2}$, $-8.8 < c_{\text{W}}/\Lambda^2 < 16\,\text{TeV}^{-2}$, and $-45 < c_{\text{B}}/\Lambda^2 < 46\,\text{TeV}^{-2}$. These results are combined with the CMS EW Zjj analysis, yielding the constraint on the c_{WWW} coupling: $-1.8 < c_{\text{WWW}}/\Lambda^2 < 2.0\,\text{TeV}^{-2}$.

1 Introduction

In proton–proton (pp) collisions at the CERN LHC, the pure electroweak (EW) production of a lepton–neutrino pair ($\ell\nu$) in association with two jets (jj) includes production via vector boson fusion (VBF). This process has a distinctive signature of two jets with large energy and separation in pseudorapidity (η), produced in association with a lepton–neutrino pair. This EW process is referred to as EW Wjj, and the two jets produced through the fragmentation of the outgoing quarks are referred to as "tagging jets".

Figure 1 shows representative Feynman diagrams for the EW Wjj signal processes, namely VBF (Fig. 1, left), bremsstrahlung-like (Fig. 1, center), and multiperipheral (Fig. 1, right) production. Gauge cancellations lead to a large negative interference between the VBF diagram and the other two diagrams, with the larger interference coming from bremsstrahlung-like production. Interference with multiperipheral production is limited to cases where the lepton–neutrino pair mass is close to the W boson mass.

In addition to the purely EW signal diagrams described above, there are other, not purely EW processes, that lead to the same $\ell\nu$jj final states and can interfere with the signal diagrams in Fig. 1. This interference effect between the signal production and the main Drell–Yan (DY) background processes (DY Wjj) is small compared to the interference effects among the EW production amplitudes, but needs to be included when measuring the signal contribution. Figure 2 (left) shows one example of W boson production in association with two jets that has the same initial and final states as those in Fig. 1. A process that does not interfere with the EW signal is shown in Fig. 2 (right).

The study of EW Wjj processes is part of a more general investigation of standard model (SM) VBF and scattering processes that includes the measurements of EW Zjj processes, Higgs boson production [1–3], and searches for physics beyond the SM [4]. The properties of EW Wjj events that are isolated from the backgrounds can be compared with SM predictions. Probing the additional hadronic activity in selected events can shed light on the modeling of the additional parton radiation [5,6], which is important for signal selection and the vetoing of background events.

Higher-dimensional operators outside the SM can generate anomalous trilinear gauge couplings (ATGCs) [7,8], so the measurement of the coupling strengths provides an indirect search for beyond-the-SM physics at mass scales not directly accessible at the LHC.

* e-mail: cms-publication-committee-chair@cern.ch

Published online: 18 January 2020

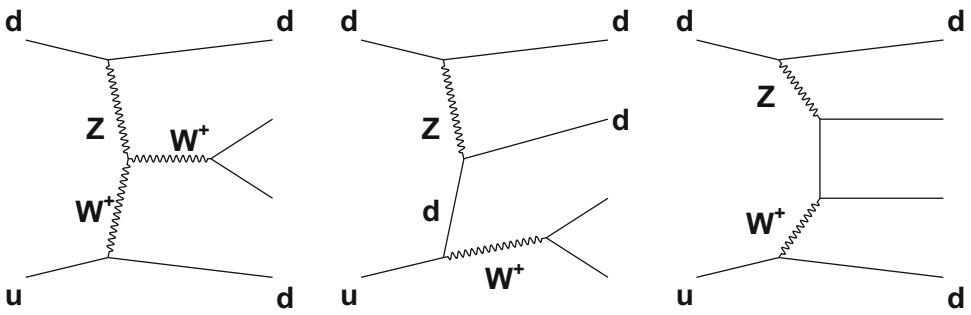

Fig. 1 Representative Feynman diagrams for lepton–neutrino production in association with two jets from purely electroweak amplitudes: vector boson fusion (left), bremsstrahlung-like (center), and multiperipheral (right) production

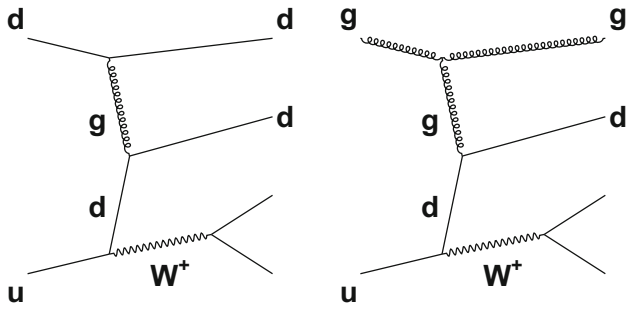

Fig. 2 Representative diagrams for W boson production in association with two jets (DY Wjj) that constitute the main background for the measurement

At the LHC, the EW Wjj process was first measured by the CMS Collaboration using pp collisions at $\sqrt{s} = 8$ TeV [9] and then by the ATLAS Collaboration at both $\sqrt{s} = 8$ TeV and $\sqrt{s} = 7$ TeV [10]. The closely related EW Zjj process was first measured during Run 1 by the CMS Collaboration using pp collisions at $\sqrt{s} = 7$ TeV [11], and then at $\sqrt{s} = 8$ TeV by both the CMS [12] and ATLAS [13] Collaborations. The EW Zjj measurements using data samples of pp collisions at $\sqrt{s} = 13$ TeV have been performed by ATLAS [14] and by CMS [15]. Considering leptonic final states in the same kinematic region the EW Wjj cross section is about a factor 10 larger than the EW Zjj cross section. All results so far agree with the expectations of the SM within a precision of 10–20%.

This paper presents measurements of the EW Wjj process with the CMS detector using pp collisions collected at $\sqrt{s}$ =13 TeV during 2016, corresponding to an integrated luminosity of 35.9 fb^{-1}. A multivariate analysis (BDT), based on the methods developed for the EW Zjj measurement [11,12], is used to separate signal events from the large W+jets background. The analysis of the 13 TeV data offers the opportunity to measure the cross section at a higher energy than previously done and to reduce the uncertainties obtained with previous measurements, given both the larger integrated luminosity and the larger predicted total cross section.

This paper is organized as follows: Sect. 2 describes the experimental apparatus and Sect. 3 the event simulations. Event selection procedures are described in Sect. 4, together with the selection efficiencies and background estimations using control regions (CRs). Section 5 describes an estimation of the multijet background from quantum chromodynamics (QCD), based on CRs in data. Section 6 discusses a correction applied to the simulation as a function of the invariant mass m_{jj}. Section 7 presents distributions of the main discriminating variables in data. Section 8 details the strategy adopted to extract the signal from the data, and the corresponding systematic uncertainties are summarized in Sect. 9. The cross section and anomalous coupling results are presented in Sects. 10 and 11, respectively. Section 12 presents a study of the additional hadronic activity in an EW Wjj enriched region. Finally, a brief summary of the results is given in Sect. 13.

2 The CMS detector and physics objects

The central feature of the CMS apparatus is a superconducting solenoid of 6 m internal diameter, providing a magnetic field of 3.8 T. Within the solenoid volume are a silicon pixel and strip tracker, a lead tungstate crystal electromagnetic calorimeter (ECAL), and a brass and scintillator hadron calorimeter, each composed of a barrel and two endcap sections. Forward calorimeters extend the η coverage provided by the barrel and endcap detectors to $|\eta| = 5.2$. Muons are measured in gas-ionization detectors embedded in the steel flux-return yoke outside the solenoid.

The tracker measures charged particles within the range $|\eta| < 2.5$. It consists of 1440 pixel and 15,148 strip detector modules. For nonisolated particles with transverse momenta $1 < p_{\mathrm{T}} < 10$ GeV and $|\eta| < 1.4$, the track resolutions are typically 1.5% in p_{T} and 25–90 (45–150) μm in the transverse (longitudinal) impact parameter [16].

The energy of electrons is measured after combining the information from the ECAL and the tracker, whereas their direction is measured by the tracker. The momentum res-

olution for electrons with $p_T \approx 45$ GeV from $Z \to ee$ decays ranges from 1.7 to 4.5%. It is generally better in the barrel region than in the endcaps, and also depends on the bremsstrahlung energy emitted by the electron as it traverses the material in front of the ECAL [17].

Muons are measured in the range $|\eta| < 2.4$, with detection planes made using three technologies: drift tubes, cathode strip chambers, and resistive-plate chambers. Matching muons to tracks measured in the silicon tracker results in a relative transverse momentum resolution for muons with $20 < p_T < 100$ GeV of 1.3–2.0% in the barrel and better than 6% in the endcaps. The p_T resolution in the barrel is better than 10% for muons with p_T up to 1 TeV [18].

Events of interest are selected using a two-tiered trigger system [19]. The first level (L1), composed of custom hardware processors, uses information from the calorimeters and muon detectors to select events at a rate of around 100 kHz within a time interval of less than 4 μs. The second level, known as the high-level trigger (HLT), consists of a farm of processors running a version of the full-event reconstruction software optimized for fast processing, and reduces the event rate to around 1 kHz before data storage.

A more detailed description of the CMS detector, together with a definition of the coordinate system used and the relevant kinematic variables, can be found in Ref. [20].

3 Simulation of signal and background events

Signal events are simulated at leading order (LO) using the MADGRAPH5_aMC@NLO (v2.3.3) Monte Carlo (MC) generator [21], interfaced with PYTHIA (v8.212) [22] for parton showering (PS) and hadronization. The NNPDF30 [23] parton distribution functions (PDFs) are used to generate the events. The underlying event is modeled using the CUETP8M1 tune [24]. The simulation does not include extra partons at matrix element (ME) level. The signal is defined in the kinematic region with parton transverse momentum $p_{Tj} > 25$ GeV, and diparton invariant mass $m_{jj} > 120$ GeV. The simulated cross section for the $\ell\nu$jj final state (with ℓ = e, μ or τ), applying the above requirements, is $\sigma_{LO}(\text{EW } \ell\nu\text{jj}) = 6.81^{+0.03}_{-0.06}\,(\text{scale}) \pm 0.26\,(\text{PDFs})$ pb, where the first uncertainty is obtained by changing simultaneously the factorization (μ_F) and renormalization (μ_R) scales by factors of 2 and 1/2, and the second one reflects the uncertainties in the NNPDF30 PDFs. The LO signal cross section and relevant kinematic distributions estimated with MADGRAPH5_aMC@NLO are in agreement within 2–5% with the next-to-leading-order (NLO) predictions of the VBFNLO generator (v2.6.3) [25–27], which include QCD NLO corrections to the LO ME-level diagrams evaluated with MADGRAPH5_aMC@NLO. For additional comparisons, signal events produced with MADGRAPH5_aMC@NLO are also processed with the HERWIG++ (v2.7.1) [28] PS, using the EE5C [29] tune.

An additional signal sample that includes NLO QCD corrections but does not include the s-channel contributions to the final state has been generated with POWHEG (v2.0) [30–32], based on the VBFNLO ME calculations [33,34]. In the POWHEG sample the $m_{jj} > 120$ GeV condition is applied on the two p_T-leading parton-level jets, after clustering the ME final state partons with the k_T-algorithm [35–37], with a distance parameter $D = 0.8$, as done in Ref. [33]. The POWHEG sample has also been processed alternatively with PYTHIA and HERWIG++ parton showering (PS) and hadronization programs, as done for the MADGRAPH5_aMC@NLO samples. In the following, results obtained with the POWHEG signal samples are given as a cross check of the main results obtained with the MADGRAPH5_aMC@NLO signal samples.

Events coming from processes including ATGCs are generated with the same settings as the SM sample, but include additional information for reweighting in the three-dimensional effective field theory (EFT) parameter space, which is described in more detail in Sect. 11. The 'EWdim6NLO' model [8,21] is used for the generation of anomalous couplings.

Background W boson events are also simulated with MADGRAPH5_aMC@NLO using (1) an NLO ME calculation with up to three final-state partons generated from QCD interactions, and (2) an LO ME calculation with up to four partons from QCD interactions. The ME-PS matching is performed following the FxFx prescription [38] for the NLO case, and the MLM prescription [39,40] for the LO case. The NLO background simulation is used to extract the final results, while the independent LO samples are used to perform the multivariate discriminant training. The inclusive W boson production is normalized to $\sigma_{th}(W) = 61.5$ nb, as computed at next-to-next-to-leading order (NNLO) with FEWZ (v3.1) [41].

The evaluation of the interference between EW Wjj and DY Wjj processes relies on the predictions obtained with MADGRAPH5_aMC@NLO. A dedicated sample of events arising from the interference terms is generated directly by selecting the contributions of order $\alpha_s\alpha_{EW}^3$, and passed through the full detector simulation to estimate the expected interference contribution.

Other backgrounds are expected from events with one electron or muon and missing transverse momentum together with jets in the final state. Events from top quark pair production are generated with POWHEG (v2.0) [30–32], and normalized to the inclusive cross section calculated at NNLO, including next-to-next-to-leading logarithmic corrections, of 832 pb [42,43]. Single top quark processes are modeled at NLO with POWHEG [30–32,44] and normalized to cross sections of 71.7 ± 2.0 pb, 217 ± 3 pb, and 10.32 ± 0.20 pb, respectively, for the tW (POWHEG v1) [45], t-, and s-channel

production [42,46]. The diboson (VV) production processes (WW, WZ, and ZZ) are generated with PYTHIA and normalized to NNLO cross section computations obtained with MCFM (v8.0) [47].

The contribution from QCD multijet processes is derived via an extrapolation from a QCD data CR with the lepton relative isolation selection inverted. All background simulations make use of the PYTHIA PS model with the CUETP8M1 tune.

A detector simulation based on GEANT4 (v9.4p03) [48,49] is applied to all the generated signal and background samples. The presence of multiple pp interactions is incorporated by simulating additional interactions (pileup), both in-time and out-of-time with respect to the hard interaction, with a multiplicity that matches the distribution observed in data. The average pileup is measured to be about 23 additional interactions per bunch crossing.

4 Reconstruction and selection of events

Events containing exactly one isolated, high-p_T lepton and at least two high-p_T jets are selected. Isolated single-lepton triggers are used to acquire the data, where the lepton is required to have $p_T > 27$ GeV for the electron trigger and $p_T > 24$ GeV for the muon trigger.

The offline analysis uses candidates reconstructed by the particle-flow (PF) algorithm [50]. In the PF event reconstruction, all stable particles in the event — i.e., electrons, muons, photons, charged and neutral hadrons — are reconstructed as PF candidates using information from all subdetectors to obtain an optimal determination of their direction, energy, and type. The PF candidates are used to reconstruct the jets and the missing transverse momentum.

The reconstructed primary vertex (PV) with the largest value of summed physics-object p_T^2 is the primary pp interaction vertex. The physics objects are the objects returned by a jet finding algorithm [51,52] applied to all charged particle tracks associated with the vertex, along with the corresponding associated missing transverse momentum. Charged tracks identified as hadrons from pileup vertices are omitted in the subsequent PF event reconstruction [50].

Offline electrons are reconstructed from clusters of energy deposits in the ECAL that match tracks extrapolated from the silicon tracker [17]. Offline muons are reconstructed by fitting trajectories based on hits in the silicon tracker and in the muon system [53]. Reconstructed electron or muon candidates are required to have $p_T > 20$ GeV. Electron candidates are required to be reconstructed within $|\eta| \leq 2.4$, excluding the barrel-to-endcap transitional region $1.444 < |\eta| < 1.566$ of the ECAL [20]. Muon candidates are required to be reconstructed in the fiducial region $|\eta| \leq 2.4$. The track associated with a lepton candidate is required to have both its transverse and longitudinal impact parameters compatible with the position of the PV of the event.

The leptons are required to be isolated; the isolation (I) variable is calculated from PF candidates and is corrected for pileup on an event-by-event basis [54]. The scalar p_T sum of all PF candidates reconstructed in an isolation cone with radius $\Delta R = \sqrt{(\Delta\eta)^2 + (\Delta\phi)^2} = 0.4$ around the lepton's momentum vector, excluding the lepton itself, is required to be less than 6% of the electron or muon p_T value. For additional offline analysis, the isolated lepton is required to have $p_T > 25$ GeV for the muon channel and $p_T > 30$ GeV for the electron channel. Events with more than one lepton satisfying the above requirements are rejected. The lepton flavor samples are exclusive and precedence is given to the selection of muons.

The missing transverse momentum vector, $\vec{p}_T^{\,\text{miss}}$, is calculated offline as the negative of the vector sum of transverse momenta of all PF objects identified in the event [55], and the magnitude of this vector is denoted p_T^{miss}. Events are required to have p_T^{miss} in excess of 20 GeV in the muon channel and 40 GeV in the electron channel. The tighter requirement for the electron channel reduces the corresponding higher background of QCD multijet events. The transverse mass (m_T) of the lepton and $\vec{p}_T^{\,\text{miss}}$ four-vector sum is then required to exceed 40 GeV in both channels.

Jets are reconstructed by clustering PF candidates with the anti-k_T algorithm [51,56] using a distance parameter of 0.4. The jet momentum is the vector sum of all particle momenta in the jet and is typically within 5–10% of the true momentum over the whole p_T spectrum and detector acceptance.

An offset correction is applied to jet energies because of the contribution from pileup. Jet energy corrections are derived from simulation, and are confirmed with in situ measurements of the energy balance in dijet, multijet, photon+jet, and Z+jets events with leptonic Z boson decays [57]. Loose jet identification criteria are applied to reject misreconstructed jets resulting from detector noise [58]. Loose criteria are also applied to remove jets heavily contaminated with pileup energy (clustering of energy deposits not associated with a parton from the primary pp interaction) [58,59]. The efficiency of the jet identification is greater than 99%, with a rejection of 90% of background pileup jets with $p_T \simeq 50$ GeV and $|\eta| \leq 2.5$. For jets with $|\eta| > 2.5$ and $30 < p_T < 50$ GeV, the efficiency is approximately 90% and the pileup jet rejection is approximately 50%. The jet energy resolution (JER) is typically ≈15% at 10 GeV, 8% at 100 GeV, and 4% at 1 TeV for jets with $|\eta| \leq 1$ [57]. Jets reconstructed with $p_T \geq 15$ GeV and $|\eta| \leq 4.7$ are used in the analysis.

The two highest p_T jets are defined as the tagging jets, and are required to have $p_T > 50$ GeV and $p_T > 30$ GeV for the leading and subleading (in p_T) jet, respectively. The

Table 1 Event yields expected for background and signal processes using the initial selections and with a selection on the multivariate analysis output (BDT) that provides similar signal and background yields. The yields are compared to the data observed in the different channels and categories. The total uncertainties quoted for signal, DY Wjj and diboson backgrounds, and processes with top quarks ($t\bar{t}$ and single top quarks) include the systematic uncertainties

Sample	Initial		BDT > 0.95	
	μ	e	μ	e
VV	$20,300 \pm 2000$	9820 ± 980	11.0 ± 2.5	9.6 ± 2.8
DY Zjj	$102,000 \pm 10,000$	$29,900 \pm 3000$	9.4 ± 5.9	7.7 ± 3.0
$t\bar{t}$	$298,000 \pm 28,000$	$164,000 \pm 15,000$	146 ± 17	102 ± 12
Single top quark	$96,000 \pm 14,000$	$45,800 \pm 6900$	35.5 ± 5.6	25.7 ± 4.2
QCD multijet	$100,000 \pm 39,000$	$65,000 \pm 21,000$	98 ± 39	17.0 ± 5.6
DY Wjj	$1,720,000 \pm 120,000$	$715,000 \pm 51,000$	356 ± 65	240 ± 41
Interference	7000 ± 2100	3400 ± 1000	18.2 ± 8.1	9.8 ± 5.5
Total backgrounds	$2,340,000 \pm 170,000$	$1,032,000 \pm 58,000$	674 ± 78	412 ± 44
EW Wjj signal	$43,100 \pm 4300$	$20,700 \pm 2100$	503 ± 54	308 ± 34
EW Zjj signal	1330 ± 130	407 ± 41	11.2 ± 1.3	6.6 ± 0.9
Total prediction	$2,390,000 \pm 170,000$	$1,054,000 \pm 58,000$	1186 ± 95	726 ± 56
Data	2,381,901	1,051,285	1138	686

invariant mass of the two tagging jets is required to satisfy $m_{jj} > 200$ GeV.

The transverse momentum of the W boson ($\vec{p}_{TW}$) is evaluated as the vector sum of the lepton p_T and $\vec{p}_T^{miss}$. The event p_T balance ($R(p_T)$) is then defined as

$$R(p_T) = \frac{|\vec{p}_{Tj_1} + \vec{p}_{Tj_2} + \vec{p}_{TW}|}{|\vec{p}_{Tj_1}| + |\vec{p}_{Tj_2}| + |\vec{p}_{TW}|} \quad (1)$$

where $\vec{p}_{Tj_1}$ and $\vec{p}_{Tj_2}$ are the transverse momenta of the two tagging jets.

Finally, events are required to have $R(p_T) < 0.2$. This has a negligible effect on the analysis sensitivity and allows the definition of a nonoverlapping control sample with $R(p_T) > 0.2$ that is used to derive a correction to the invariant mass based on a CR in data, as described in Sect. 6.

A multivariate analysis technique, described in Sect. 8, is used to provide an optimal separation of the DY Wjj and EW Wjj components of the inclusive $\ell\nu$jj spectrum. The main discriminating variables are the dijet invariant mass m_{jj} and pseudorapidity separation $\Delta\eta_{jj}$.

Angular variables useful for signal discrimination include the y^* Zeppenfeld variable [6], defined as the difference between the rapidity of the W boson y_W and the average rapidity of the two tagging jets, i.e.,

$$y^* = y_W - \frac{1}{2}(y_{j_1} + y_{j_2}), \quad (2)$$

and the z^* Zeppenfeld variable [6] defined as

$$z^* = \frac{y^*}{\Delta y_{jj}}, \quad (3)$$

where Δy_{jj} is the dijet rapidity separation.

Table 1 reports the expected and observed event yields after the initial selection and after imposing a minimum value for the final multivariate discriminant output applied to define the signal-enriched region used for the studies of additional hadronic activity described in Sect. 12.

4.1 Discriminating quarks from gluons

Jets in signal events are expected to originate from quarks, whereas for background events it is more probable that jets are initiated by a gluon. A quark-gluon likelihood (QGL) discriminant [11] is evaluated for the two tagging jets with the intent of distinguishing the nature of each jet.

The QGL discriminant exploits differences in the showering and fragmentation of quarks and gluons, making use of the following internal jet composition observables: (1) the particle multiplicity of the jet, (2) the minor root-mean-square of distance between the jet constituents in the η–ϕ plane, and (3) the p_T distribution function of the jet constituents, as defined in Ref. [60].

The variables are used as inputs to a likelihood discriminant on gluon and quark jets constructed from simulated dijet events. The performance of the QGL discriminant is evaluated and validated using independent, exclusive samples of Z+jet and dijet data [60]. Corrections to the simulated QGL distributions and related systematic uncertainties are derived from a comparison of simulation and data distributions.

5 The QCD multijet background

The QCD multijet contribution is estimated by defining a multijet-enriched CR with inverted lepton isolation criteria

for both the muon and electron channels. In the nominal selection both lepton types are required to pass the relative isolation requirement $I < 0.06$, whereas the multijet-enriched CRs are defined with the same event selection but with isolation requirements $0.06 < I < 0.12$ and $0.06 < I < 0.15$, for the muon and electron channel respectively. It is then assumed that the $p_{\mathrm{T}}^{\mathrm{miss}}$ distribution of QCD events has the same shape in both the nominal and the multijet-enriched CR.

The various components, with floating W+jets and QCD multijet background scale factors, are simultaneously fitted to the $p_{\mathrm{T}}^{\mathrm{miss}}$ data distributions, independently in the muon and electron channels, and the expected QCD multijet yields in the nominal regions are derived.

The contribution of QCD multijet processes in any other observable (x) used in the analysis is then normalized to the yields obtained above from the fit to the $p_{\mathrm{T}}^{\mathrm{miss}}$ distribution, and the shape for the distribution x is taken as the difference between data and all simulated background contributions in the x distribution in the multijet-enriched CR.

The estimation of the QCD multijet contribution based on a CR in data is validated by checking the modeling of other variables that discriminate QCD multijets from W+jets such as the W transverse mass and the minimum difference in ϕ between the missing transerse energy and the jets. Good agreement with the data is observed in all distributions. The stability of the W+jets fitted normalization is checked by varying the selection requirements for the fitted region and repeating the QCD extraction fit. The observed variations in fitted normalization when varying the $m_{\mathrm{T}}(\mathrm{W})$ and $p_{\mathrm{T}}^{\mathrm{miss}}$ selection requirements with respect to the fit region definition are much smaller than systematic uncertainties.

Although b tagging is not used in this analysis, a b-tagging discriminant output [61] is used to check the fitted W+jets background normalization as well as the $\mathrm{t\bar{t}}$ normalization from simulation, and they agree with data within the uncertainties. Finally, the selections on m_{jj}, $p_{\mathrm{T}}^{\mathrm{miss}}$, and $m_{\mathrm{T}}(\mathrm{W})$ are also loosened in order to verify that the W+jets background scale factor is not biased by these requirements.

6 The m_{jj} correction

A systematic overestimation of the simulation yields is caused by a partial mistiming of the signals in the forward region of the ECAL endcaps ($2.5 < |\eta| < 3.0$). This effect, which increases with increasing m_{jj}, is observed in both electron and muon channels. A correction for this effect is derived in the nonoverlapping signal-depleted CR obtained by requiring that the event transverse momentum balance $R(p_{\mathrm{T}})$, defined in Sect. 4, exceeds 0.2.

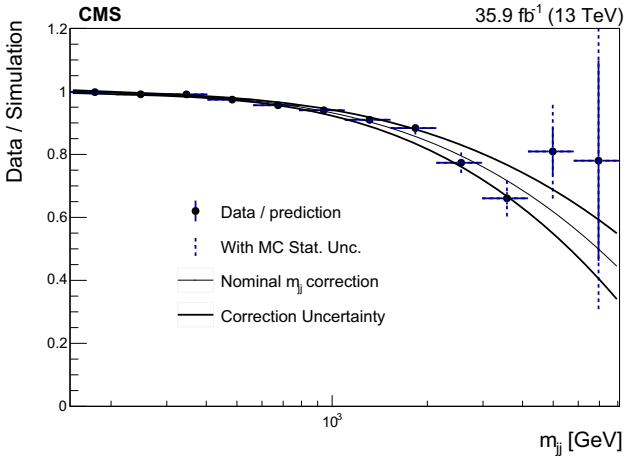

Fig. 3 Data divided by simulation as a function of $\ln(m_{\mathrm{jj}}/\,\mathrm{GeV})$ in a signal-depleted control sample with $R(p_{\mathrm{T}}) > 0.2$. This distribution is fit by a third-order polynomial (solid black line) in order to derive a correction on the simulation m_{jj} prediction. The points are varied by the uncertainty, including the effect of the limited number of simulated events and refitted in order to derive the systematic variations on the correction (dashed lines) corresponding to a standard deviation (SD)

A third-order polynomial correction is first applied to the W+jets simulation separately in the muon and electron channels in order to match the $R(p_{\mathrm{T}})$ distribution in data. The magnitude of the applied $R(p_{\mathrm{T}})$ corrections is about 10%. The uncertainty in this correction due to the limited statistical precision of the simulation as well as data is propagated to the fitted W+jets templates.

A correction to the m_{jj} prediction from simulation is derived in the signal-depleted $R(p_{\mathrm{T}}) > 0.2$ CR via a third-order polynomial fit to the ratio of data to the overall prediction from simulation for signal and background as a function of $\ln(m_{\mathrm{jj}}/\,\mathrm{GeV})$. The electron and muon channels are combined when deriving the m_{jj} correction. The uncertainty in the correction includes the data statistical component as well as the systematic uncertainty due to the limited statistical precision of the simulation.

Figure 3 shows the fitted correction including the uncertainty. This correction is applied to all simulated results, including the signal, and the corresponding uncertainty is propagated to the signal extraction fits.

7 Distributions of discriminating variables

Figure 4 shows the $p_{\mathrm{T}}^{\mathrm{miss}}$ and $m_{\mathrm{T}}(\mathrm{W})$ distributions after the event preselection. The dijet invariant mass and pseudorapidity difference ($\Delta\eta_{\mathrm{jj}}$) after preselection are presented in Fig. 5, and Fig. 6 shows the $y^{\star}$ and $z^{\star}$ distributions after the event preselection. The distributions of the QGL likelihood output values in data and simulation for the two tagging jets are shown in Fig. 7. The prediction from simulated events and

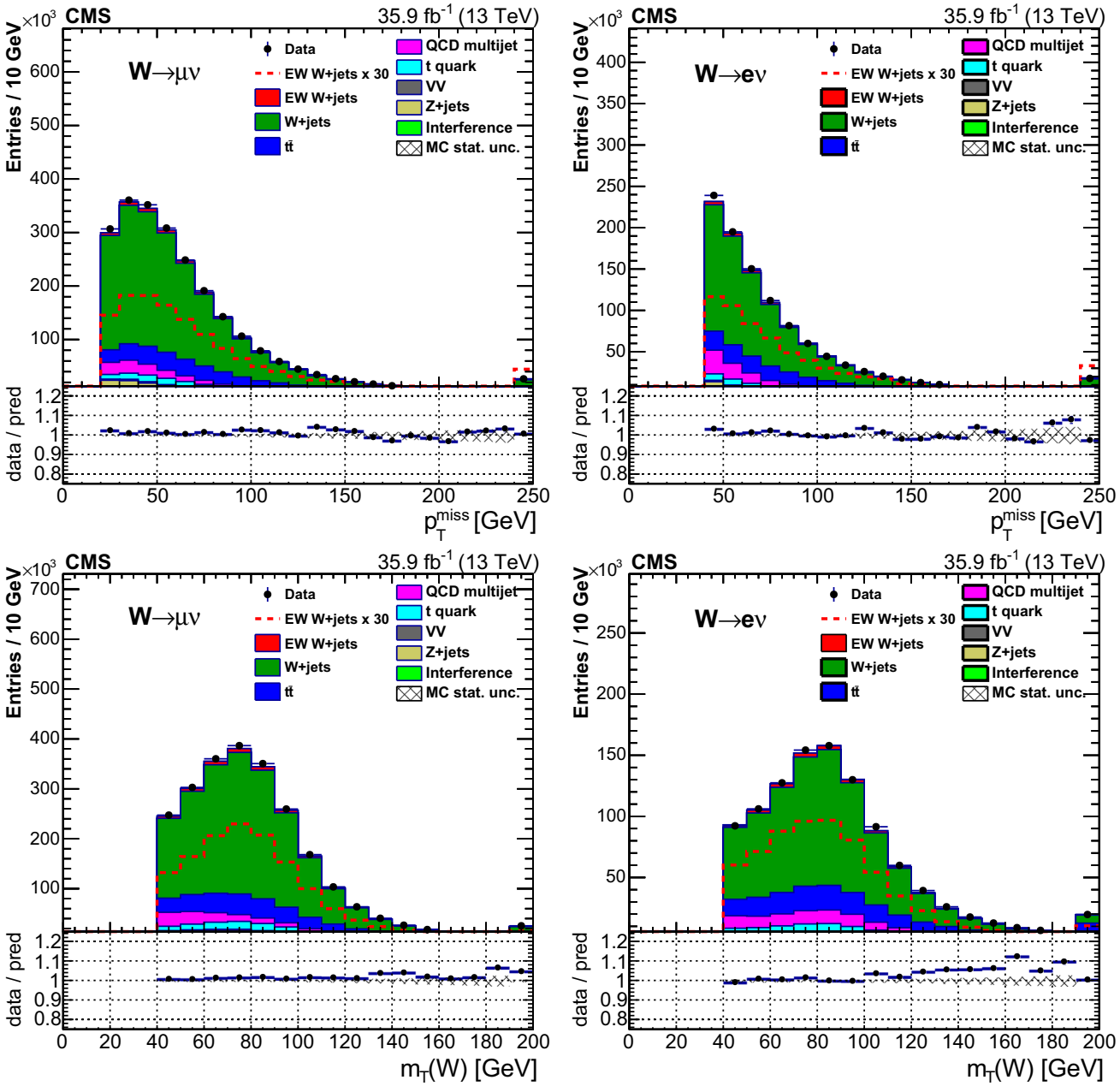

Fig. 4 Distribution of the missing transverse momentum (upper) and the lepton–$p_{\mathrm{T}}^{\mathrm{miss}}$ system transverse mass (lower) after the event preselection for the selected leading lepton in the event, in the muon (left) and electron (right) channels. In all plots the last bin contains overflow events

the data agree within total uncertainties for all discriminating variables.

8 Signal discriminants and extraction procedure

The EW Wjj signal is characterized by a large pseudorapidity separation between the tagging jets, due to the small-angle scattering of the two initial partons. Because of both the topological configuration and the large energy of the outgoing partons, m_{jj} is also expected to be large, and can be used to distinguish the EW Wjj and DY Wjj processes. The correlation between $\Delta\eta_{\mathrm{jj}}$ and m_{jj} is expected to be different in signal and background events, therefore these characteristics are expected to yield a high separation power between EW Wjj and DY Wjj production. In addition, in signal events it is expected that the W boson candidate is produced centrally in the rapidity region defined by the two tagging jets.

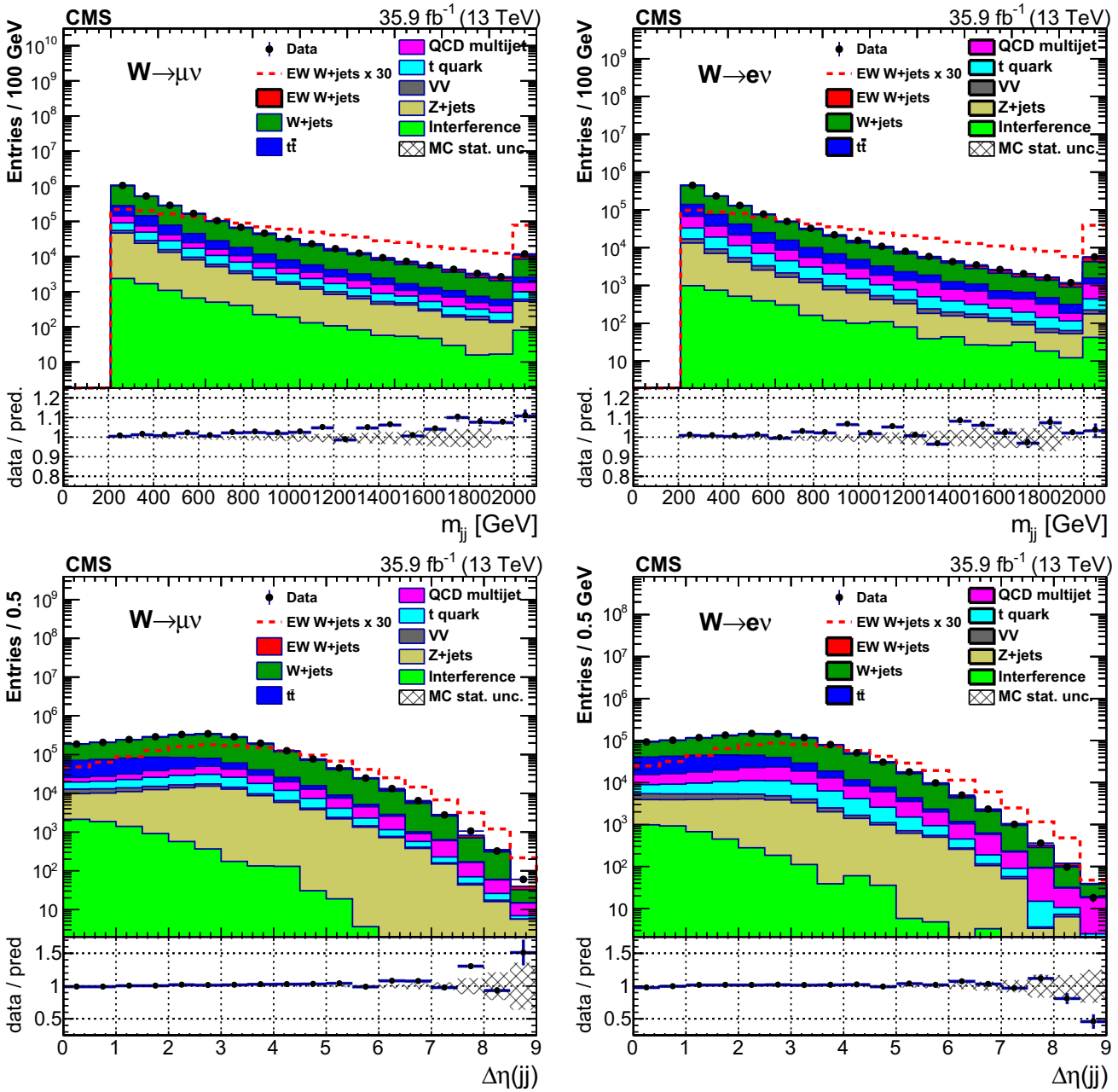

Fig. 5 Dijet invariant mass (upper) and pseudorapidity difference (lower) distributions after the event preselection, in the muon (left) and electron (right) channels. In all plots the last bin contains overflow events

As a consequence, signal events are expected to yield lower values of z^* compared to the DY background. Other variables that are used to enhance the signal-to-background separation are related to the kinematics of the event or to the properties of the jets that are expected to be initiated by quarks. The variables that are used in the multivariate analysis are: (1) m_{jj}, (2) $\Delta\eta_{jj}$, (3) z^*, and (4) the QGL values of the two tagging jets.

The output is built by training a boosted decision tree (BDT) discriminator with the TMVA package [62] to achieve an optimal separation between the EW Wjj and DY Wjj processes. The simulated events that are used for the BDT training are not used for the signal extraction.

To improve the sensitivity for the extraction of the signal component, the transformation that originally projects the BDT output value in the $[-1,+1]$ interval is changed to $\mathrm{BDT}' = \tanh^{-1}((\mathrm{BDT}+1)/2)$. This allows the purest signal region of the BDT output to be better sampled while keeping an equal-width binning of the BDT variable.

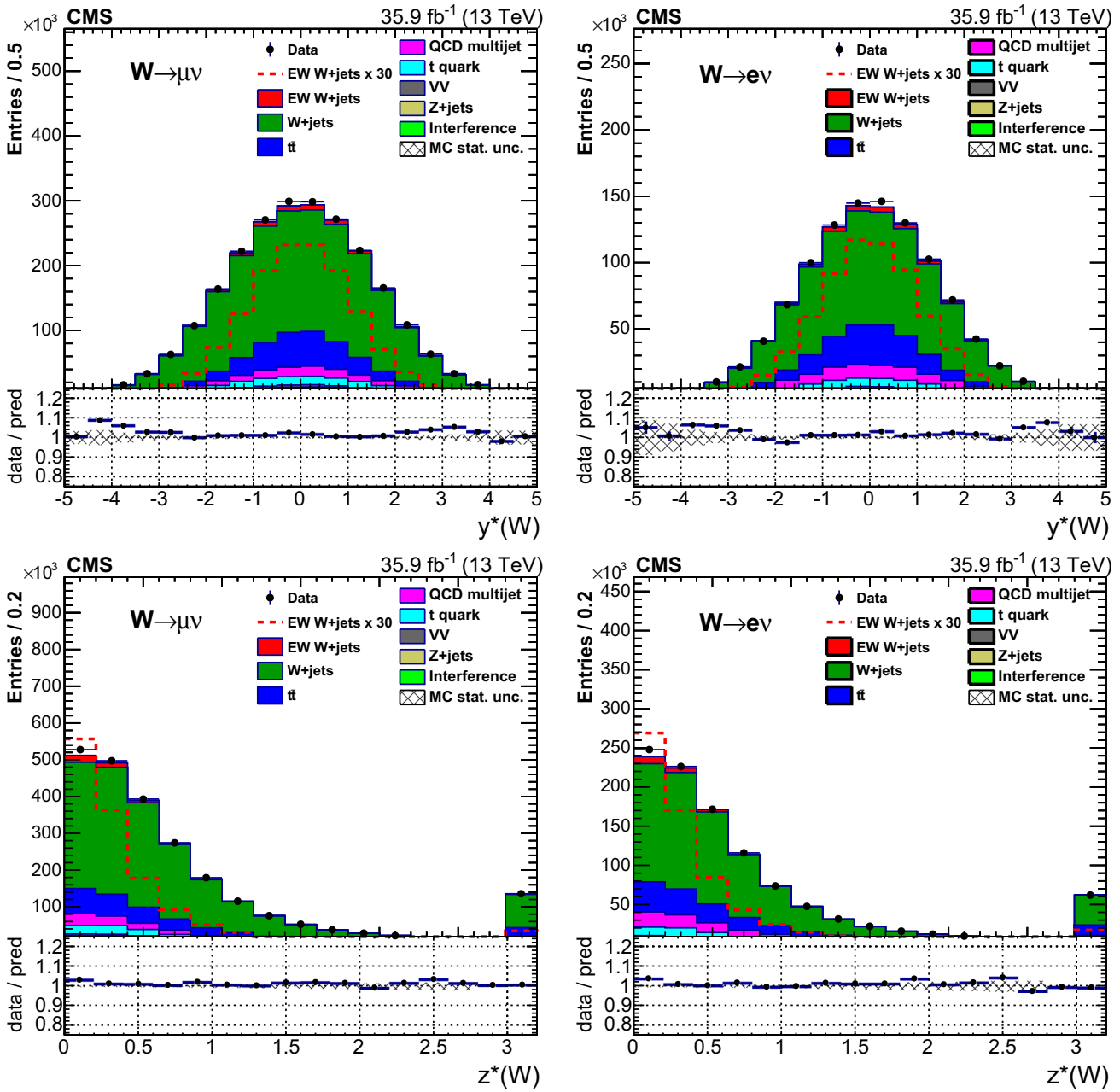

Fig. 6 Distributions of the "Zeppenfeld" variables $y^{\star}$(W) (upper) and $z^{\star}$(W) (lower) after event preselection in the muon (left) and electron (right) channels. In all plots the first and last bins contain overflow events

Figure 8 shows the distributions of the discriminants for the two leptonic channels. Good overall agreement between simulation and data is observed in all distributions, and the signal presence is visible at high BDT' values.

A binned maximum likelihood is built from the expected rates for each process, as a function of the value of the discriminant, which is fit to extract the strength modifiers for the EW Wjj and DY Wjj processes, $\mu = \sigma(\text{EW Wjj})/\sigma_{\text{LO}}$ (EW $\ell\nu$jj) and $\upsilon = \sigma(\text{W})/\sigma_{\text{NNLO}}(\text{W})$. Nuisance parameters are added to modify the expected rates and shapes according to the estimate of the systematic uncertainties affecting the measurement.

The interference between the EW Wjj and DY Wjj processes is included in the fit procedure, and its strength scales as $\sqrt{\mu\upsilon}$. The interference model is derived from the MADGRAPH5_aMC@NLO simulation described in Sect. 3.

The parameters of the model (μ and υ) are determined by maximizing the likelihood. The statistical methodology follows the one used in other analyses [63] using asymptotic formulas [64]. In this procedure the systematic uncertain-

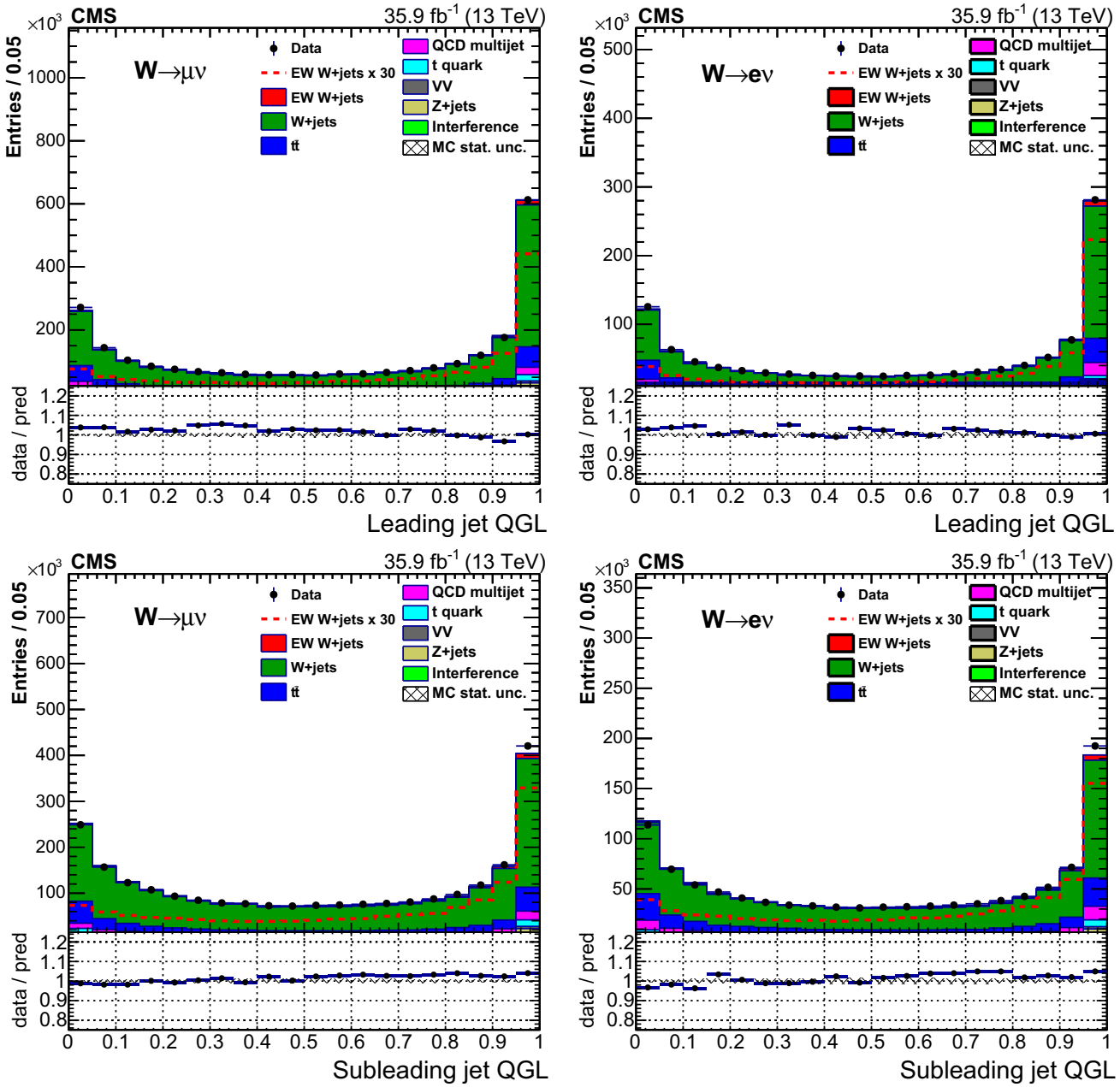

Fig. 7 The QGL output for the leading (upper) and subleading (lower) quark jet candidates in the preselected muon (left) and electron (right) samples

ties affecting the measurement of the signal and background strengths (μ and υ) are constrained with log-normal probability distributions.

9 Systematic uncertainties

The main systematic uncertainties affecting the measurement are classified into experimental and theoretical according to their sources. Some uncertainties affect only normalizations, whereas others affect both the normalization and shape of the BDT output distribution.

9.1 Experimental uncertainties

The following experimental uncertainties are considered.

Integrated luminosity. A 2.5% uncertainty is assigned to the value of the integrated luminosity [65].

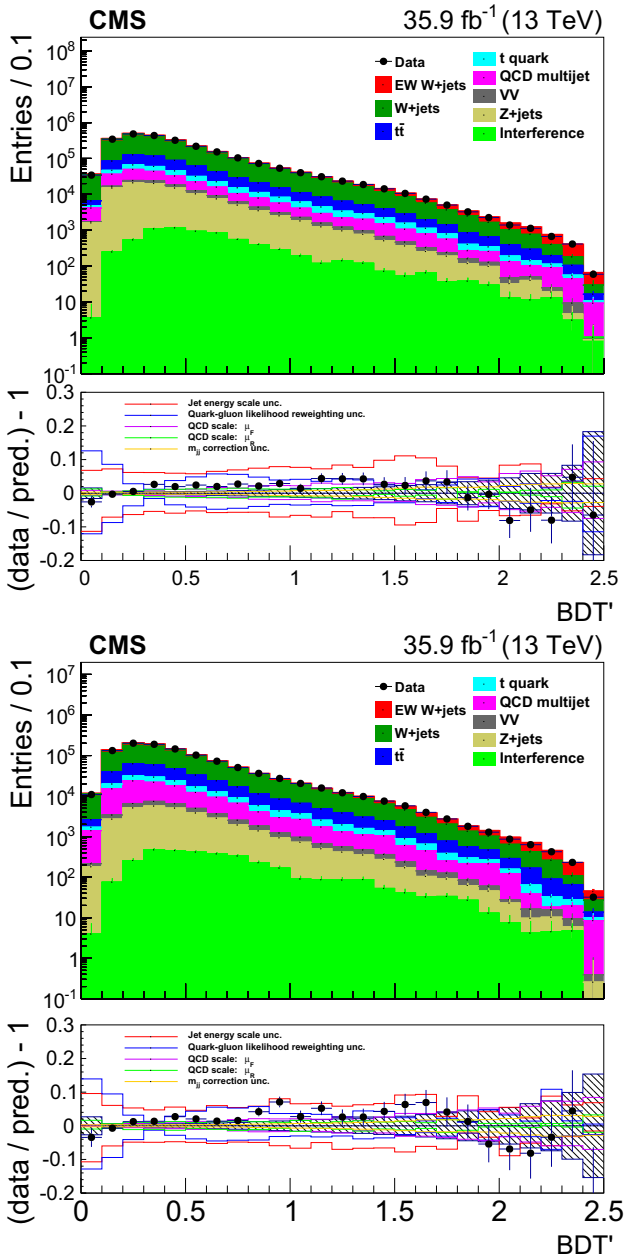

Fig. 8 Data and MC simulation BDT' output distributions for the muon (upper) and electron (lower) channels, using the BDT output transformed with the $\tanh^{-1}$ function to enhance the purest signal region. The ratio panel shows the statistical uncertainty from the simulation as well as the independent systematic uncertainties front the leading sources

Trigger and selection efficiencies. Uncertainties in the efficiency corrections based on control samples in data for the leptonic trigger and offline selections are included and amount to a total of 2–3% depending on the lepton p_{T} and η, for both the e and μ channels. These uncertainties are estimated by comparing the lepton efficiencies expected in simulation and measured in data with a "tag-and-probe" method [66].

Jet energy scale and resolution. The uncertainty in the energy of the jets affects the event selection and the computation of the kinematic variables used to calculate the discriminants. Therefore, the uncertainty in the jet energy scale (JES) affects both the expected event yields and the final shapes. The effect of the JES uncertainty is studied by rescaling up and down the reconstructed jet energy by p_{T}- and η-dependent scale factors [57]. An analogous approach is used for the JER.

QGL discriminator. The uncertainty in the performance of the QGL discriminator is measured using independent Z+jet and dijet data, after comparing with the corresponding simulation predictions [60]. Shape variations corresponding to the full differences between the data and the simulation are used as estimates of the uncertainty.

Pileup. Pileup can affect the identification and isolation of the leptons or the corrected energy of the jets. When the jet clustering algorithm is run, pileup can distort the reconstructed dijet system because of the contamination of tracks and calorimetric deposits. This uncertainty is evaluated by generating alternative distributions of the number of pileup interactions, corresponding to a 4.6% uncertainty in the total inelastic pp cross section at $\sqrt{s} = 13\,\mathrm{TeV}$ [67].

Limited number of simulated events. For each signal and background simulation, shape variations for the distributions are considered by shifting the content of each bin up or down by its statistical uncertainty [68]. This generates alternatives to the nominal shape that are used to describe the uncertainty from the limited number of simulated events.

m_{jj} correction. As described in Sect. 6, the m_{jj} prediction from simulation is corrected to match the distribution in data in a signal-depleted $R(p_{\mathrm{T}}) > 0.2$ control region. The uncertainty in this correction is derived by varying the fitted points within the statistical uncertainty from data and simulation combined and refitting the correction.

QCD multijet background template. As described in Sect. 5, the QCD multijet prediction is extrapolated from the data in a nonoverlapping CR. The uncertainty in the QCD multijet background template shape is derived by taking the envelope of the shape obtained when varying the lepton isolation requirement used to define the multijet-enriched CR. A 50% uncertainty in the QCD multijet background normalization is also included.

9.2 Theoretical uncertainties

The following theoretical uncertainties are considered in the analysis.

PDF. The PDF uncertainties are evaluated by comparing the nominal distributions to those obtained when using the

alternative PDFs of the NNPDF set, including α_s variations.

Factorization and renormalization scales. To account for theoretical uncertainties, signal and background shape variations are built by changing the values of μ_F and μ_R from their defaults by factors of 2 or 1/2 in the ME calculation, simultaneously for μ_F and μ_R, but independently for each simulated sample.

Signal acceptance. A 5% uncertainty on the signal yield is assigned to account for differences between the prediction for the LO signal with respect to the NLO predictions of the VBFNLO generator (v2.6.3).

Normalization of top quark and diboson backgrounds. Diboson and top quark production processes are modeled with MC simulations. An uncertainty in the normalization of these backgrounds is assigned based on the PDF and μ_F, μ_R uncertainties, following calculations in Refs. [42,43,47].

Interference between EW Wjj and DY Wjj. An overall normalization and a shape uncertainty are assigned to the interference term in the fit, based on an envelope of predictions with different μ_F, μ_R scales.

Parton showering model. The uncertainty in the PS model and the event tune is assessed as the full difference of the acceptance and shape predictions using PYTHIA and HERWIG++.

$R(p_T)$ correction. As described in Sect. 6, the $R(p_T)$ prediction from W+jets simulation is corrected to match the distribution in data with all expected contributions other than W+jets subtracted. The uncertainty in this correction is derived by varying the fitted points within the statistical uncertainty from data and simulation combined and refitting the correction.

10 Measurement of the EW Wjj production cross section

The signal strength, defined with the $\ell\nu$jj final state in the kinematic region described in Sect. 3, is extracted from the fit to the BDT output distribution as discussed in Sect. 8. Figure 9 shows the BDT distribution in the muon and electron channels for data and simulation after the fit, where the grey uncertainty band includes all systematic uncertainties. Good agreement is observed between the data and simulation within the uncertainties.

In the muon channel, the signal strength is measured to be

$$\mu = 0.91 \pm 0.02\,(\text{stat}) \pm 0.12\,(\text{syst}) = 0.91 \pm 0.12\,(\text{total}),$$

corresponding to a measured signal cross section

$$\begin{aligned}\sigma(\text{EW } \ell\nu\text{jj}) &= 6.22 \pm 0.12\,(\text{stat}) \pm 0.74\,(\text{syst})\,\text{pb}\\ &= 6.22 \pm 0.75\,(\text{total})\,\text{pb}.\end{aligned}$$

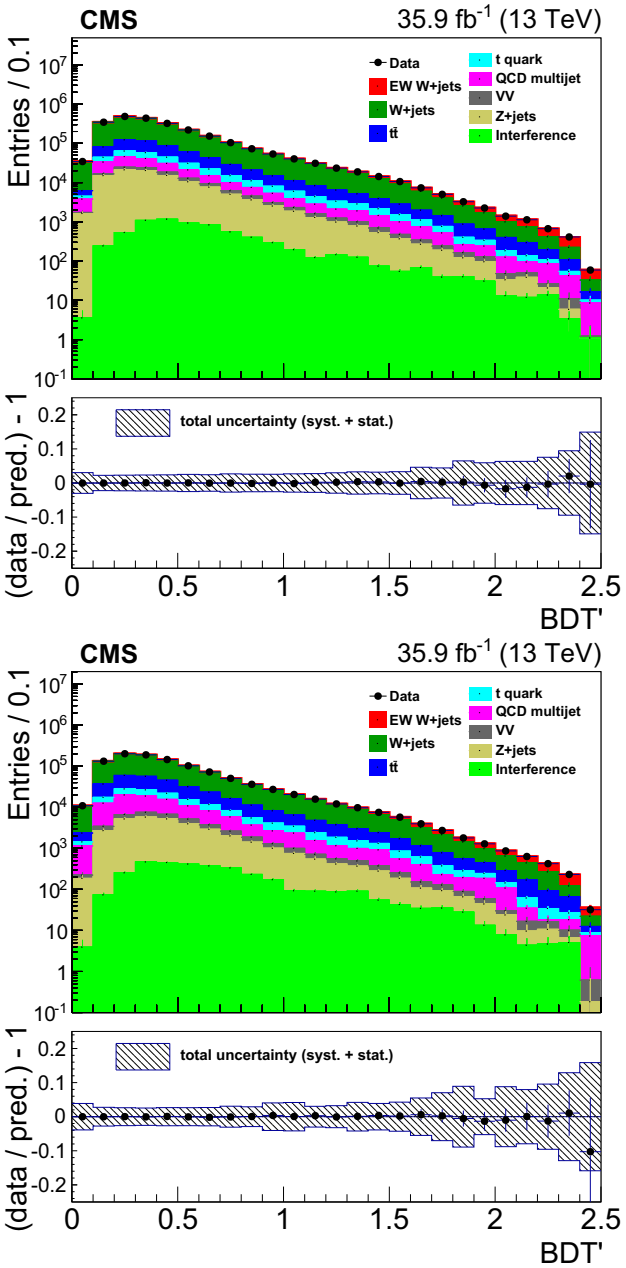

Fig. 9 Data compared with simulation for the BDT' output distribution for the muon (upper) and electron (lower) channels, after the fit. The grey uncertainty band in the ratio panel includes all systematic uncertainties

In the electron channel, the signal strength is measured to be

$$\mu = 0.92 \pm 0.03\,(\text{stat}) \pm 0.13\,(\text{syst}) = 0.92 \pm 0.13\,(\text{total}),$$

corresponding to a measured signal cross section

$$\begin{aligned}\sigma(\text{EW } \ell\nu\text{jj}) &= 6.27 \pm 0.19\,(\text{stat}) \pm 0.80\,(\text{syst})\,\text{pb}\\ &= 6.27 \pm 0.82\,(\text{total})\,\text{pb}.\end{aligned}$$

Table 2 Major sources of uncertainty in the measurement of the signal strength μ, and their impact. The total uncertainty is separated into four components: statistical, number of simulated events, experimental, and theory. The experimental and theory components are further decomposed into their primary individual uncertainty sources

Uncertainty source	$\Delta\mu$	
Statistical	+0.02	−0.02
Size of simulated samples	+0.05	−0.05
Experimental	+0.07	−0.07
Jet energy scale and resolution	+0.03	−0.01
QCD multijet estimation	+0.03	−0.03
m_{jj} correction	+0.05	−0.05
Background normalization	+0.02	−0.02
Other experimental uncertainties	< 0.01	
Theory	+0.07	−0.07
QCD scale and PDF	+0.05	−0.05
Interference	+0.02	−0.02
Signal acceptance	+0.05	−0.05
Other theory uncertainties	+0.01	−0.01
Total	+0.10	−0.10

The results obtained for the different lepton channels are compatible with each other, and in agreement with the SM predictions.

From the combined fit of the two channels, the signal strength is measured to be

$$\mu = 0.91 \pm 0.02\,(\text{stat}) \pm 0.10\,(\text{syst}) = 0.91 \pm 0.10\,(\text{total}),$$

corresponding to a measured signal cross section

$$\begin{aligned}\sigma(\text{EW}\ \ell\nu\text{jj}) &= 6.23 \pm 0.12\,(\text{stat}) \pm 0.61\,(\text{syst})\,\text{pb}\\ &= 6.23 \pm 0.62\,(\text{total})\,\text{pb},\end{aligned}$$

in agreement with the MADGRAPH5_aMC@NLO LO prediction $\sigma_{\text{LO}}(\text{EW}\ \ell\nu\text{jj}) = 6.81^{+0.03}_{-0.06}\,(\text{scale}) \pm 0.26\,(\text{PDF})\,\text{pb}$. In the combined fit, the DY strength is $\nu = 0.88 \pm 0.07$. Using the statistical methodology described in Sect. 8, the background-only hypotheses in the electron, muon, and combined channels are all excluded with significance above five standard deviations. Table 2 lists the major sources of uncertainty and their impact on the measured precision of μ. The largest sources of experimental uncertainty are the m_{jj} correction, the JES, and the limited number of simulated events, while the largest sources of theoretical uncertainty are the μ_{F}, μ_{R} scale uncertainties and the uncertainty in the signal acceptance, derived by comparing the LO signal prediction with the prediction from the VBFNLO generator.

The signal strength is also measured with respect to the NLO signal prediction, as described in Sect. 3. In the muon channel, the signal strength is measured to be

$$\begin{aligned}\mu_{\text{NLO}} &= 0.91 \pm 0.02\,(\text{stat}) \pm 0.12\,(\text{syst})\\ &= 0.91 \pm 0.12\,(\text{total}).\end{aligned}$$

In the electron channel, the signal strength is measured to be

$$\begin{aligned}\mu_{\text{NLO}} &= 0.89 \pm 0.03\,(\text{stat}) \pm 0.12\,(\text{syst})\\ &= 0.89 \pm 0.12\,(\text{total}).\end{aligned}$$

From the combined fit of the two channels, the signal strength is measured to be

$$\begin{aligned}\mu_{\text{NLO}} &= 0.90 \pm 0.02\,(\text{stat}) \pm 0.10\,(\text{syst})\\ &= 0.90 \pm 0.10\,(\text{total}),\end{aligned}$$

corresponding to a measured signal cross section

$$\begin{aligned}\sigma(\text{EW}\ \ell\nu\text{jj}) &= 6.07 \pm 0.12\,(\text{stat}) \pm 0.57\,(\text{syst})\,\text{pb}\\ &= 6.07 \pm 0.58\,(\text{total})\,\text{pb},\end{aligned}$$

in agreement with the POWHEG NLO prediction $\sigma_{\text{NLO}}(\text{EW}\ \ell\nu\text{jj}) = 6.74^{+0.02}_{-0.04}\,(\text{scale}) \pm 0.26\,(\text{PDF})\,\text{pb}$.

11 Limits on anomalous gauge couplings

It is useful to look for signs of new physics via a model-independent EFT framework. In the framework of EFT, new physics can be described as an infinite series of new interaction terms organized as an expansion in the mass dimension of the operators.

In the EW sector of the SM, the first higher-dimensional operators containing bosons are six-dimensional [8]:

$$\begin{aligned}\mathcal{O}_{WWW} &= \frac{c_{WWW}}{\Lambda^2} W_{\mu\nu} W^{\nu\rho} W^{\mu}_{\rho},\\ \mathcal{O}_{W} &= \frac{c_{W}}{\Lambda^2} (D^{\mu}\Phi)^{\dagger} W_{\mu\nu} (D^{\nu}\Phi),\\ \mathcal{O}_{B} &= \frac{c_{B}}{\Lambda^2} (D^{\mu}\Phi)^{\dagger} B_{\mu\nu} (D^{\nu}\Phi),\\ \widetilde{\mathcal{O}}_{WWW} &= \frac{\widetilde{c}_{WWW}}{\Lambda^2} \widetilde{W}_{\mu\nu} W^{\nu\rho} W^{\mu}_{\rho},\\ \widetilde{\mathcal{O}}_{W} &= \frac{\widetilde{c}_{W}}{\Lambda^2} (D^{\mu}\Phi)^{\dagger} \widetilde{W}_{\mu\nu} (D^{\nu}\Phi),\end{aligned} \tag{4}$$

where, as is customary, group indices are suppressed and the mass scale Λ is factorized from the coupling constants c. In Eq. (4), $W_{\mu\nu}$ is the SU(2) field strength, $B_{\mu\nu}$ is the U(1) field strength, Φ is the Higgs doublet, and operators with a tilde are the magnetic duals of the field strengths. The first three operators are charge and parity conserving, whereas the last two are not. Models with operators that preserve charge conjugation and parity symmetries can be included in the calculation either individually or in pairs. With these assumptions, the values of coupling constants divided by the mass scale c/Λ^2 are measured.

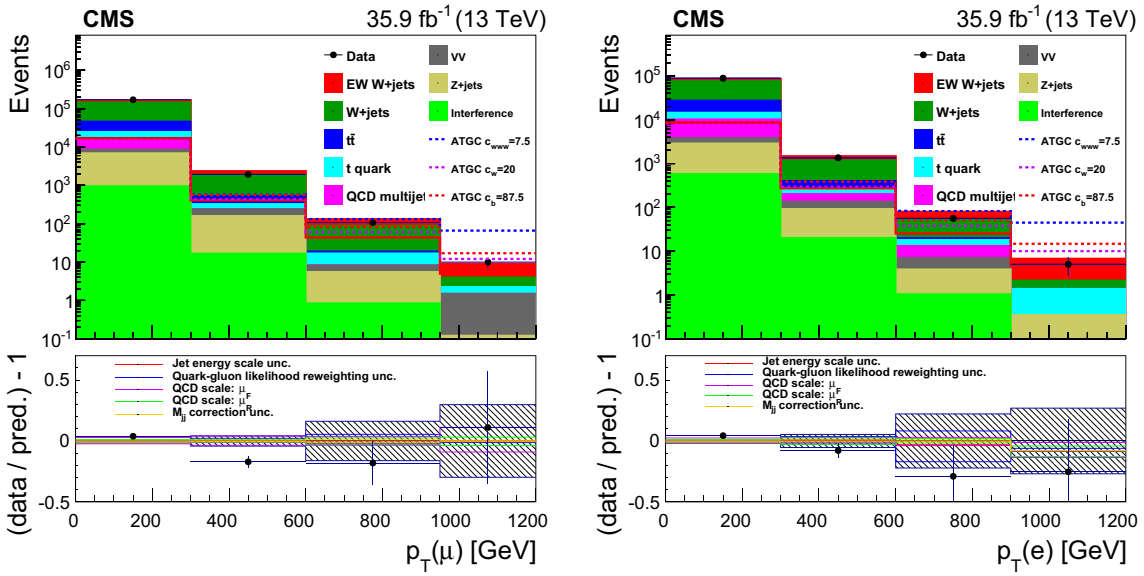

Fig. 10 Distributions of p_{T}^{ℓ} in data and SM backgrounds, and various ATGC scenarios in the muon (left) and electron (right) channels, before the fit. For each ATGC scenario plotted a particular parameter is varied while the other ATGC parameters are fixed to zero. The lower panels show the ratio between data and prediction minus one with the statistical uncertainty from simulation (grey hatched band) as well as the leading systematic uncertainties in the shape of the p_{T}^{ℓ} distribution

These operators have a rich phenomenology since they contribute to many multiboson scattering processes at tree level. The operator $\mathcal{O}_{WWW}$ modifies vertices with three or six vector bosons, whereas the operators $\mathcal{O}_W$ and $\mathcal{O}_B$ modify both the HVV vertices and vertices with three or four vector bosons. A more detailed description of the phenomenology of these operators can be found in Ref. [69]. Modifications to the ZWW and γWW vertices are investigated in this analysis, since these modify the pp $\rightarrow$ Wjj cross section.

Previously, modifications to these vertices have been studied using anomalous trilinear gauge couplings [70]. The relationship between the dimension-six operators in Eq. (4) and ATGCs can be found in Ref. [8]. Most stringent limits on ATGC parameters were previously set by LEP [71], CDF [72], D0 [73], ATLAS [74,75], and CMS [76,77].

11.1 Statistical analysis

The measurement of the coupling constants uses templates in the p_{T} of the lepton from the $W \rightarrow \ell\nu$ decay. Because this is well measured and longitudinally Lorentz invariant, this variable is robust against mismodeling and ideal for this purpose. An additional requirement of BDT > 0.5 has been applied, which is optimized based on the expected sensitivity to the ATGC signal. The expected limits are subsequently improved by 20–25% with respect to the expected limits without a BDT selection. In each channel, four bins from $0 < p_{\mathrm{T}}^{\ell} < 1.2$ TeV are used, where the last bin contains overflow and its lower bin edge boundary has been optimized separately for each channel.

For each signal MC event, 125 weights are assigned that correspond to a 5×5×5 grid in (c_{WWW}/Λ^2) (c_W/Λ^2) (c_B/Λ^2). Equal bins are used in the interval $[-15, 15]$ TeV^{-2} for c_{WWW}/Λ^2, $[-40, 40]$ TeV^{-2} for c_W/Λ^2, and equal bins in the interval $[-175, 175]$ TeV^{-2} for c_B/Λ^2.

To construct the p_{T}^{ℓ} templates, the associated weights calculated for each event are used to construct a parametrized model of the expected yield in each bin as a function of the values of the dimension-six operators' coupling constants. For each bin, the ratios of the expected signal yield with dimension-six operators to the one without (leaving only the SM contribution) are fitted at each point of the grid to a quadratic polynomial. The highest p_{T}^{ℓ} bin has the largest statistical power to detect the presence of higher-dimensional operators. Figure 10 shows examples of the final templates, with the expected signal overlaid on the background expectation, for three different hypotheses of dimension-six operators. The SM distribution is normalized to the expected cross section.

A simultaneous binned fit for the values of the ATGCs is performed in the two lepton channels. A profile likelihood method, the Wald Gaussian approximation, and Wilks' theorem [78] are used to derive confidence intervals at 95% confidence level (CL). One-dimensional and two-dimensional limits are derived on each of the three ATGC parameters and each combination of two ATGC parameters while all other parameters are set to their SM values. Systematic and theoret-

Table 3 One-dimensional limits on the ATGC EFT parameters at 95% CL

Coupling constant	Expected 95% CL interval (TeV^{-2})	Observed 95% CL interval (TeV^{-2})
c_{WWW}/Λ^2	$[-2.5, 2.5]$	$[-2.3, 2.5]$
c_W/Λ^2	$[-16, 19]$	$[-8.8, 16]$
c_B/Λ^2	$[-62, 61]$	$[-45, 46]$

Table 4 One-dimensional limits on the ATGC effective Lagrangian (LEP parametrization) parameters at 95% CL

Coupling constant	Expected 95% CL interval	Observed 95% CL interval
λ^Z	$[-0.0094, 0.0097]$	$[-0.0088, 0.0095]$
Δg_1^Z	$[-0.046, 0.053]$	$[-0.029, 0.044]$
$\Delta\kappa_1^Z$	$[-0.059, 0.059]$	$[-0.044, 0.044]$

ical uncertainties are represented by the individual nuisance parameters with log-normal distributions and are profiled in the fit.

11.2 Results

No significant deviation from the SM expectation is observed. Limits on the EFT parameters are reported and also translated into the equivalent parameters defined in an effective Lagrangian (LEP parametrization) in Ref. [79], without form factors: $\lambda^\gamma = \lambda^Z = \lambda$, $\Delta\kappa^Z = \Delta g_1^Z - \Delta\kappa^\gamma \tan^2\theta_W$. The parameters λ, $\Delta\kappa^Z$, and Δg_1^Z are considered, where the Δ symbols represent deviations from their respective SM values.

Results for the one-dimensional limits are listed in Table 3 for c_{WWW}, c_W and c_B, and in Table 4 for λ, Δg_1^Z and $\Delta\kappa_1^Z$; two-dimensions limits are shown in Figs. 11 and 12. The results are dominated by the sensitivity in the muon channel due to the larger acceptance for muons. An ATGC signal is not included in the interference between EW and DY production. The effect on the limits is small (<3%). The LHC semileptonic WZ analysis using 13 TeV data currently sets the most stringent limits on c_{WWW}/Λ^2 and c_W/Λ^2, while the WW analysis using 8 TeV data currently sets the tightest limits on c_B/Λ^2. This analysis is most sensitive to c_{WWW}/Λ^2, where the limit is slightly less restrictive but comparable.

11.3 Combination with the VBF Z boson production analysis

As mentioned in Sect. 1, the closely-related EW Zjj process has been measured by CMS at $\sqrt{s} = 13$ TeV [15].

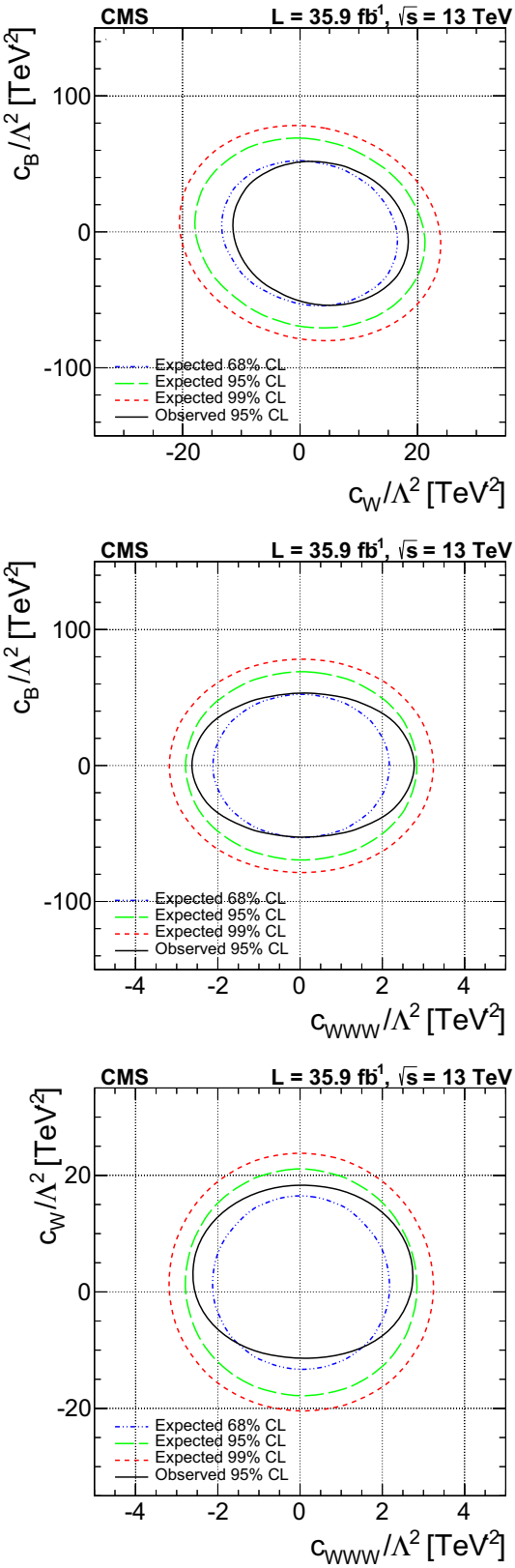

Fig. 11 Expected and observed two-dimensional limits on the EFT parameters at 95% CL

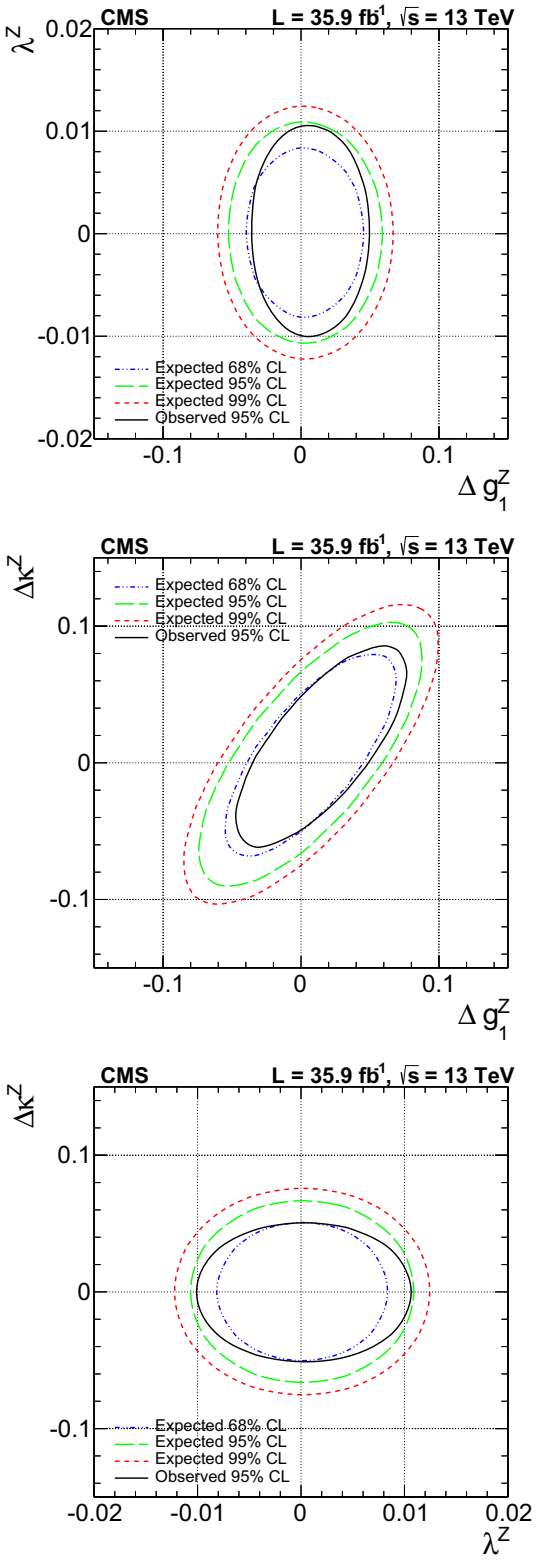

Fig. 12 Expected and observed two-dimensional limits on the ATGC effective Lagrangian (LEP parametrization) parameters at 95% CL

Table 5 One-dimensional limits on the ATGC EFT parameters at 95% CL from the combination of EW Wjj and EW Zjj analyses

Coupling constant	Expected 95% CL interval (TeV^{-2})	Observed 95% CL interval (TeV^{-2})
c_{WWW}/Λ^2	$[-2.3, 2.4]$	$[-1.8, 2.0]$
c_W/Λ^2	$[-11, 14]$	$[-5.8, 10.0]$
c_B/Λ^2	$[-61, 61]$	$[-43, 45]$

Table 6 One-dimensional limits on the ATGC effective Lagrangian (LEP parametrization) parameters at 95% CL from the combination of EW Wjj and EW Zjj analyses

Coupling constant	Expected 95% CL interval	Observed 95% CL interval
λ^Z	$[-0.0089, 0.0091]$	$[-0.0071, 0.0076]$
Δg_1^Z	$[-0.040, 0.047]$	$[-0.021, 0.034]$
$\Delta\kappa_1^Z$	$[-0.058, 0.059]$	$[-0.043, 0.042]$

This result included constraints on ATGC EFT parameters obtained via a fit to the p_{T}(Z) distribution, an experimentally clean observable sensitive to deviations from zero in the ATGC parameters. Both the EW Zjj and EW Wjj analyses are sensitive to anomalous couplings related to the WWZ vertex. A simultaneous binned likelihood fit for the ATGC parameters is performed to the p_{T}(Z) distribution in the EW Zjj production and and p_{T}^{ℓ} in the EW Wjj production. In the combined fit, the primary uncertainty sources are correlated including the JES and JER uncertainties. Results for the one-dimensional limits are listed in Table 5 for c_{WWW}, c_W and c_B, and in Table 6 for λ, Δg_1^Z, and $\Delta\kappa_1^Z$; two-dimensions limits are shown in Figs. 13 and 14.

12 Study of the hadronic and jet activity in W+jet events

Having established the presence of the SM signal, the properties of the hadronic activity in the selected events can be examined, in particular in the the region in rapidity between the two tagging jets, with low expected hadron activity (rapidity gap). The production of additional jets in the rapidity gap, in a region with a larger contribution of EW Wjj processes is explored in Sect. 12.1. Studies of the rapidity gap hadronic activity using track-only observables, are presented in Sect. 12.2. Finally, a study of hadronic activity vetoes, using both PF jets and track-only observables, is presented in Sect. 12.3. A significant suppression of the hadronic activ-

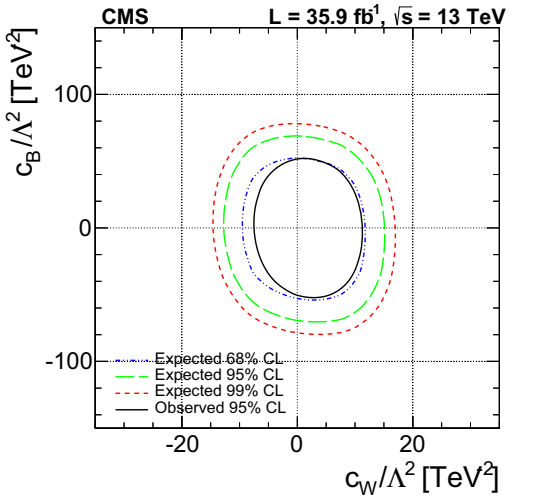

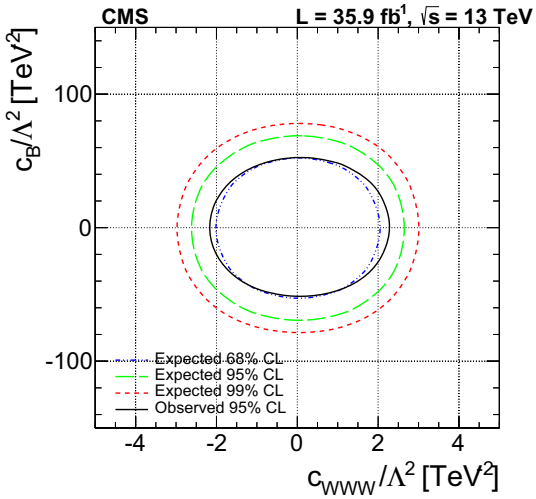

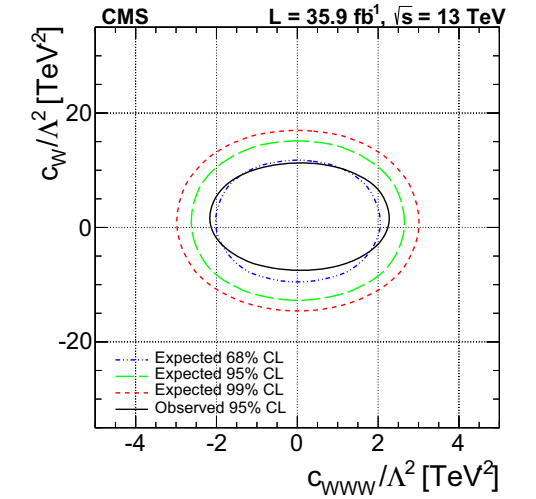

Fig. 13 Expected and observed two-dimensional limits on the EFT parameters at 95% CL from the combination of EW Wjj and EW Zjj analyses

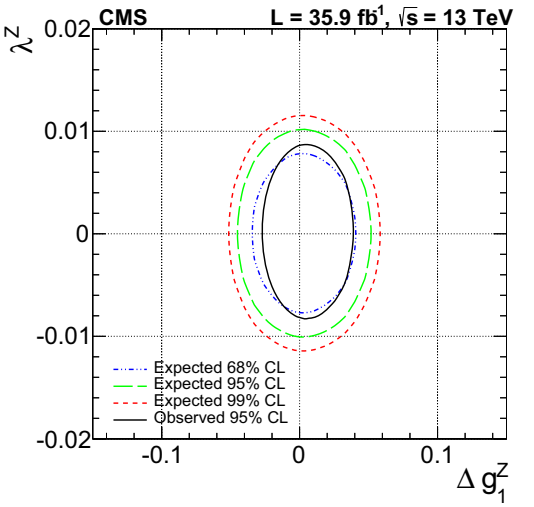

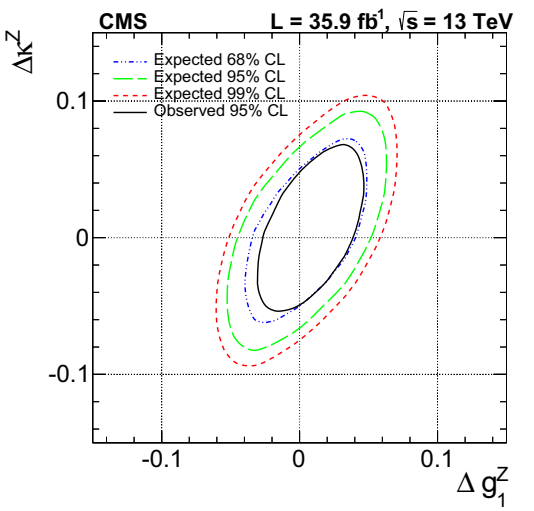

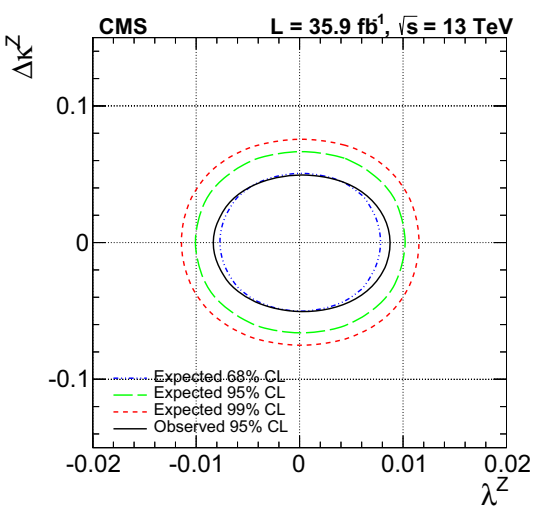

Fig. 14 Expected and observed two-dimensional limits on the ATGC effective Lagrangian (LEP parametrization) parameters at 95% CL from the combination of EW Wjj and EW Zjj analyses

ity in signal events is expected because the final-state objects originate from EW interactions, in contrast with the radiative QCD production of jets in DY Wjj events.

In all these studies, event distributions are shown with a selection on the output value at BDT $>$ 0.95, which allows a signal-enriched region to be selected with a sim-

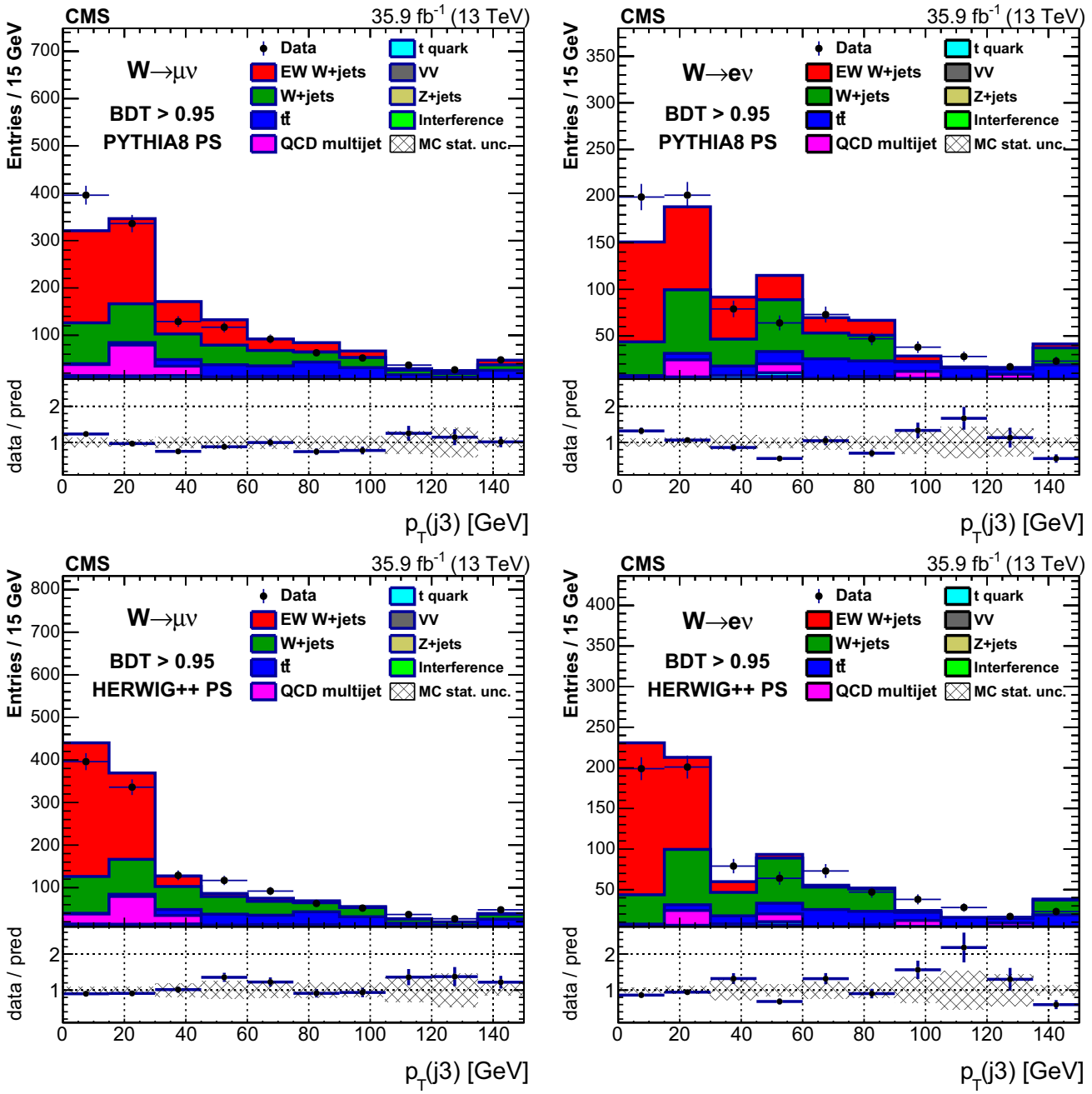

Fig. 15 Leading additional jet p_{T} (p_{T} (j3)) for BDT $>$ 0.95 in the muon (left) and electron (right) channels including the signal prediction from MadGraph5_aMC@NLO interfaced with Pythia parton showering (upper) and Herwig++ parton showering (lower). In all plots the last bin contains overflow events, and the first bin contains events where no additional jet with $p_{\mathrm{T}} > 15$ GeV is present

ilar fraction of signal and background events. None of the BDT input observables listed in Sect. 8 are related to additional hadronic activity observables, as a consequence there is no bias on the additional hadronic activity observables due to the BDT output cut. The reconstructed distributions are compared directly to the prediction obtained with a full simulation of the CMS detector. In the BDT $>$ 0.95 region, the dominant uncertainty on the prediction from simulation is due to the limited number of generated events.

12.1 Jet activity studies in a high-purity region

For this study, aside from the two tagging jets used in the preselection, all PF jets with $p_{\mathrm{T}} > 15$ GeV found within the pseudorapidity gap of the tagging jets, $\eta_{\mathrm{min}}^{\mathrm{tag\ jet}} < \eta < \eta_{\mathrm{max}}^{\mathrm{tag\ jet}}$,

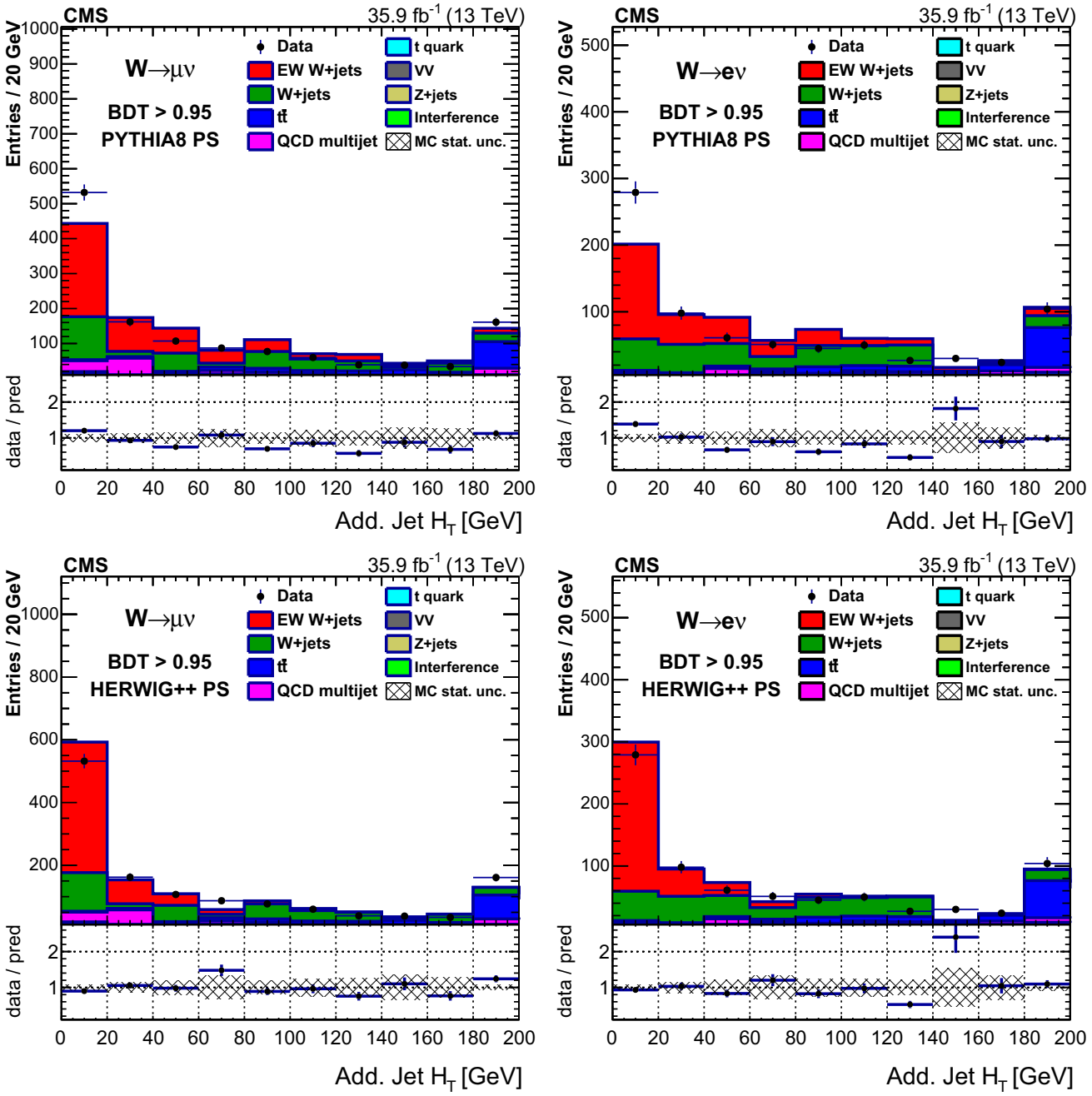

Fig. 16 Total H_T of the additional jets for BDT $>$ 0.95 in the muon (left) and electron (right) channels including the signal prediction from MADGRAPH5_aMC@NLO interfaced with PYTHIA parton showering (upper) and HERWIG++ parton showering (lower). In all plots the last bin contains overflow events, and the first bin contains events where no additional jet with $p_T > 15$ GeV is present

are used. For the estimation of the background contributions, the normalizations obtained from the fit discussed in Sect. 10 are used.

The p_T of the leading additional jet in Wjj events, as well as the scalar p_T sum (H_T) of all additional jets, are shown in Figs. 15 and 16, comparing data and simulations including the signal prediction from MADGRAPH5_aMC@NLO interfaced with either PYTHIA or HERWIG++ parton showering. The comparison reveals a deficit in the simulation predictions with PYTHIA parton showering for the rate of events with lower additional jet activity, whereas the tail of higher additional activity is generally in better agreement.

A suppression of additional jets is observed in data compared with the background-only simulation shapes. In

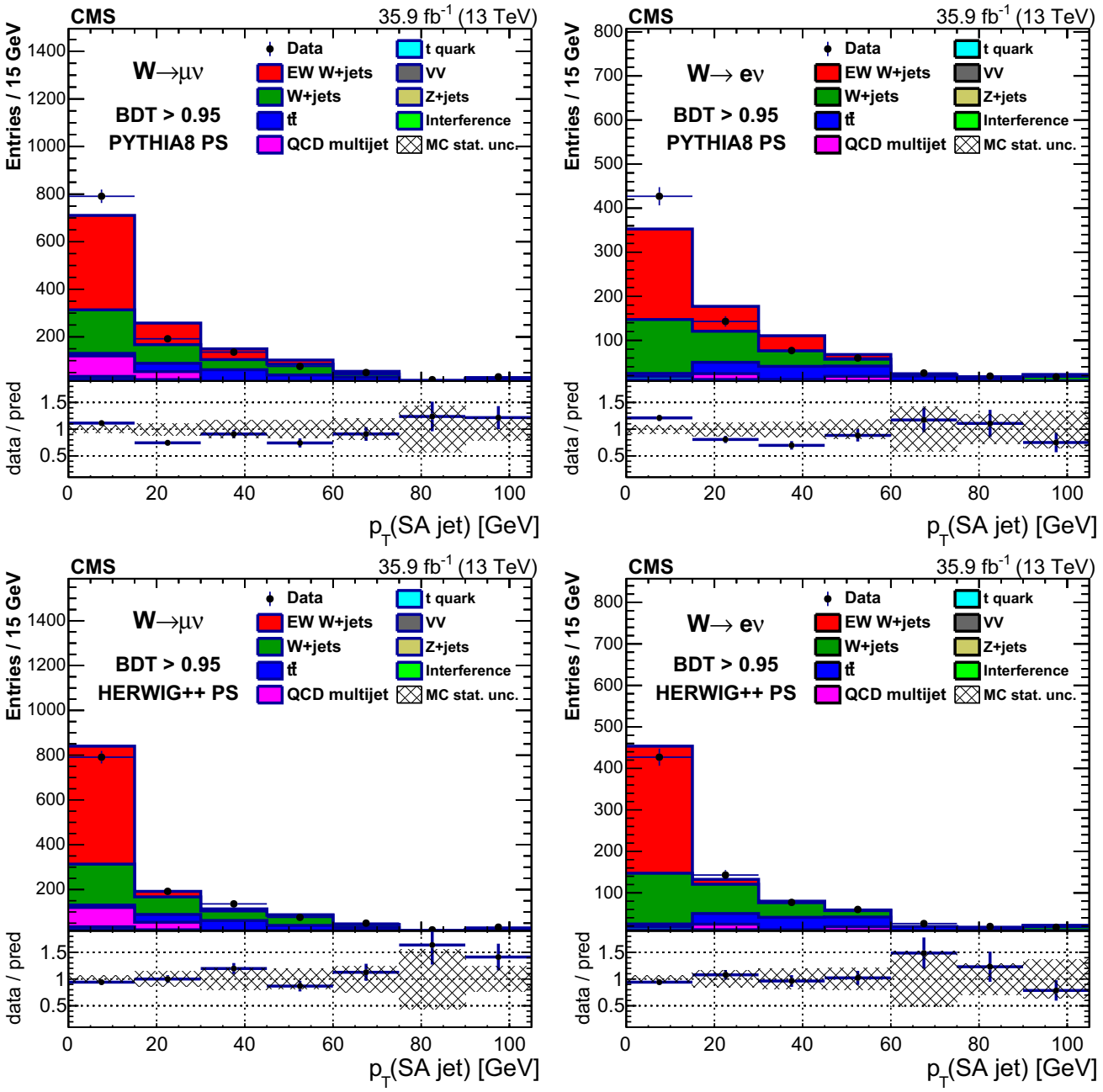

Fig. 17 Leading additional soft-activity (SA) jet p_{T} for BDT > 0.95 in the muon (left) and electron (right) channels including the signal prediction from MADGRAPH5_aMC@NLO interfaced with PYTHIA parton showering (upper) and HERWIG++ parton showering (lower)

the simulation of the signal, the additional jets are produced by the PS (see Sect. 3), so studying these distributions provides insight on the PS model in the rapidity gap region.

12.2 Study of charged hadron activity

For this study, a collection is formed of high-purity tracks [80] with $p_{\mathrm{T}} > 0.3$ GeV, uniquely associated with the main PV in the event. Tracks associated with the lepton or with the tagging jets are excluded from the selection. The association between the selected tracks and the reconstructed PVs is carried out by minimizing the longitudinal impact parameter, which is defined as the z-distance between the PV and the point of closest approach of the track helix to the PV, labeled d_z^{PV}. The association is required to satisfy the conditions $d_z^{\mathrm{PV}} < 2$ mm and $d_z^{\mathrm{PV}} < 3\delta d_z^{\mathrm{PV}}$, where δd_z^{PV} is the uncertainty in d_z^{PV}.

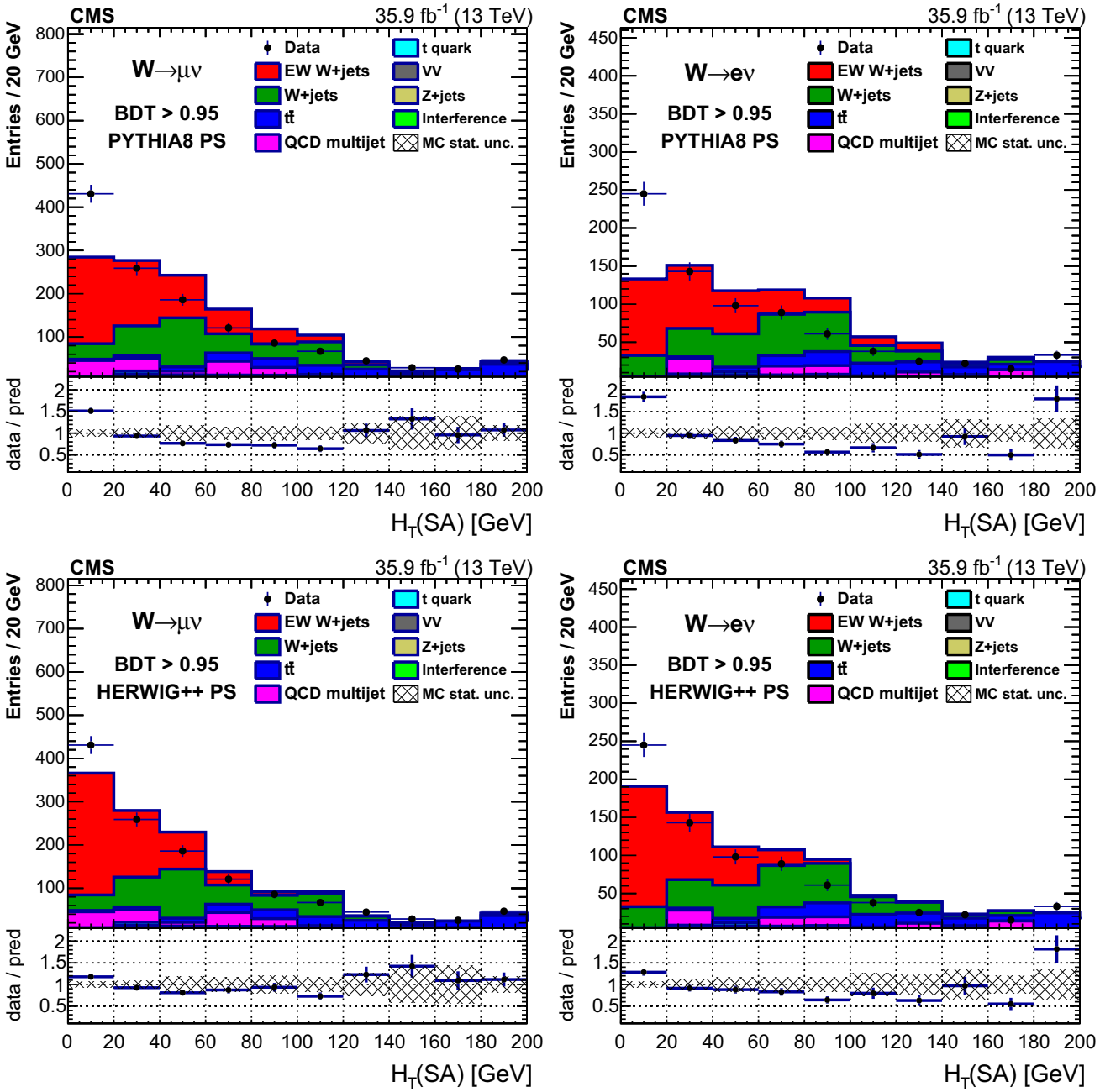

Fig. 18 Total soft activity (SA) jet H_T for BDT $>$ 0.95 in the muon (left) and electron (right) channels including the signal prediction from MadGraph5_aMC@NLO interfaced with Pythia parton showering (upper) and Herwig++ parton showering (lower). In all plots the last bin contains overflow events

A collection of "soft-track" jets is defined by clustering the selected tracks using the anti-k_T clustering algorithm [51] with a distance parameter of $R = 0.4$. The use of track jets represents a clean and well-understood method [81] to reconstruct jets with energy as low as a few GeV. These jets are not affected by pileup because of the association of the constituent tracks with the hard scattering vertex [82].

Track jets of low p_T and within $\eta_{\text{min}}^{\text{tag jet}} < \eta < \eta_{\text{max}}^{\text{tag jet}}$ are considered for the study of the hadronic activity between the tagging jets, and referred to as "soft activity" (SA). For each event, the scalar p_T sum of the soft-track jets with $p_T > 1$ GeV is computed, and referred to as the "soft H_T" variable. Figures 17 and 18 show the distribution of the leading soft-track jet p_T and soft H_T in the signal-enriched region (BDT $>$ 0.95), for the electron and muon channels, compared to predictions from Pythia and Herwig++ PS models. The plots show some disagreement between the data and the predictions, in particular in the regions of small additional activity, when compared with the Pythia predictions.

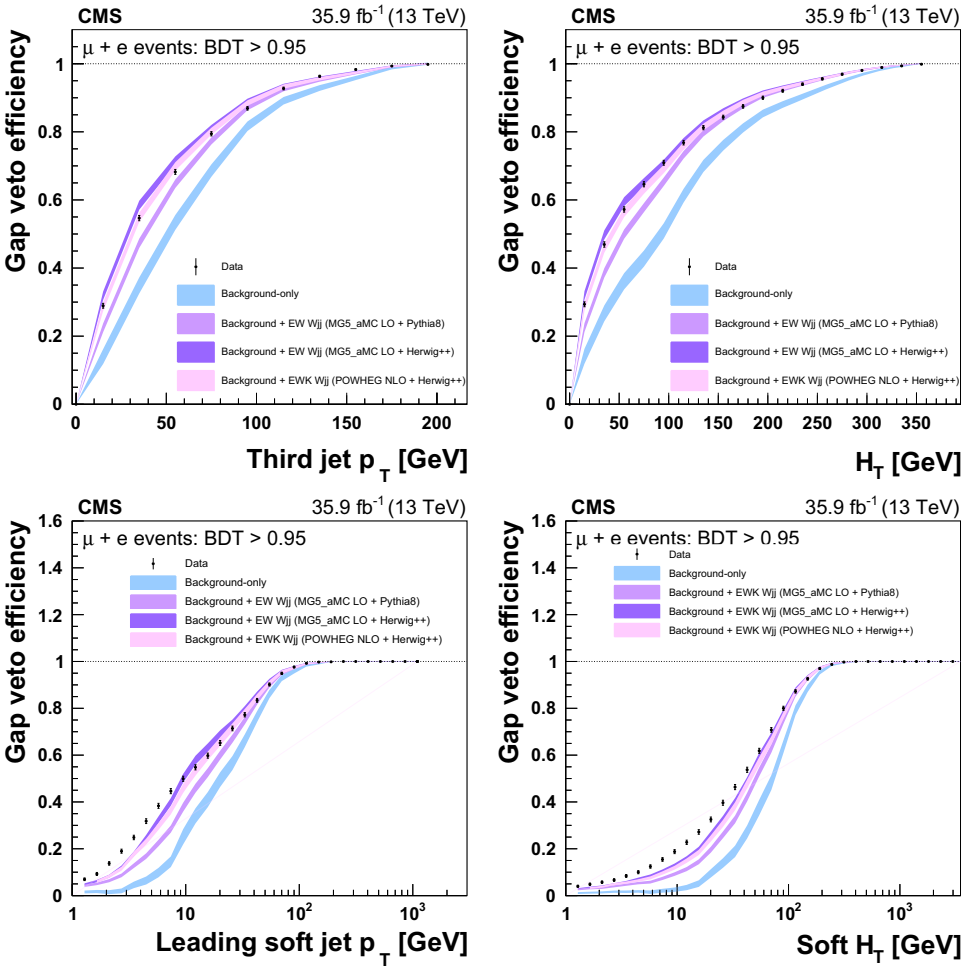

Fig. 19 Hadronic activity veto efficiencies in the signal-enriched BDT > 0.95 region for the muon and electron channels combined, as a function of the leading additional jet p_{T} (upper left), additional jet H_{T} (upper right), leading soft-activity jet p_{T} (lower left), and soft-activity jet H_{T} (lower right). The data are compared with the background-only prediction as well as background+signal with PYTHIA parton showering and background+signal with HERWIG++ parton showering. In addition, the background+signal prediction from POWHEG plus HERWIG++ parton showering is included. The uncertainty bands include only the statistical uncertainty in the prediction from simulation, and the data points include only the statistical uncertainty in data

12.3 Study of hadronic activity vetoes

The efficiency of a hadronic activity veto corresponds to the fraction of events with a measured gap activity below a given threshold. This efficiency is studied as a function of the applied threshold for various gap activity observables. The veto thresholds studied here start at 15 GeV for gap activities measured with standard PF jets, while they go down to 1 GeV for gap activities measured with soft-track jets.

Figure 19 shows the gap activity veto efficiency of combined muon and electron events in the signal-enriched region when placing an upper threshold on the p_{T} of the additional third jet, on the H_{T} of all additional jets, on the leading soft-activity jet p_{T}, or on the soft-activity H_{T}. The observed efficiency in data is compared to expected efficiencies for background-only events, and efficiencies for background plus signal events where the signal is modeled with PYTHIA or HERWIG++. Data points clearly disfavor the background-only predictions and are in reasonable agreement with the presence of the signal with the HERWIG++ PS predictions for gap activities above 20 GeV, while the signal with PYTHIA PS seems to generally overestimate the gap activity. In the events with very low gap activity, in particular below 10 GeV as measured with the soft track jets, the data indicates gap activities also below the HERWIG++ PS predictions. In addition, the expected efficiencies are included for background plus signal events where the signal is modeled with POWHEG (Sect. 3) with HERWIG++ PS. The POWHEG plus HERWIG++ prediction is in good agreement with the LO plus HERWIG++ prediction.

13 Summary

The cross section of the electroweak production of a W boson in association with two jets is measured in the kinematic region defined as invariant mass $m_{\mathrm{jj}} > 120$ GeV and transverse momenta $p_{\mathrm{Tj}} > 25$ GeV. The data sample corresponds to an integrated luminosity of 35.9 fb^{-1} of proton–proton collisions at centre-of-mass energy $\sqrt{s} =$ 13 TeV recorded by the CMS Collaboration at the LHC. The

measured cross section $\sigma_{\mathrm{EW}}(\mathrm{Wjj}) = 6.23 \pm 0.12\,(\mathrm{stat}) \pm 0.61\,(\mathrm{syst})$ pb agrees with the leading order standard model prediction. This is the first observation of this process at $\sqrt{s} = 13$ TeV.

A search is performed for anomalous trilinear gauge couplings associated with dimension-six operators as given in the framework of an effective field theory. No evidence for ATGCs is found, and the corresponding 95% confidence level intervals on the dimension-six operators are $-2.3 < c_{\mathrm{WWW}}/\Lambda^2 < 2.5\,\mathrm{TeV}^{-2}$, $-8.8 < c_{\mathrm{W}}/\Lambda^2 < 16\,\mathrm{TeV}^{-2}$, and $-45 < c_{\mathrm{B}}/\Lambda^2 < 46\,\mathrm{TeV}^{-2}$. These results are combined with previous results on the electroweak production of a Z boson in association with two jets, yielding the limit on the c_{WWW} coupling $-1.8 < c_{\mathrm{WWW}}/\Lambda^2 < 2.0\,\mathrm{TeV}^{-2}$.

The additional hadronic activity, as well as the efficiencies for gap activity vetos, are studied in a signal-enriched region. Generally reasonable agreement is found between the data and the quantum chromodynamics predictions with the HERWIG++ parton shower and hadronization model, while the PYTHIA model predictions typically show greater activity in the rapidity gap between the two tagging jets.

Acknowledgements We congratulate our colleagues in the CERN accelerator departments for the excellent performance of the LHC and thank the technical and administrative staffs at CERN and at other CMS institutes for their contributions to the success of the CMS effort. In addition, we gratefully acknowledge the computing centers and personnel of the Worldwide LHC Computing Grid for delivering so effectively the computing infrastructure essential to our analyses. Finally, we acknowledge the enduring support for the construction and operation of the LHC and the CMS detector provided by the following funding agencies: BMBWF and FWF (Austria); FNRS and FWO (Belgium); CNPq, CAPES, FAPERJ, FAPERGS, and FAPESP (Brazil); MES (Bulgaria); CERN; CAS, MoST, and NSFC (China); COLCIENCIAS (Colombia); MSES and CSF (Croatia); RPF (Cyprus); SENESCYT (Ecuador); MoER, ERC IUT, and ERDF (Estonia); Academy of Finland, MEC, and HIP (Finland); CEA and CNRS/IN2P3 (France); BMBF, DFG, and HGF (Germany); GSRT (Greece); NKFIA (Hungary); DAE and DST (India); IPM (Iran); SFI (Ireland); INFN (Italy); MSIP and NRF (Republic of Korea); MES (Latvia); LAS (Lithuania); MOE and UM (Malaysia); BUAP, CINVESTAV, CONACYT, LNS, SEP, and UASLP-FAI (Mexico); MOS (Montenegro); MBIE (New Zealand); PAEC (Pakistan); MSHE and NSC (Poland); FCT (Portugal); JINR (Dubna); MON, RosAtom, RAS, RFBR, and NRC KI (Russia); MESTD (Serbia); SEIDI, CPAN, PCTI, and FEDER (Spain); MOSTR (Sri Lanka); Swiss Funding Agencies (Switzerland); MST (Taipei); ThEPCenter, IPST, STAR, and NSTDA (Thailand); TUBITAK and TAEK (Turkey); NASU and SFFR (Ukraine); STFC (United Kingdom); DOE and NSF (USA).

Individuals have received support from the Marie-Curie program and the European Research Council and Horizon 2020 Grant, contract Nos. 675440 and 765710 (European Union); the Leventis Foundation; the A.P. Sloan Foundation; the Alexander von Humboldt Foundation; the Belgian Federal Science Policy Office; the Fonds pour la Formation à la Recherche dans l'Industrie et dans l'Agriculture (FRIA-Belgium); the Agentschap voor Innovatie door Wetenschap en Technologie (IWT-Belgium); the F.R.S.-FNRS and FWO (Belgium) under the "Excellence of Science – EOS" – be.h project n. 30820817; the Beijing Municipal Science & Technology Commission, No. Z181100004218003; the Ministry of Education, Youth and Sports (MEYS) of the Czech Republic; the Lendület ("Momentum") Program and the János Bolyai Research Scholarship of the Hungarian Academy of Sciences, the New National Excellence Program ÚNKP, the NKFIA research Grants 123842, 123959, 124845, 124850, 125105, 128713, 128786, and 129058 (Hungary); the Council of Science and Industrial Research, India; the HOMING PLUS program of the Foundation for Polish Science, cofinanced from European Union, Regional Development Fund, the Mobility Plus program of the Ministry of Science and Higher Education, the National Science Center (Poland), contracts Harmonia 2014/14/M/ST2/00428, Opus 2014/13/B/ST2/02543, 2014/15/B/ST2/03998, and 2015/19/B/ST2/02861, Sonata-bis 2012/07/E/ST2/01406; the National Priorities Research Program by Qatar National Research Fund; the Programa Estatal de Fomento de la Investigación Científica y Técnica de Excelencia María de Maeztu, Grant MDM-2015-0509 and the Programa Severo Ochoa del Principado de Asturias; the Thalis and Aristeia programs cofinanced by EU-ESF and the Greek NSRF; the Rachadapisek Sompot Fund for Postdoctoral Fellowship, Chulalongkorn University and the Chulalongkorn Academic into Its 2nd Century Project Advancement Project (Thailand); the Welch Foundation, contract C-1845; and the Weston Havens Foundation (USA).

Data Availability Statement This manuscript has no associated data or the data will not be deposited. [Authors' comment: Release and preservation of data used by the CMS Collaboration as the basis for publications is guided by the CMS policy as written in its document "CMS data preservation, re-use and open access policy" (https://cms-docdb.cern.ch/cgi-bin/PublicDocDB/RetrieveFile?docid=6032&filename=CMSDataPolicyV1.2.pdf&version=2).]

Funded by SCOAP[3].

A Additional rapidity gap observables

A set of rapidity gap observables in the high signal purity region BDT > 0.95 is studied in addition to the results described in Sect. 12. The number of soft activity jets, defined in Sect. 12.2, in the rapidity gap between the two tag jets is shown for soft activity jet $p_{\mathrm{T}} > 10$, 5, and 2 GeV in Figures 20, 21, and 22, respectively. These distributions are consistent with the general underestimation of the simulation with respect to data at low activity values, particularly for the PYTHIA parton showering.

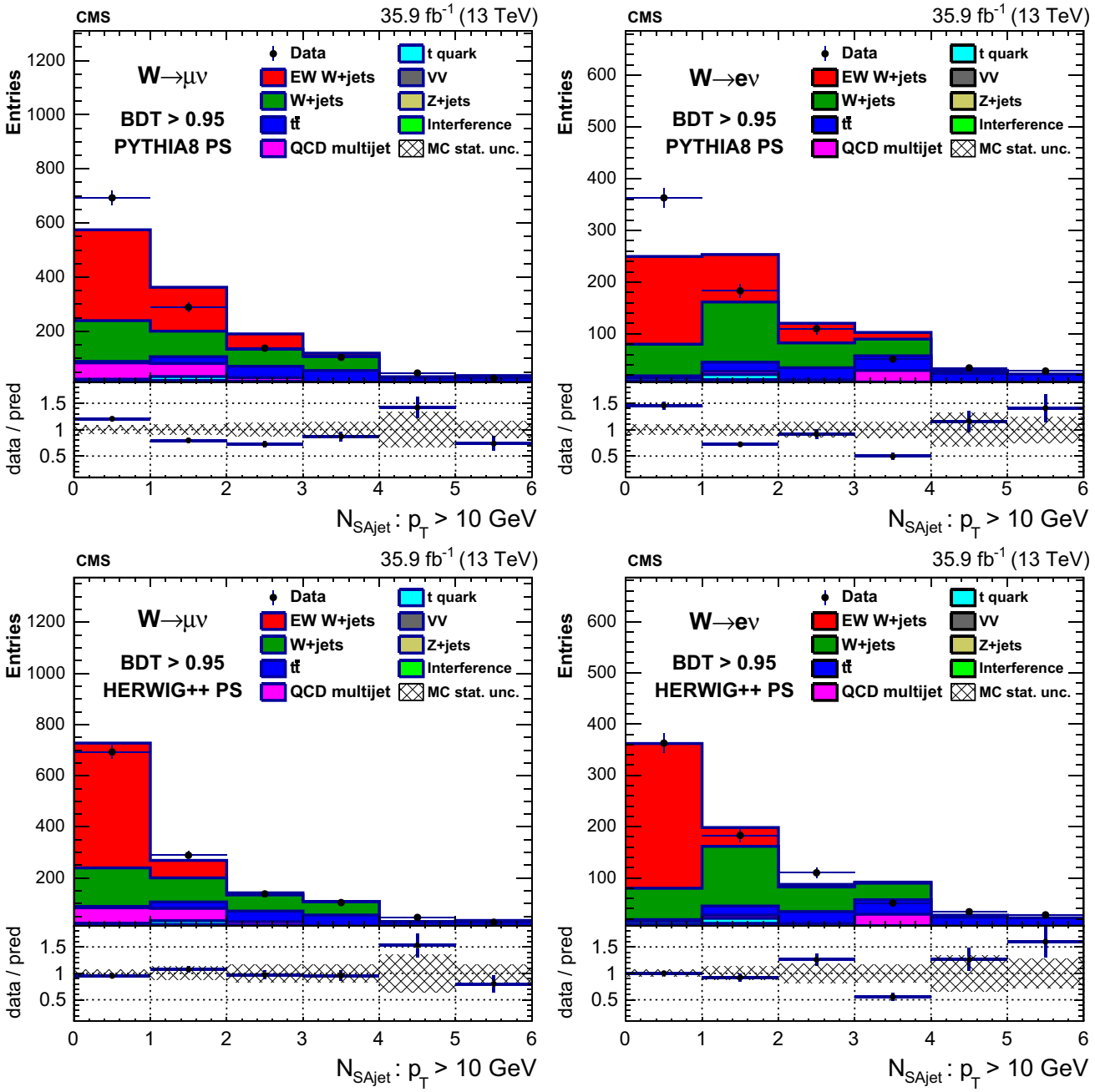

Fig. 20 Number of soft activity jets with $p_{\mathrm{T}} > 10\,\mathrm{GeV}$ in the rapidity gap for BDT > 0.95 in the muon (left) and electron (right) channels including signal with PYTHIA parton showering (upper) and HERWIG++ parton showering (lower). In all plots the last bin contains overflow events

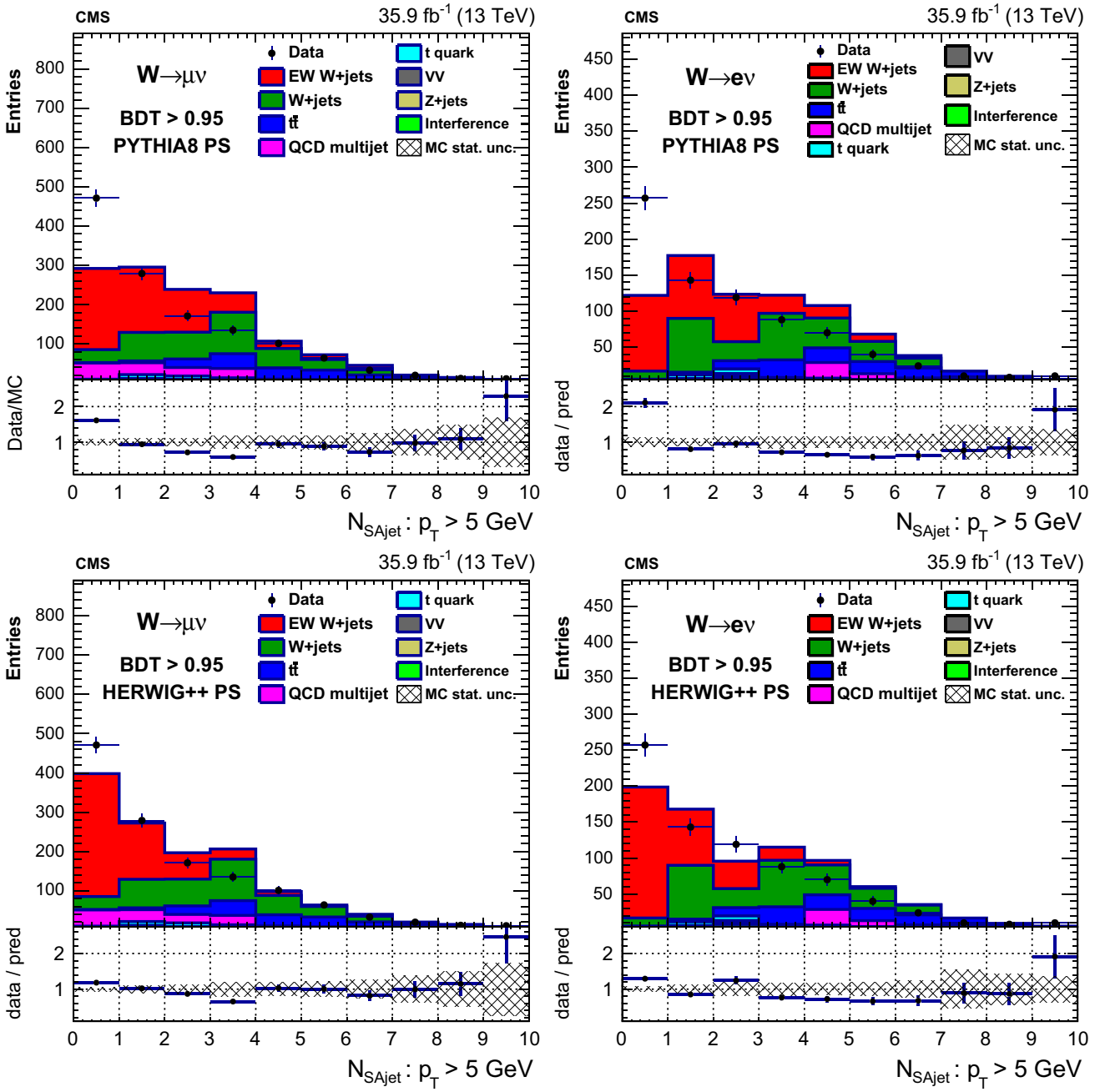

Fig. 21 Number of soft activity jets with $p_{\mathrm{T}} > 5$ GeV in the rapidity gap for BDT > 0.95 in the muon (left) and electron (right) channels including signal with PYTHIA parton showering (upper) and HERWIG++ parton showering (lower)

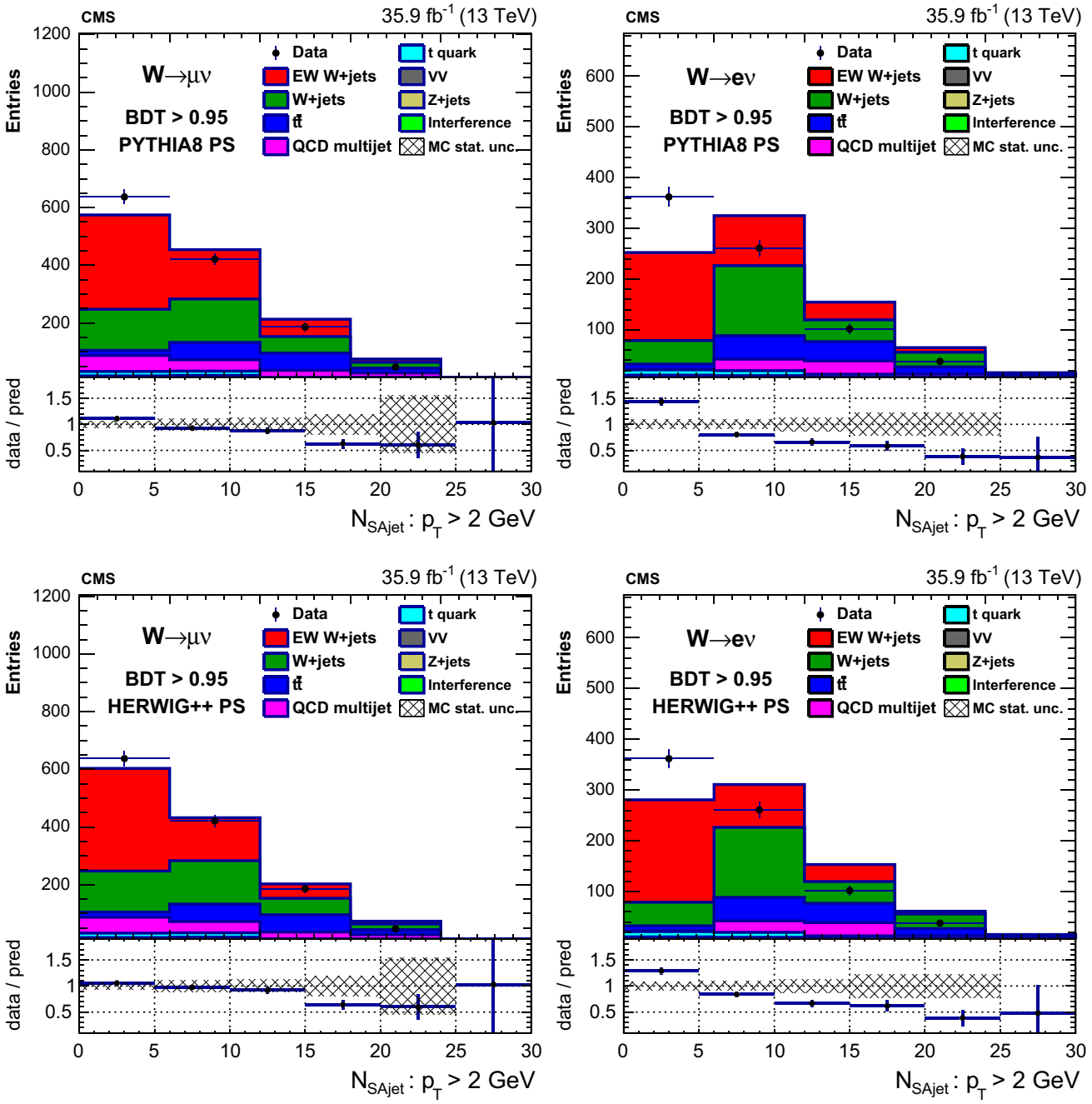

Fig. 22 Number of soft activity jets with $p_{\mathrm{T}} > 2$ GeV in the rapidity gap for BDT > 0.95 in the muon (left) and electron (right) channels including signal with PYTHIA parton showering (upper) and HERWIG++ parton showering (lower)

B Jet activity in signal-depleted region

Section 12 shows a comparison of the data with simulation with PYTHIA and HERWIG++ parton showering separately in a high purity signal region with BDT > 0.95. The agreement of the simulation with data for the background prediction is validated for the rapidity gap observables in the signal-depleted region BDT < 0.95, where the signal purity is less than 2%. Figures 23, 24, 25, and 26 show the leading additional jet p_{T}, the total H_{T} of the additional jets, the leading soft activity jet p_{T}, and the total soft activity jet H_{T}, respectively, in the region BDT < 0.95. Good agreement is observed between the background prediction and the data for all observables.

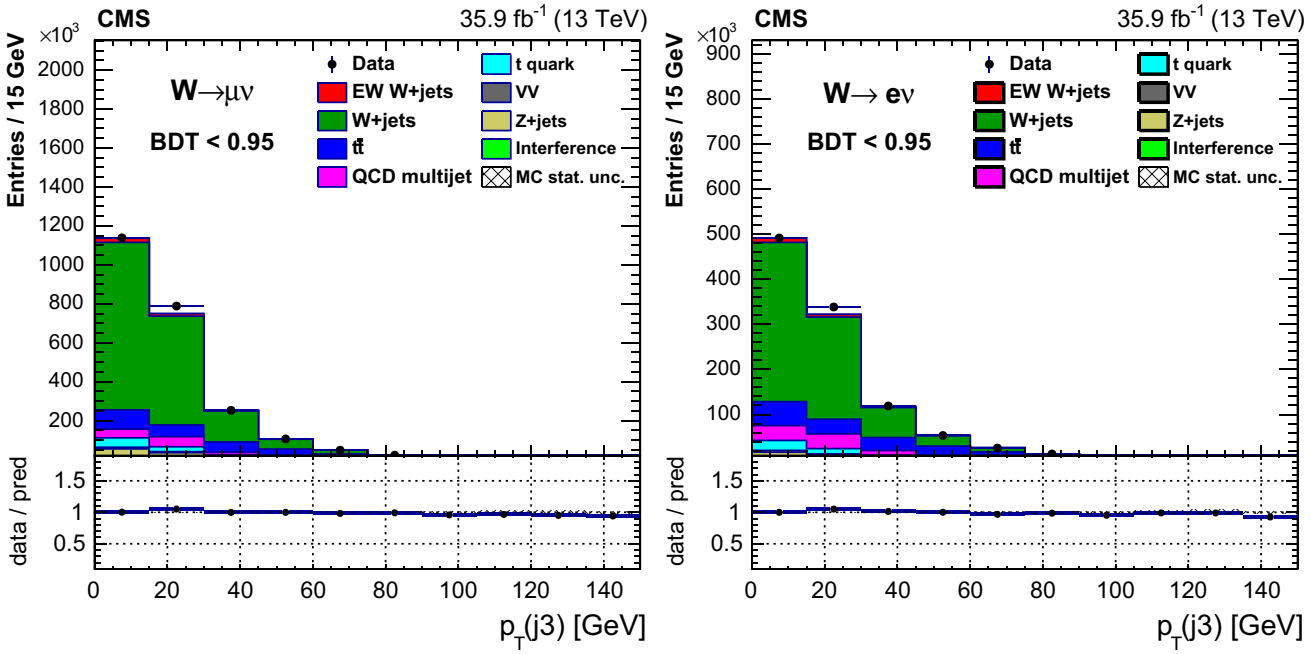

Fig. 23 Leading additional jet p_T (p_T (j3)) for BDT < 0.95 in the muon (left) and electron (right) channels. In all plots the first bin contains events where no additional jet with $p_T > 15$ GeV is present

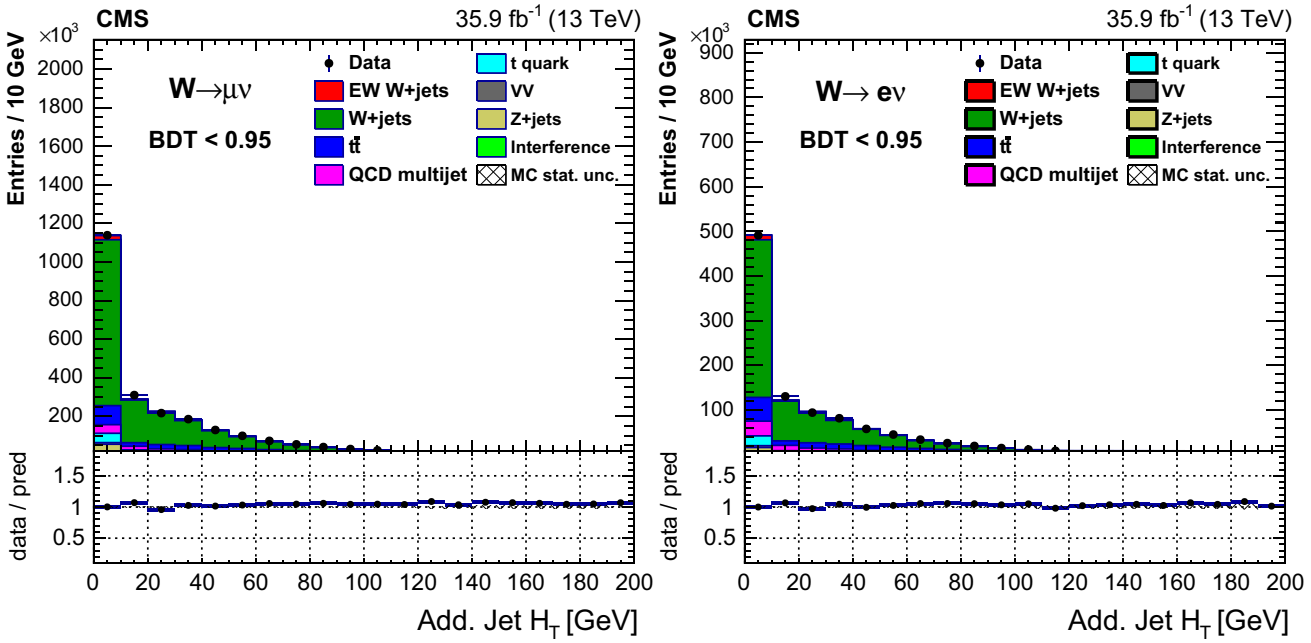

Fig. 24 Total H_T of the additional jets for BDT < 0.95 in the muon (left) and electron (right) channels. In all plots the fist bin contains events where no additional jet with $p_T > 15$ GeV is present

B.1 Hadronic activity vetoes

The efficiency of a hadronic activity veto, as described in Sect. 12.3, is studied in the signal-depleted BDT < 0.95 region. Figure 27 shows the gap activity veto efficiency of combined muon and electron events in the signal-depleted region when placing an upper threshold on the p_T of the additional third jet, on the H_T of all additional jets, on the leading soft-activity jet p_T, or on the soft-activity H_T. There is very little difference between the background-only prediction and the predictions including signal with either PYTHIA or HERWIG++ parton showering due to the very small fraction

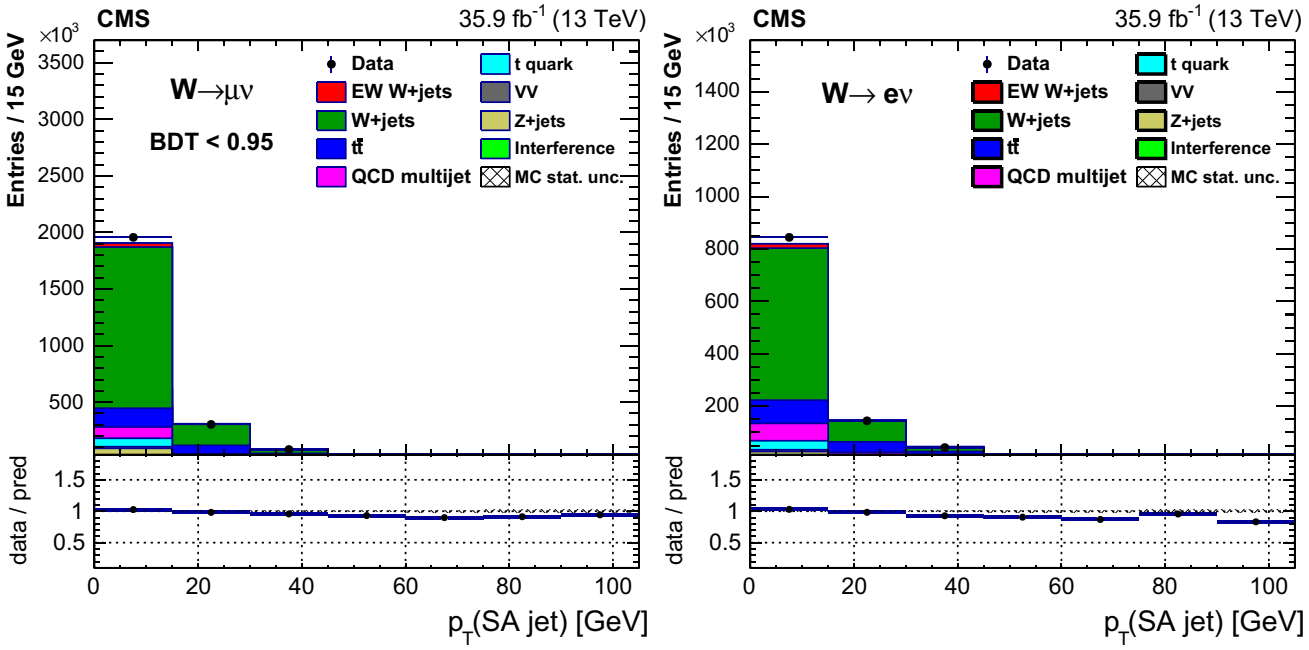

Fig. 25 Leading additional soft-activity (SA) jet p_{T} for BDT < 0.95 in the muon (left) and electron (right)

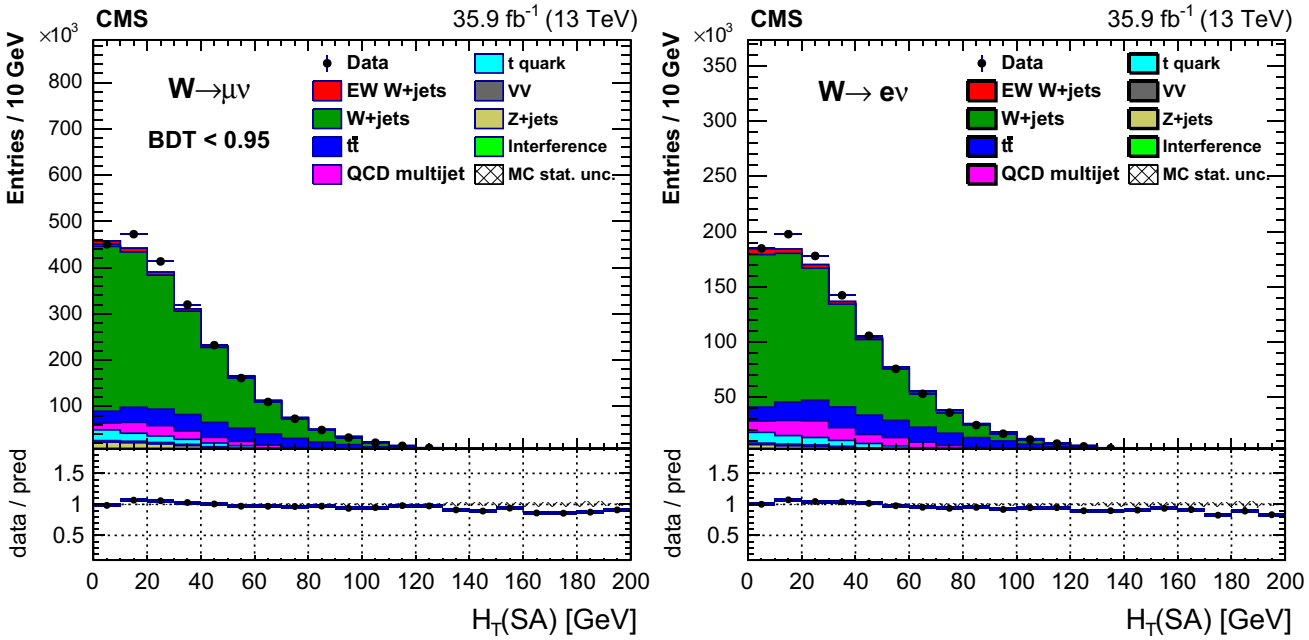

Fig. 26 Total soft activity (SA) jet H_{T} for BDT < 0.95 in the muon (left) and electron (right) channels

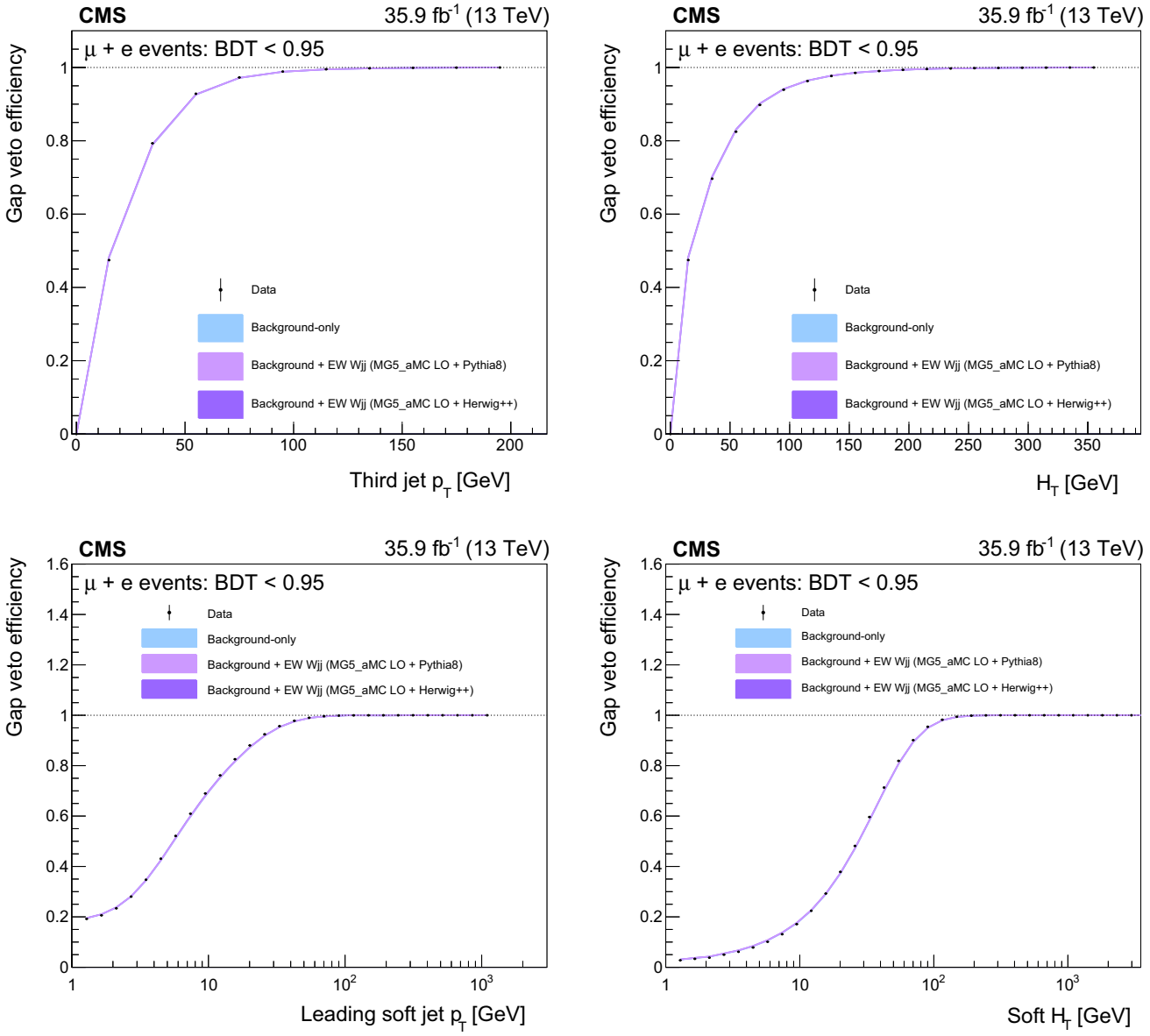

Fig. 27 Hadronic activity veto efficiencies in the signal-depleted BDT < 0.95 region for the muon and electron channels combined, as a function of the leading additional jet p_{T} (upper left), additional jet H_{T} (upper right), leading soft-activity jet p_{T} (lower left), and soft-activity jet H_{T} (lower right). The data are compared with the background-only prediction as well as background+signal with PYTHIA parton showering and background+signal with HERWIG++ parton showering. The uncertainty bands include only the statistical uncertainty in the prediction from simulation. There is very little difference between the predictions due to the small fraction of signal in this region

of signal in this region. Good agreement is observed between the data and the simulation, giving further confidence in the modelling of the background observables for the rapidity gap studies.

References

1. ATLAS Collaboration, Observation of a new particle in the search for the standard model Higgs boson with the ATLAS detector at the LHC. Phys. Lett. B **716**, 1 (2012). https://doi.org/10.1016/j.physletb.2012.08.020. arXiv:1207.7214
2. CMS Collaboration, Observation of a new boson at a mass of 125 GeV with the CMS experiment at the LHC. Phys. Lett. B **716**, 30 (2012). https://doi.org/10.1016/j.physletb.2012.08.021. arXiv:1207.7235
3. CMS Collaboration, Observation of a new boson with mass near 125 GeV in pp collisions at $\sqrt{s} = 7$ and 8 TeV. JHEP **06**, 081 (2013). https://doi.org/10.1007/JHEP06(2013)081. arXiv:1303.4571
4. G.-C. Cho et al., Weak boson fusion production of supersymmetric particles at the CERN LHC. Phys. Rev. D

73, 054002 (2006). https://doi.org/10.1103/PhysRevD.73.054002. arXiv:hep-ph/0601063
5. J.D. Bjorken, Rapidity gaps and jets as a new physics signature in very high-energy hadron hadron collisions. Phys. Rev. D **47**, 101 (1993). https://doi.org/10.1103/PhysRevD.47.101
6. F. Schissler, D. Zeppenfeld, Parton shower effects on W and Z production via vector boson fusion at NLO QCD. JHEP **04**, 057 (2013). https://doi.org/10.1007/JHEP04(2013)057. arXiv:1302.2884
7. K. Hagiwara, S. Ishihara, R. Szalapski, D. Zeppenfeld, Low-energy effects of new interactions in the electroweak boson sector. Phys. Rev. D **48**, 2182 (1993). https://doi.org/10.1103/PhysRevD.48.2182
8. C. Degrande et al., Effective field theory: a modern approach to anomalous couplings. Ann. Phys. **335**, 21 (2013). https://doi.org/10.1016/j.aop.2013.04.016. arXiv:1205.4231
9. CMS Collaboration, Measurement of electroweak production of a W boson and two forward jets in proton-proton collisions at $\sqrt{s} = 8$ TeV. JHEP **11**, 147 (2016). https://doi.org/10.1007/JHEP11(2016)147. arXiv:1607.06975
10. ATLAS Collaboration, Measurements of electroweak Wjj production and constraints on anomalous gauge couplings with the ATLAS detector. Eur. Phys. J. C **77**, 474 (2017). https://doi.org/10.1140/epjc/s10052-017-5007-2. arXiv:1703.04362
11. CMS Collaboration, Measurement of the hadronic activity in events with a Z and two jets and extraction of the cross section for the electroweak production of a Z with two jets in pp collisions at $\sqrt{s} = 7$ TeV. JHEP **10**, 062 (2013). https://doi.org/10.1007/JHEP10(2013)062. arXiv:1305.7389
12. CMS Collaboration, Measurement of electroweak production of two jets in association with a Z boson in proton-proton collisions at $\sqrt{s} = 8$ TeV. Eur. Phys. J. C **75**, 66 (2015). https://doi.org/10.1140/epjc/s10052-014-3232-5. arXiv:1410.3153
13. ATLAS Collaboration, Measurement of the electroweak production of dijets in association with a Z boson and distributions sensitive to vector boson fusion in proton-proton collisions at $\sqrt{s} = 8$ TeV using the ATLAS detector. JHEP **04**, 031 (2014). https://doi.org/10.1007/JHEP04(2014)031. arXiv:1401.7610
14. ATLAS Collaboration, Measurement of the cross-section for electroweak production of dijets in association with a Z boson in pp collisions at $\sqrt{s} = 13$ TeV with the ATLAS detector. Phys. Lett. B **775**, 206 (2017). https://doi.org/10.1016/j.physletb.2017.10.040. arXiv:1709.10264
15. CMS Collaboration, Electroweak production of two jets in association with a Z boson in proton-proton collisions at $\sqrt{s} = 13$ TeV. Eur. Phys. J. C **78**, 589 (2018). https://doi.org/10.1140/epjc/s10052-018-6049-9. arXiv:1712.09814
16. CMS Collaboration, Description and performance of track and primary-vertex reconstruction with the CMS tracker. JINST **9**, P10009 (2014). https://doi.org/10.1088/1748-0221/9/10/P10009. arXiv:1405.6569
17. CMS Collaboration, Performance of electron reconstruction and selection with the CMS detector in proton-proton collisions at $\sqrt{s} = 8$ TeV. JINST **10**, P06005 (2015). https://doi.org/10.1088/1748-0221/10/06/P06005. arXiv:1502.02701
18. CMS Collaboration, Performance of the CMS muon detector and muon reconstruction with proton-proton collisions at $\sqrt{s} = 13$ TeV. JINST **13**, P06015 (2018). https://doi.org/10.1088/1748-0221/13/06/P06015. arXiv:1804.04528
19. CMS Collaboration, The CMS trigger system. JINST **12**, P01020 (2017). https://doi.org/10.1088/1748-0221/12/01/P01020. arXiv:1609.02366
20. CMS Collaboration, The CMS experiment at the CERN LHC. JINST **3**, S08004 (2008). https://doi.org/10.1088/1748-0221/3/08/S08004
21. J. Alwall et al., The automated computation of tree-level and next-to-leading order differential cross sections, and their matching to parton shower simulations. JHEP **07**, 079 (2014). https://doi.org/10.1007/JHEP07(2014)079. arXiv:1405.0301
22. T. Sjöstrand et al., An introduction to PYTHIA 8.2. Comput. Phys. Commun. **191**, 159 (2015). https://doi.org/10.1016/j.cpc.2015.01.024. arXiv:1410.3012
23. NNPDF Collaboration, Unbiased global determination of parton distributions and their uncertainties at NNLO and at LO. Nucl. Phys. B **855**, 153 (2012). https://doi.org/10.1016/j.nuclphysb.2011.09.024. arXiv:1107.2652
24. CMS Collaboration, Event generator tunes obtained from underlying event and multiparton scattering measurements. Eur. Phys. J. C **76**, 155 (2016). https://doi.org/10.1140/epjc/s10052-016-3988-x. arXiv:1512.00815
25. K. Arnold et al., VBFNLO: a parton level Monte Carlo for processes with electroweak bosons. Comput. Phys. Commun. **180**, 1661 (2009). https://doi.org/10.1016/j.cpc.2009.03.006. arXiv:0811.4559
26. J. Baglio et al., VBFNLO: a parton level Monte Carlo for processes with electroweak bosons—manual for version 2.7.0, (2011). arXiv:1107.4038
27. K. Arnold et al., Release note—VBFNLO-2.6.0, (2012). arXiv:1207.4975
28. M. Bähr et al., Herwig++ physics and manual. Eur. Phys. J. C **58**, 639 (2008). https://doi.org/10.1140/epjc/s10052-008-0798-9. arXiv:0803.0883
29. M.H. Seymour, A. Siodmok, Constraining MPI models using σ_{eff} and recent Tevatron and LHC Underlying Event data. JHEP **10**, 113 (2013). https://doi.org/10.1007/JHEP10(2013)113. arXiv:1307.5015
30. P. Nason, A new method for combining NLO QCD with shower Monte Carlo algorithms. JHEP **11**, 040 (2004). https://doi.org/10.1088/1126-6708/2004/11/040. arXiv:hep-ph/0409146
31. S. Frixione, P. Nason, C. Oleari, Matching NLO QCD computations with parton shower simulations: the POWHEG method. JHEP **11**, 070 (2007). https://doi.org/10.1088/1126-6708/2007/11/070. arXiv:0709.2092
32. S. Alioli, P. Nason, C. Oleari, E. Re, A general framework for implementing NLO calculations in shower Monte Carlo programs: the POWHEG BOX. JHEP **06**, 043 (2010). https://doi.org/10.1007/JHEP06(2010)043. arXiv:1002.2581
33. C. Oleari, D. Zeppenfeld, QCD corrections to electroweak $\ell\nu_\ell$jj and $\ell^+\ell^-$jj production. Phys. Rev. D **69**, 093004 (2004). https://doi.org/10.1103/PhysRevD.69.093004. arXiv:hep-ph/0310156
34. B. Jager, S. Schneider, G. Zanderighi, Next-to-leading order QCD corrections to electroweak Zjj production in the POWHEG BOX. JHEP **09**, 083 (2012). https://doi.org/10.1007/JHEP09(2012)083. arXiv:1207.2626
35. S. Catani, Y .L. Dokshitzer, B .R. Webber, The K^- perpendicular clustering algorithm for jets in deep inelastic scattering and hadron collisions. Phys. Lett.B **285**, 291 (1992). https://doi.org/10.1016/0370-2693(92)91467-N
36. S. Catani, Y.L. Dokshitzer, M.H. Seymour, B.R. Webber, Longitudinally invariant K_t clustering algorithms for hadron hadron collisions. Nucl. Phys. B **406**, 187 (1993). https://doi.org/10.1016/0550-3213(93)90166-M
37. S.D. Ellis, D.E. Soper, Successive combination jet algorithm for hadron collisions. Phys. Rev. D **48**, 3160 (1993). https://doi.org/10.1103/PhysRevD.48.3160. arXiv:hep-ph/9305266
38. R. Frederix, S. Frixione, Merging meets matching in MC@NLO. JHEP **12**, 061 (2012). https://doi.org/10.1007/JHEP12(2012)061. arXiv:1209.6215
39. M.L. Mangano, M. Moretti, F. Piccinini, M. Treccani, Matching matrix elements and shower evolution for top-quark production in hadronic collisions. JHEP **01**, 013 (2007). https://doi.org/10.1088/1126-6708/2007/01/013. arXiv:hep-ph/0611129

40. J. Alwall et al., Comparative study of various algorithms for the merging of parton showers and matrix elements in hadronic collisions. Eur. Phys. J. C **53**, 473 (2008). https://doi.org/10.1140/epjc/s10052-007-0490-5. arXiv:0706.2569
41. K. Melnikov, F. Petriello, Electroweak gauge boson production at hadron colliders through $O(\alpha_S^2)$. Phys. Rev. D **74**, 114017 (2006). https://doi.org/10.1103/PhysRevD.74.114017. arXiv:hep-ph/0609070
42. N. Kidonakis, Differential and total cross sections for top pair and single top production. In: Proceedings of the XX International Workshop on Deep-Inelastic Scattering and Related Subjects. Bonn, Germany (2012). https://doi.org/10.3204/DESY-PROC-2012-02/251. arXiv:1205.3453
43. M. Czakon, P. Fiedler, A. Mitov, Total top quark pair production cross section at hadron colliders through $O(\alpha_S^4)$. Phys. Rev. Lett. **110**, 252004 (2013). https://doi.org/10.1103/PhysRevLett.110.252004. arXiv:1303.6254
44. S. Alioli, P. Nason, C. Oleari, E. Re, NLO single-top production matched with shower in POWHEG: s- and t-channel contributions. JHEP **09**, 111 (2009). https://doi.org/10.1088/1126-6708/2009/09/111. arXiv:0907.4076. [Erratum: https://doi.org/10.1007/JHEP02(2010)011]
45. E. Re, Single-top Wt-channel production matched with parton showers using the POWHEG method. Eur. Phys. J. C **71**, 1547 (2011). https://doi.org/10.1140/epjc/s10052-011-1547-z. arXiv:1009.2450
46. N. Kidonakis, Top quark production (2013). arXiv:1311.0283
47. J.M. Campbell, R.K. Ellis, MCFM for the Tevatron and the LHC. Nucl. Phys. B Proc. Suppl. **205–206**, 10 (2010). https://doi.org/10.1016/j.nuclphysbps.2010.08.011. arXiv:1007.3492
48. GEANT4 Collaboration, GEANT4–a simulation toolkit. Nucl. Instrum. Meth. A **506**, 250 (2003). https://doi.org/10.1016/S0168-9002(03)01368-8
49. J. Allison et al., GEANT4 developments and applications. IEEE Trans. Nucl. Sci. **53**, 270 (2006). https://doi.org/10.1109/TNS.2006.869826
50. CMS Collaboration, Particle-flow reconstruction and global event description with the CMS detector. JINST **12**, P10003 (2017). https://doi.org/10.1088/1748-0221/12/10/P10003. arXiv:1706.04965
51. M. Cacciari, G.P. Salam, G. Soyez, The anti-k_T jet clustering algorithm. JHEP **04**, 063 (2008). https://doi.org/10.1088/1126-6708/2008/04/063. arXiv:0802.1189
52. M. Cacciari, G.P. Salam, G. Soyez, FastJet user manual. Eur. Phys. J. C **72**, 1896 (2012). https://doi.org/10.1140/epjc/s10052-012-1896-2. arXiv:1111.6097
53. CMS Collaboration, Performance of CMS muon reconstruction in pp collision events at $\sqrt{s} = 7$ TeV. JINST **7**, P10002 (2012). https://doi.org/10.1088/1748-0221/7/10/P10002. arXiv:1206.4071
54. M. Cacciari, G.P. Salam, Pileup subtraction using jet areas. Phys. Lett. B **659**, 119 (2008). https://doi.org/10.1016/j.physletb.2007.09.077. arXiv:0707.1378
55. CMS Collaboration, Performance of missing energy reconstruction in 13 TeV pp collision data using the CMS detector. CMS Physics Analysis Summary CMS-PAS-JME-16-004 (2016)
56. M. Cacciari, G.P. Salam, Dispelling the N^3 myth for the k_T jet-finder. Phys. Lett. B **641**, 57 (2006). https://doi.org/10.1016/j.physletb.2006.08.037. arXiv:hep-ph/0512210
57. CMS Collaboration, Determination of jet energy calibration and transverse momentum resolution in CMS. JINST **6**, P11002 (2011). https://doi.org/10.1088/1748-0221/6/11/P11002. arXiv:1107.4277
58. CMS Collaboration, Jet algorithms performance in 13 TeV data. CMS Physics Analysis Summary CMS-PAS-JME-16-003 (2017)
59. CMS Collaboration, Pileup jet identification. CMS Physics Analysis Summary CMS-PAS-JME-13-005 (2013)
60. CMS Collaboration, Performance of quark/gluon discrimination using pp collision data at $\sqrt{s} = 8$ TeV. CMS Physics Analysis Summary CMS-PAS-JME-13-002 (2013)
61. CMS Collaboration, Identification of heavy-flavour jets with the CMS detector in pp collisions at 13 TeV. JINST **13**, P05011 (2018). https://doi.org/10.1088/1748-0221/13/05/P05011. arXiv:1712.07158
62. H. Voss, A. Höcker, J. Stelzer, and F. Tegenfeldt, TMVA, the toolkit for multivariate data analysis with ROOT. In: XIth International Workshop on Advanced Computing and Analysis Techniques in Physics Research (ACAT), p. 40 (2007). arXiv:physics/0703039
63. The ATLAS Collaboration, The CMS Collaboration, The LHC Higgs Combination Group, Procedure for the LHC Higgs boson search combination in Summer 2011. Technical Report CMS-NOTE-2011-005. ATL-PHYS-PUB-2011-11 (2011)
64. G. Cowan, K. Cranmer, E. Gross, O. Vitells, Asymptotic formulae for likelihood-based tests of new physics. Eur. Phys. J. C **71**, 1554 (2011). https://doi.org/10.1140/epjc/s10052-011-1554-0. arXiv:1007.1727. [Erratum: https://doi.org/10.1140/epjc/s10052-013-2501-z]
65. CMS Collaboration, CMS luminosity measurements for the 2016 data taking period. CMS Physics Analysis Summary CMS-PAS-LUM-17-001 (2017)
66. CMS Collaboration, Measurements of inclusive W and Z cross sections in pp collisions at $\sqrt{s} = 7$ TeV. JHEP **01**, 080 (2011). https://doi.org/10.1007/JHEP01(2011)080. arXiv:1012.2466
67. CMS Collaboration, Measurement of the inelastic proton-proton cross section at $\sqrt{s} = 13$ TeV. JHEP **07**, 161 (2018). https://doi.org/10.1007/JHEP07(2018)161. arXiv:1802.02613
68. R.J. Barlow, C. Beeston, Fitting using finite Monte Carlo samples. Comput. Phys. Commun. **77**, 219 (1993). https://doi.org/10.1016/0010-4655(93)90005-W
69. C. Degrande et al., Studies of vector boson scattering and triboson production with DELPHES parametrized fast simulation for Snowmass 2013 (2013). arXiv:1309.7452
70. Particle Data Group, K. Nakamura et al., Review of particle physics. J. Phys. G **37**, 075021 (2010). https://doi.org/10.1088/0954-3899/37/7A/075021
71. The LEP Electroweak Working Group, Electroweak measurements in electron-positron collisions at W-boson-pair energies at LEP. Phys. Rep. **532**, 119 (2013). https://doi.org/10.1016/j.physrep.2013.07.004. arXiv:1302.3415
72. CDF Collaboration, Measurement of the WZ Cross Section and Triple Gauge Couplings in $p\bar{p}$ Collisions at $\sqrt{s} = 1.96$ TeV. Phys. Rev. D **86**, 031104 (2012). https://doi.org/10.1103/PhysRevD.86.031104. arXiv:1202.6629
73. D0 Collaboration, Limits on anomalous trilinear gauge boson couplings from WW, WZ and $W\gamma$ production in $p\bar{p}$ collisions at $\sqrt{s} = 1.96$ TeV. Phys. Lett. B **718**, 451 (2012). https://doi.org/10.1016/j.physletb.2012.10.062. arXiv:1208.5458
74. ATLAS Collaboration, Measurement of WW/WZ $\to \ell\nu$qq$'$ production with the hadronically decaying boson reconstructed as one or two jets in pp collisions at $\sqrt{s} = 8$ TeV with ATLAS, and constraints on anomalous gauge couplings. Eur. Phys. J. C **77**, 563 (2017). https://doi.org/10.1140/epjc/s10052-017-5084-2. arXiv:1706.01702
75. ATLAS Collaboration, Measurements of $W^{\pm}Z$ production cross sections in pp collisions at $\sqrt{s} = 8$ TeV with the ATLAS detector and limits on anomalous gauge boson self-couplings. Phys. Rev. D **93**, 092004 (2016). https://doi.org/10.1103/PhysRevD.93.092004. arXiv:1603.02151
76. CMS Collaboration, Search for anomalous couplings in boosted WW/WZ$\to \ell\nu q\bar{q}$ production in proton-proton collisions at $\sqrt{s} =$ 8 TeV. Phys. Lett. B **772**, 21 (2017). https://doi.org/10.1016/j.physletb.2017.06.009. arXiv:1703.06095

77. CMS Collaboration, Measurement of the WZ production cross section in pp collisions at $\sqrt{s} = 7$ and 8 TeV and search for anomalous triple gauge couplings at $\sqrt{s} = 8$ TeV. Eur. Phys. J. C **77**, 236 (2017). https://doi.org/10.1140/epjc/s10052-017-4730-z. arXiv:1609.05721
78. CMS Collaboration, Precise determination of the mass of the Higgs boson and tests of compatibility of its couplings with the standard model predictions using proton collisions at 7 and 8 TeV. Eur. Phys. J. C **75**, 212 (2015). https://doi.org/10.1140/epjc/s10052-015-3351-7. arXiv:1412.8662
79. K. Hagiwara, R.D. Peccei, D. Zeppenfeld, Probing the weak boson sector in $e^+e^- \to W^+W^-$. Nucl. Phys. B **282**, 253 (1987). https://doi.org/10.1016/0550-3213(87)90685-7
80. CMS Collaboration, Tracking and primary vertex results in first 7 TeV collisions. CMS Physics Analysis Summary CMS-PAS-TRK-10-005 (2010)
81. CMS Collaboration, Commissioning of TrackJets in pp collisions at $\sqrt{s} = 7$ TeV. CMS Physics Analysis Summary CMS-PAS-JME-10-006, (2010)
82. CMS Collaboration, Performance of jet reconstruction with charged tracks only. CMS Physics Analysis Summary CMS-PAS-JME-08-001 (2009)

CMS Collaboration

Yerevan Physics Institute, Yerevan, Armenia
A. M. Sirunyan, A. Tumasyan

Institut für Hochenergiephysik, Wien, Austria
W. Adam, F. Ambrogi, E. Asilar, T. Bergauer, J. Brandstetter, M. Dragicevic, J. Erö, A. Escalante Del Valle, M. Flechl, R. Frühwirth[1], V. M. Ghete, J. Hrubec, M. Jeitler[1], N. Krammer, I. Krätschmer, D. Liko, T. Madlener, I. Mikulec, N. Rad, H. Rohringer, J. Schieck[1], R. Schöfbeck, M. Spanring, D. Spitzbart, W. Waltenberger, J. Wittmann, C.-E. Wulz[1], M. Zarucki

Institute for Nuclear Problems, Minsk, Belarus
V. Chekhovsky, V. Mossolov, J. Suarez Gonzalez

Universiteit Antwerpen, Antwerp, Belgium
E. A. De Wolf, D. Di Croce, X. Janssen, J. Lauwers, A. Lelek, M. Pieters, H. Van Haevermaet, P. Van Mechelen, N. Van Remortel

Vrije Universiteit Brussel, Brussels, Belgium
F. Blekman, J. D'Hondt, J. De Clercq, K. Deroover, G. Flouris, D. Lontkovskyi, S. Lowette, I. Marchesini, S. Moortgat, L. Moreels, Q. Python, K. Skovpen, S. Tavernier, W. Van Doninck, P. Van Mulders, I. Van Parijs

Université Libre de Bruxelles, Bruxelles, Belgium
D. Beghin, B. Bilin, H. Brun, B. Clerbaux, G. De Lentdecker, H. Delannoy, B. Dorney, L. Favart, A. Grebenyuk, A. K. Kalsi, J. Luetic, A. Popov[2], N. Postiau, E. Starling, L. Thomas, C. Vander Velde, P. Vanlaer, D. Vannerom, Q. Wang

Ghent University, Ghent, Belgium
T. Cornelis, D. Dobur, A. Fagot, M. Gul, I. Khvastunov[3], C. Roskas, D. Trocino, M. Tytgat, W. Verbeke, B. Vermassen, M. Vit, N. Zaganidis

Université Catholique de Louvain, Louvain-la-Neuve, Belgium
O. Bondu, G. Bruno, C. Caputo, P. David, C. Delaere, M. Delcourt, A. Giammanco, G. Krintiras, V. Lemaitre, A. Magitteri, K. Piotrzkowski, A. Saggio, M. Vidal Marono, P. Vischia, J. Zobec

Centro Brasileiro de Pesquisas Fisicas, Rio de Janeiro, Brazil
F. L. Alves, G. A. Alves, G. Correia Silva, C. Hensel, A. Moraes, M. E. Pol, P. Rebello Teles

Universidade do Estado do Rio de Janeiro, Rio de Janeiro, Brazil
E. Belchior Batista Das Chagas, W. Carvalho, J. Chinellato[4], E. Coelho, E. M. Da Costa, G. G. Da Silveira[5], D. De Jesus Damiao, C. De Oliveira Martins, S. Fonseca De Souza, L. M. Huertas Guativa, H. Malbouisson, D. Matos Figueiredo, M. Melo De Almeida, C. Mora Herrera, L. Mundim, H. Nogima, W. L. Prado Da Silva, L. J. Sanchez Rosas, A. Santoro, A. Sznajder, M. Thiel, E. J. Tonelli Manganote[4], F. Torres Da Silva De Araujo, A. Vilela Pereira

Universidade Estadual Paulista[a], Universidade Federal do ABC[b], São Paulo, Brazil
S. Ahuja[a], C. A. Bernardes[a], L. Calligaris[a], T. R. Fernandez Perez Tomei[a], E. M. Gregores[b], P. G. Mercadante[b], S. F. Novaes[a], SandraS. Padula[a]

Institute for Nuclear Research and Nuclear Energy, Bulgarian Academy of Sciences, Sofia, Bulgaria
A. Aleksandrov, R. Hadjiiska, P. Iaydjiev, A. Marinov, M. Misheva, M. Rodozov, M. Shopova, G. Sultanov

University of Sofia, Sofia, Bulgaria
A. Dimitrov, L. Litov, B. Pavlov, P. Petkov

Beihang University, Beijing, China
W. Fang[6], X. Gao[6], L. Yuan

Institute of High Energy Physics, Beijing, China
M. Ahmad, J. G. Bian, G. M. Chen, H. S. Chen, M. Chen, Y. Chen, C. H. Jiang, D. Leggat, H. Liao, Z. Liu, S. M. Shaheen[7], A. Spiezia, J. Tao, E. Yazgan, H. Zhang, S. Zhang[7], J. Zhao

State Key Laboratory of Nuclear Physics and Technology, Peking University, Beijing, China
Y. Ban, G. Chen, A. Levin, J. Li, L. Li, Q. Li, Y. Mao, S. J. Qian, D. Wang

Tsinghua University, Beijing, China
Y. Wang

Universidad de Los Andes, Bogota, Colombia
C. Avila, A. Cabrera, C. A. Carrillo Montoya, L. F. Chaparro Sierra, C. Florez, C. F. González Hernández, M. A. Segura Delgado

Universidad de Antioquia, Medellin, Colombia
J. D. Ruiz Alvarez

University of Split, Faculty of Electrical Engineering, Mechanical Engineering and Naval Architecture, Split, Croatia
N. Godinovic, D. Lelas, I. Puljak, T. Sculac

University of Split, Faculty of Science, Split, Croatia
Z. Antunovic, M. Kovac

Institute Rudjer Boskovic, Zagreb, Croatia
V. Brigljevic, D. Ferencek, K. Kadija, B. Mesic, M. Roguljic, A. Starodumov[8], T. Susa

University of Cyprus, Nicosia, Cyprus
M. W. Ather, A. Attikis, M. Kolosova, S. Konstantinou, G. Mavromanolakis, J. Mousa, C. Nicolaou, F. Ptochos, P. A. Razis, H. Rykaczewski

Charles University, Prague, Czech Republic
M. Finger[9], M. Finger Jr.[9]

Escuela Politecnica Nacional, Quito, Ecuador
E. Ayala

Universidad San Francisco de Quito, Quito, Ecuador
E. Carrera Jarrin

Academy of Scientific Research and Technology of the Arab Republic of Egypt, Egyptian Network of High Energy Physics, Cairo, Egypt
A. A. Abdelalim[10,11], A. Ellithi Kamel[12], E. Salama[13,14]

National Institute of Chemical Physics and Biophysics, Tallinn, Estonia
S. Bhowmik, A. Carvalho Antunes De Oliveira, R. K. Dewanjee, K. Ehataht, M. Kadastik, M. Raidal, C. Veelken

Department of Physics, University of Helsinki, Helsinki, Finland
P. Eerola, H. Kirschenmann, J. Pekkanen, M. Voutilainen

Helsinki Institute of Physics, Helsinki, Finland
J. Havukainen, J. K. Heikkilä, T. Järvinen, V. Karimäki, R. Kinnunen, T. Lampén, K. Lassila-Perini, S. Laurila, S. Lehti, T. Lindén, P. Luukka, T. Mäenpää, H. Siikonen, E. Tuominen, J. Tuominiemi

Lappeenranta University of Technology, Lappeenranta, Finland
T. Tuuva

IRFU, CEA, Université Paris-Saclay, Gif-sur-Yvette, France
M. Besancon, F. Couderc, M. Dejardin, D. Denegri, J. L. Faure, F. Ferri, S. Ganjour, A. Givernaud, P. Gras, G. Hamel de Monchenault, P. Jarry, C. Leloup, E. Locci, J. Malcles, J. Rander, A. Rosowsky, M. Ö. Sahin, A. Savoy-Navarro[15], M. Titov

Laboratoire Leprince-Ringuet, CNRS/IN2P3, Ecole Polytechnique, Institut Polytechnique de Paris, Palaiseau, France
C. Amendola, F. Beaudette, P. Busson, C. Charlot, B. Diab, R. Granier de Cassagnac, I. Kucher, A. Lobanov, J. Martin Blanco, C. Martin Perez, M. Nguyen, C. Ochando, G. Ortona, P. Paganini, J. Rembser, R. Salerno, J. B. Sauvan, Y. Sirois, A. Zabi, A. Zghiche

Université de Strasbourg, CNRS, IPHC UMR 7178, Strasbourg, France
J.-L. Agram[16], J. Andrea, D. Bloch, G. Bourgatte, J.-M. Brom, E. C. Chabert, C. Collard, E. Conte[16], J.-C. Fontaine[16], D. Gelé, U. Goerlach, M. Jansová, A.-C. Le Bihan, N. Tonon, P. Van Hove

Centre de Calcul de l'Institut National de Physique Nucleaire et de Physique des Particules, CNRS/IN2P3, Villeurbanne, France
S. Gadrat

Université de Lyon, Université Claude Bernard Lyon 1, CNRS-IN2P3, Institut de Physique Nucléaire de Lyon, Villeurbanne, France
S. Beauceron, C. Bernet, G. Boudoul, N. Chanon, R. Chierici, D. Contardo, P. Depasse, H. El Mamouni, J. Fay, S. Gascon, M. Gouzevitch, G. Grenier, B. Ille, F. Lagarde, I. B. Laktineh, H. Lattaud, M. Lethuillier, L. Mirabito, S. Perries, V. Sordini, G. Touquet, M. Vander Donckt, S. Viret

Georgian Technical University, Tbilisi, Georgia
T. Toriashvili[17]

Tbilisi State University, Tbilisi, Georgia
I. Bagaturia[18]

RWTH Aachen University, I. Physikalisches Institut, Aachen, Germany
C. Autermann, L. Feld, M. K. Kiesel, K. Klein, M. Lipinski, D. Meuser, A. Pauls, M. Preuten, M. P. Rauch, C. Schomakers, J. Schulz, M. Teroerde, B. Wittmer

RWTH Aachen University, III. Physikalisches Institut A, Aachen, Germany
A. Albert, M. Erdmann, S. Erdweg, T. Esch, R. Fischer, S. Ghosh, T. Hebbeker, C. Heidemann, K. Hoepfner, H. Keller, L. Mastrolorenzo, M. Merschmeyer, A. Meyer, P. Millet, S. Mukherjee, A. Novak, T. Pook, A. Pozdnyakov, M. Radziej, H. Reithler, M. Rieger, A. Schmidt, A. Sharma, D. Teyssier, S. Thüer

RWTH Aachen University, III. Physikalisches Institut B, Aachen, Germany
G. Flügge, O. Hlushchenko, T. Kress, T. Müller, A. Nehrkorn, A. Nowack, C. Pistone, O. Pooth, D. Roy, H. Sert, A. Stahl[19]

Deutsches Elektronen-Synchrotron, Hamburg, Germany
M. Aldaya Martin, T. Arndt, C. Asawatangtrakuldee, I. Babounikau, H. Bakhshiansohi, K. Beernaert, O. Behnke, U. Behrens, A. Bermúdez Martínez, D. Bertsche, A. A. Bin Anuar, K. Borras[20], V. Botta, A. Campbell, P. Connor, C. Contreras-Campana, V. Danilov, A. De Wit, M. M. Defranchis, C. Diez Pardos, D. Domínguez Damiani, G. Eckerlin, T. Eichhorn, A. Elwood, E. Eren, E. Gallo[21], A. Geiser, J. M. Grados Luyando, A. Grohsjean, M. Guthoff, M. Haranko, A. Harb, N. Z. Jomhari, H. Jung, M. Kasemann, J. Keaveney, C. Kleinwort, J. Knolle, D. Krücker, W. Lange, T. Lenz, J. Leonard, K. Lipka, W. Lohmann[22], R. Mankel, I.-A. Melzer-Pellmann, A. B. Meyer, M. Meyer, M. Missiroli, G. Mittag, J. Mnich, V. Myronenko, S. K. Pflitsch, D. Pitzl, A. Raspereza, A. Saibel, M. Savitskyi, P. Saxena, V. Scheurer, P. Schütze,

C. Schwanenberger, R. Shevchenko, A. Singh, H. Tholen, O. Turkot, A. Vagnerini, M. Van De Klundert, G. P. Van Onsem, R. Walsh, Y. Wen, K. Wichmann, C. Wissing, O. Zenaiev

University of Hamburg, Hamburg, Germany
R. Aggleton, S. Bein, L. Benato, A. Benecke, V. Blobel, T. Dreyer, A. Ebrahimi, E. Garutti, D. Gonzalez, P. Gunnellini, J. Haller, A. Hinzmann, A. Karavdina, G. Kasieczka, R. Klanner, R. Kogler, N. Kovalchuk, S. Kurz, V. Kutzner, J. Lange, D. Marconi, J. Multhaup, M. Niedziela, C. E. N. Niemeyer, D. Nowatschin, A. Perieanu, A. Reimers, O. Rieger, C. Scharf, P. Schleper, S. Schumann, J. Schwandt, J. Sonneveld, H. Stadie, G. Steinbrück, F. M. Stober, M. Stöver, B. Vormwald, I. Zoi

Karlsruher Institut fuer Technologie, Karlsruhe, Germany
M. Akbiyik, C. Barth, M. Baselga, S. Baur, T. Berger, E. Butz, R. Caspart, T. Chwalek, W. De Boer, A. Dierlamm, K. El Morabit, N. Faltermann, M. Giffels, M. A. Harrendorf, F. Hartmann[19], U. Husemann, I. Katkov[2], S. Kudella, S. Mitra, M. U. Mozer, Th. Müller, M. Musich, G. Quast, K. Rabbertz, M. Schröder, I. Shvetsov, H. J. Simonis, R. Ulrich, M. Weber, C. Wöhrmann, R. Wolf

Institute of Nuclear and Particle Physics (INPP), NCSR Demokritos, Aghia Paraskevi, Greece
G. Anagnostou, G. Daskalakis, T. Geralis, A. Kyriakis, D. Loukas, G. Paspalaki

National and Kapodistrian University of Athens, Athens, Greece
A. Agapitos, G. Karathanasis, P. Kontaxakis, A. Panagiotou, I. Papavergou, N. Saoulidou, K. Vellidis

National Technical University of Athens, Athens, Greece
G. Bakas, K. Kousouris, I. Papakrivopoulos, G. Tsipolitis

University of Ioánnina, Ioánnina, Greece
I. Evangelou, C. Foudas, P. Gianneios, P. Katsoulis, P. Kokkas, S. Mallios, K. Manitara, N. Manthos, I. Papadopoulos, E. Paradas, J. Strologas, F. A. Triantis, D. Tsitsonis

MTA-ELTE Lendület CMS Particle and Nuclear Physics Group, Eötvös Loránd University, Budapest, Hungary
M. Bartók[23], M. Csanad, N. Filipovic, P. Major, K. Mandal, A. Mehta, M. I. Nagy, G. Pasztor, O. Surányi, G. I. Veres

Wigner Research Centre for Physics, Budapest, Hungary
G. Bencze, C. Hajdu, D. Horvath[24], Hunyadi, F. Sikler, T. Vámi, V. Veszpremi, G. Vesztergombi[†]

Institute of Nuclear Research ATOMKI, Debrecen, Hungary
N. Beni, S. Czellar, J. Karancsi[23], A. Makovec, J. Molnar, Z. Szillasi

Institute of Physics, University of Debrecen, Debrecen, Hungary
P. Raics, Z. L. Trocsanyi, B. Ujvari

Indian Institute of Science (IISc), Bangalore, India
S. Choudhury, J. R. Komaragiri, P. C. Tiwari

National Institute of Science Education and Research, HBNI, Bhubaneswar, India
S. Bahinipati[26], C. Kar, P. Mal, A. Nayak[27], S. Roy Chowdhury, D. K. Sahoo[26], S. K. Swain

Panjab University, Chandigarh, India
S. Bansal, S. B. Beri, V. Bhatnagar, S. Chauhan, R. Chawla, N. Dhingra, R. Gupta, A. Kaur, M. Kaur, S. Kaur, P. Kumari, M. Lohan, M. Meena, K. Sandeep, S. Sharma, J. B. Singh, A. K. Virdi, G. Walia

University of Delhi, Delhi, India
A. Bhardwaj, B. C. Choudhary, R. B. Garg, M. Gola, S. Keshri, Ashok Kumar, S. Malhotra, M. Naimuddin, P. Priyanka, K. Ranjan, Aashaq Shah, R. Sharma

Saha Institute of Nuclear Physics, HBNI, Kolkata, India
R. Bhardwaj[28], M. Bharti[28], R. Bhattacharya, S. Bhattacharya, U. Bhawandeep[28], D. Bhowmik, S. Dey, S. Dutt[28], S. Dutta, S. Ghosh, M. Maity[29], K. Mondal, S. Nandan, A. Purohit, P. K. Rout, A. Roy, G. Saha, S. Sarkar, T. Sarkar[29], M. Sharan, B. Singh[28], S. Thakur[28]

Indian Institute of Technology Madras, Madras, India
P. K. Behera, A. Muhammad

Bhabha Atomic Research Centre, Mumbai, India
R. Chudasama, D. Dutta, V. Jha, V. Kumar, D. K. Mishra, P. K. Netrakanti, L. M. Pant, P. Shukla, P. Suggisetti

Tata Institute of Fundamental Research-A, Mumbai, India
T. Aziz, M. A. Bhat, S. Dugad, G. B. Mohanty, N. Sur, RavindraKumar Verma

Tata Institute of Fundamental Research-B, Mumbai, India
S. Banerjee, S. Bhattacharya, S. Chatterjee, P. Das, M. Guchait, Sa. Jain, S. Karmakar, S. Kumar, G. Majumder, K. Mazumdar, N. Sahoo, S. Sawant

Indian Institute of Science Education and Research (IISER), Pune, India
S. Chauhan, S. Dube, V. Hegde, A. Kapoor, K. Kothekar, S. Pandey, A. Rane, A. Rastogi, S. Sharma

Institute for Research in Fundamental Sciences (IPM), Tehran, Iran
S. Chenarani[30], E. Eskandari Tadavani, S. M. Etesami[30], M. Khakzad, M. Mohammadi Najafabadi, M. Naseri, F. Rezaei Hosseinabadi, B. Safarzadeh[31], M. Zeinali

University College Dublin, Dublin, Ireland
M. Felcini, M. Grunewald

INFN Sezione di Bari[a], Università di Bari[b], Politecnico di Bari[c], Bari, Italy
M. Abbrescia[a,b], C. Calabria[a,b], A. Colaleo[a], D. Creanza[a,c], L. Cristella[a,b], N. De Filippis[a,c], M. De Palma[a,b], A. Di Florio[a,b], F. Errico[a,b], L. Fiore[a], A. Gelmi[a,b], G. Iaselli[a,c], M. Ince[a,b], S. Lezki[a,b], G. Maggi[a,c], M. Maggi[a], G. Miniello[a,b], S. My[a,b], S. Nuzzo[a,b], A. Pompili[a,b], G. Pugliese[a,c], R. Radogna[a], A. Ranieri[a], G. Selvaggi[a,b], L. Silvestris[a], R. Venditti[a], P. Verwilligen[a]

INFN Sezione di Bologna[a], Università di Bologna[b], Bologna, Italy
G. Abbiendi[a], C. Battilana[a,b], D. Bonacorsi[a,b], L. Borgonovi[a,b], S. Braibant-Giacomelli[a,b], R. Campanini[a,b], P. Capiluppi[a,b], A. Castro[a,b], F. R. Cavallo[a], S. S. Chhibra[a,b], G. Codispoti[a,b], M. Cuffiani[a,b], G. M. Dallavalle[a], F. Fabbri[a], A. Fanfani[a,b], E. Fontanesi, P. Giacomelli[a], C. Grandi[a], L. Guiducci[a,b], F. Iemmi[a,b], S. Lo Meo[a,32], S. Marcellini[a], G. Masetti[a], A. Montanari[a], F. L. Navarria[a,b], A. Perrotta[a], F. Primavera[a,b], A. M. Rossi[a,b], T. Rovelli[a,b], G. P. Siroli[a,b], N. Tosi[a]

INFN Sezione di Catania[a], Università di Catania[b], Catania, Italy
S. Albergo[a,b,33], A. Di Mattia[a], R. Potenza[a,b], A. Tricomi[a,b,33], C. Tuve[a,b]

INFN Sezione di Firenze[a], Università di Firenze[b], Firenze, Italy
G. Barbagli[a], K. Chatterjee[a,b], V. Ciulli[a,b], C. Civinini[a], R. D'Alessandro[a,b], E. Focardi[a,b], G. Latino, P. Lenzi[a,b], M. Meschini[a], S. Paoletti[a], L. Russo[a,34], G. Sguazzoni[a], D. Strom[a], L. Viliani[a]

INFN Laboratori Nazionali di Frascati, Frascati, Italy
L. Benussi, S. Bianco, F. Fabbri, D. Piccolo

INFN Sezione di Genova[a], Università di Genova[b], Genova, Italy
F. Ferro[a], R. Mulargia[a,b], E. Robutti[a], S. Tosi[a,b]

INFN Sezione di Milano-Bicocca[a], Università di Milano-Bicocca[b], Milan, Italy
A. Benaglia[a], A. Beschi[b], F. Brivio[a,b], V. Ciriolo[a,b,19], S. Di Guida[a,b,19], M. E. Dinardo[a,b], S. Fiorendi[a,b], S. Gennai[a], A. Ghezzi[a,b], P. Govoni[a,b], M. Malberti[a,b], S. Malvezzi[a], D. Menasce[a], F. Monti, L. Moroni[a], M. Paganoni[a,b], D. Pedrini[a], S. Ragazzi[a,b], T. Tabarelli de Fatis[a,b], D. Zuolo[a,b]

INFN Sezione di Napoli[a], Università di Napoli 'Federico II' [b], Naples, Italy, Università della Basilicata[c], Potenza, Italy, Università G. Marconi[d], Rome, Italy
S. Buontempo[a], N. Cavallo[a,c], A. De Iorio[a,b], A. Di Crescenzo[a,b], F. Fabozzi[a,c], F. Fienga[a], G. Galati[a], A. O. M. Iorio[a,b], L. Lista[a,b], S. Meola[a,d,19], P. Paolucci[a,19], C. Sciacca[a,b], E. Voevodina[a,b]

INFN Sezione di Padova[a], Università di Padova[b], Padova, Italy, Università di Trento[c], Trento, Italy
P. Azzi[a], N. Bacchetta[a], D. Bisello[a,b], A. Boletti[a,b], A. Bragagnolo, R. Carlin[a,b], P. Checchia[a], M. Dall'Osso[a,b], P. De Castro Manzano[a], T. Dorigo[a], U. Dosselli[a], F. Gasparini[a,b], U. Gasparini[a,b], A. Gozzelino[a], S. Y. Hoh, S. Lacaprara[a], P. Lujan, M. Margoni[a,b], A. T. Meneguzzo[a,b], J. Pazzini[a,b], M. Presilla[b], P. Ronchese[a,b], R. Rossin[a,b], F. Simonetto[a,b], A. Tiko, E. Torassa[a], M. Tosi[a,b], M. Zanetti[a,b], P. Zotto[a,b], G. Zumerle[a,b]

INFN Sezione di Pavia[a], Università di Pavia[b], Pavia, Italy
A. Braghieri[a], A. Magnani[a], P. Montagna[a,b], S. P. Ratti[a,b], V. Re[a], M. Ressegotti[a,b], C. Riccardi[a,b], P. Salvini[a], I. Vai[a,b], P. Vitulo[a,b]

INFN Sezione di Perugia[a], Università di Perugia[b], Perugia, Italy
M. Biasini[a,b], G. M. Bilei[a], C. Cecchi[a,b], D. Ciangottini[a,b], L. Fanò[a,b], P. Lariccia[a,b], R. Leonardi[a,b], E. Manoni[a], G. Mantovani[a,b], V. Mariani[a,b], M. Menichelli[a], A. Rossi[a,b], A. Santocchia[a,b], D. Spiga[a]

INFN Sezione di Pisa[a], Università di Pisa[b], Scuola Normale Superiore di Pisa[c], Pisa, Italy
K. Androsov[a], P. Azzurri[a], G. Bagliesi[a], L. Bianchini[a], T. Boccali[a], L. Borrello, R. Castaldi[a], M. A. Ciocci[a,b], R. Dell'Orso[a], G. Fedi[a], F. Fiori[a,c], L. Giannini[a,c], A. Giassi[a], M. T. Grippo[a], F. Ligabue[a,c], E. Manca[a,c], G. Mandorli[a,c], A. Messineo[a,b], F. Palla[a], A. Rizzi[a,b], G. Rolandi[35], A. Scribano[a], P. Spagnolo[a], R. Tenchini[a], G. Tonelli[a,b], A. Venturi[a], P. G. Verdini[a]

INFN Sezione di Roma[a], Sapienza Università di Roma[b], Rome, Italy
L. Barone[a,b], F. Cavallari[a], M. Cipriani[a,b], D. Del Re[a,b], E. Di Marco[a,b], M. Diemoz[a], S. Gelli[a,b], E. Longo[a,b], B. Marzocchi[a,b], P. Meridiani[a], G. Organtini[a,b], F. Pandolfi[a], R. Paramatti[a,b], F. Preiato[a,b], C. Quaranta[a,b], S. Rahatlou[a,b], C. Rovelli[a], F. Santanastasio[a,b]

INFN Sezione di Torino[a], Università di Torino[b], Torino, Italy, Università del Piemonte Orientale[c], Novara, Italy
N. Amapane[a,b], R. Arcidiacono[a,c], S. Argiro[a,b], M. Arneodo[a,c], N. Bartosik[a], R. Bellan[a,b], C. Biino[a], A. Cappati[a,b], N. Cartiglia[a], F. Cenna[a,b], S. Cometti[a], M. Costa[a,b], R. Covarelli[a,b], N. Demaria[a], B. Kiani[a,b], C. Mariotti[a], S. Maselli[a], E. Migliore[a,b], V. Monaco[a,b], E. Monteil[a,b], M. Monteno[a], M. M. Obertino[a,b], L. Pacher[a,b], N. Pastrone[a], M. Pelliccioni[a], G. L. Pinna Angioni[a,b], A. Romero[a,b], M. Ruspa[a,c], R. Sacchi[a,b], R. Salvatico[a,b], K. Shchelina[a,b], V. Sola[a], A. Solano[a,b], D. Soldi[a,b], A. Staiano[a]

INFN Sezione di Trieste[a], Università di Trieste[b], Trieste, Italy
S. Belforte[a], V. Candelise[a,b], M. Casarsa[a], F. Cossutti[a], A. Da Rold[a,b], G. Della Ricca[a,b], F. Vazzoler[a,b], A. Zanetti[a]

Kyungpook National University, Taegu, Korea
D. H. Kim, G. N. Kim, M. S. Kim, J. Lee, S. W. Lee, C. S. Moon, Y. D. Oh, S. I. Pak, S. Sekmen, D. C. Son, Y. C. Yang

Chonnam National University, Institute for Universe and Elementary Particles, Kwangju, Korea
H. Kim, D. H. Moon, G. Oh

Hanyang University, Seoul, Korea
B. Francois, J. Goh[36], T. J. Kim

Korea University, Seoul, Korea
S. Cho, S. Choi, Y. Go, D. Gyun, S. Ha, B. Hong, Y. Jo, K. Lee, K. S. Lee, S. Lee, J. Lim, S. K. Park, Y. Roh

Sejong University, Seoul, Korea
H. S. Kim

Seoul National University, Seoul, Korea
J. Almond, J. Kim, J. S. Kim, H. Lee, K. Lee, S. Lee, K. Nam, S. B. Oh, B. C. Radburn-Smith, S. h. Seo, U. K. Yang, H. D. Yoo, G. B. Yu

University of Seoul, Seoul, Korea
D. Jeon, H. Kim, J. H. Kim, J. S. H. Lee, I. C. Park

Sungkyunkwan University, Suwon, Korea
Y. Choi, C. Hwang, J. Lee, I. Yu

Riga Technical University, Riga, Latvia
V. Veckalns[37]

Vilnius University, Vilnius, Lithuania
V. Dudenas, A. Juodagalvis, J. Vaitkus

National Centre for Particle Physics, Universiti Malaya, Kuala Lumpur, Malaysia
Z. A. Ibrahim, M. A. B. Md Ali[38], F. Mohamad Idris[39], W. A. T. Wan Abdullah, M. N. Yusli, Z. Zolkapli

Universidad de Sonora (UNISON), Hermosillo, Mexico
J. F. Benitez, A. Castaneda Hernandez, J. A. Murillo Quijada

Centro de Investigacion y de Estudios Avanzados del IPN, Mexico, Mexico
H. Castilla-Valdez, E. De La Cruz-Burelo, M. C. Duran-Osuna, I. Heredia-De La Cruz[40], R. Lopez-Fernandez, R. I. Rabadan-Trejo, G. Ramirez-Sanchez, R. Reyes-Almanza, A. Sanchez-Hernandez

Universidad Iberoamericana, Mexico, Mexico
S. Carrillo Moreno, C. Oropeza Barrera, M. Ramirez-Garcia, F. Vazquez Valencia

Benemerita Universidad Autonoma de Puebla, Puebla, Mexico
J. Eysermans, I. Pedraza, H. A. Salazar Ibarguen, C. Uribe Estrada

Universidad Autónoma de San Luis Potosí, San Luis Potosí, Mexico
A. Morelos Pineda

University of Montenegro, Podgorica, Montenegro
N. Raicevic

University of Auckland, Auckland, New Zealand
D. Krofcheck

University of Canterbury, Christchurch, New Zealand
S. Bheesette, P. H. Butler

National Centre for Physics, Quaid-I-Azam University, Islamabad, Pakistan
A. Ahmad, M. Ahmad, M. I. Asghar, Q. Hassan, H. R. Hoorani, W. A. Khan, M. A. Shah, M. Shoaib, M. Waqas

National Centre for Nuclear Research, Swierk, Poland
H. Bialkowska, M. Bluj, B. Boimska, T. Frueboes, M. Górski, M. Kazana, M. Szleper, P. Traczyk, P. Zalewski

Institute of Experimental Physics, Faculty of Physics, University of Warsaw, Warsaw, Poland
K. Bunkowski, A. Byszuk[41], K. Doroba, A. Kalinowski, M. Konecki, J. Krolikowski, M. Misiura, M. Olszewski, A. Pyskir, M. Walczak

Laboratório de Instrumentação e Física Experimental de Partículas, Lisbon, Portugal
M. Araujo, P. Bargassa, D. Bastos, C. Beirão Da Cruz E Silva, A. Di Francesco, P. Faccioli, B. Galinhas, M. Gallinaro, J. Hollar, N. Leonardo, J. Seixas, G. Strong, O. Toldaiev, J. Varela

Joint Institute for Nuclear Research, Dubna, Russia
S. Afanasiev, P. Bunin, M. Gavrilenko, I. Golutvin, I. Gorbunov, A. Kamenev, V. Karjavine, A. Lanev, A. Malakhov, V. Matveev[42,43], P. Moisenz, V. Palichik, V. Perelygin, S. Shmatov, S. Shulha, N. Skatchkov, V. Smirnov, N. Voytishin, A. Zarubin

Petersburg Nuclear Physics Institute, Gatchina (St. Petersburg), Russia
V. Golovtsov, Y. Ivanov, V. Kim[44], E. Kuznetsova[45], P. Levchenko, V. Murzin, V. Oreshkin, I. Smirnov, D. Sosnov, V. Sulimov, L. Uvarov, S. Vavilov, A. Vorobyev

Institute for Nuclear Research, Moscow, Russia
Yu. Andreev, A. Dermenev, S. Gninenko, N. Golubev, A. Karneyeu, M. Kirsanov, N. Krasnikov, A. Pashenkov, A. Shabanov, D. Tlisov, A. Toropin

Institute for Theoretical and Experimental Physics named by A.I. Alikhanov of NRC 'Kurchatov Institute', Moscow, Russia
V. Epshteyn, V. Gavrilov, N. Lychkovskaya, V. Popov, I. Pozdnyakov, G. Safronov, A. Spiridonov, A. Stepennov, V. Stolin, M. Toms, E. Vlasov, A. Zhokin

Moscow Institute of Physics and Technology, Moscow, Russia
T. Aushev

National Research Nuclear University 'Moscow Engineering Physics Institute' (MEPhI), Moscow, Russia
M. Chadeeva[46], D. Philippov, E. Popova, V. Rusinov

P.N. Lebedev Physical Institute, Moscow, Russia
V. Andreev, M. Azarkin, I. Dremin[43], M. Kirakosyan, A. Terkulov

Skobeltsyn Institute of Nuclear Physics, Lomonosov Moscow State University, Moscow, Russia
A. Belyaev, E. Boos, M. Dubinin[47], L. Dudko, A. Ershov, A. Gribushin, V. Klyukhin, O. Kodolova, I. Lokhtin, S. Obraztsov, S. Petrushanko, V. Savrin, A. Snigirev

Novosibirsk State University (NSU), Novosibirsk, Russia
A. Barnyakov[48], V. Blinov[48], T. Dimova[48], L. Kardapoltsev[48], Y. Skovpen[48]

Institute for High Energy Physics of National Research Centre 'Kurchatov Institute', Protvino, Russia
I. Azhgirey, I. Bayshev, S. Bitioukov, V. Kachanov, A. Kalinin, D. Konstantinov, P. Mandrik, V. Petrov, R. Ryutin, S. Slabospitskii, A. Sobol, S. Troshin, N. Tyurin, A. Uzunian, A. Volkov

National Research Tomsk Polytechnic University, Tomsk, Russia
A. Babaev, S. Baidali, A. Iuzhakov, V. Okhotnikov

University of Belgrade: Faculty of Physics and VINCA Institute of Nuclear Sciences, Beograde, Serbia
P. Adzic[49], P. Cirkovic, D. Devetak, M. Dordevic, P. Milenovic[50], J. Milosevic

Centro de Investigaciones Energéticas Medioambientales y Tecnológicas (CIEMAT), Madrid, Spain
J. Alcaraz Maestre, A. lvarez Fernández, I. Bachiller, M. Barrio Luna, J. A. Brochero Cifuentes, M. Cerrada, N. Colino, B. De La Cruz, A. Delgado Peris, C. Fernandez Bedoya, J. P. Fernández Ramos, J. Flix, M. C. Fouz, O. Gonzalez Lopez, S. Goy Lopez, J. M. Hernandez, M. I. Josa, D. Moran, A. Pérez-Calero Yzquierdo, J. Puerta Pelayo, I. Redondo, L. Romero, S. Sánchez Navas, M. S. Soares, A. Triossi

Universidad Autónoma de Madrid, Madrid, Spain
C. Albajar, J. F. de Trocóniz

Universidad de Oviedo, Instituto Universitario de Ciencias y Tecnologías Espaciales de Asturias (ICTEA), Oviedo, Spain
J. Cuevas, C. Erice, J. Fernandez Menendez, S. Folgueras, I. Gonzalez Caballero, J. R. González Fernández, E. Palencia Cortezon, V. Rodríguez Bouza, S. Sanchez Cruz, J. M. Vizan Garcia

Instituto de Física de Cantabria (IFCA), CSIC-Universidad de Cantabria, Santander, Spain
I. J. Cabrillo, A. Calderon, B. Chazin Quero, J. Duarte Campderros, M. Fernandez, P. J. Fernández Manteca, A. García Alonso, G. Gomez, A. Lopez Virto, C. Martinez Rivero, P. Martinez Ruiz del Arbol, F. Matorras, J. Piedra Gomez, C. Prieels, T. Rodrigo, A. Ruiz-Jimeno, L. Scodellaro, N. Trevisani, I. Vila

Department of Physics, University of Ruhuna, Matara, Sri Lanka
N. Wickramage

CERN, European Organization for Nuclear Research, Geneva, Switzerland
D. Abbaneo, B. Akgun, E. Auffray, G. Auzinger, P. Baillon†, A. H. Ball, D. Barney, J. Bendavid, M. Bianco, A. Bocci, C. Botta, E. Brondolin, T. Camporesi, M. Cepeda, G. Cerminara, E. Chapon, Y. Chen, G. Cucciati, D. d'Enterria, A. Dabrowski, N. Daci, V. Daponte, A. David, A. De Roeck, N. Deelen, M. Dobson, M. Dünser, N. Dupont, A. Elliott-Peisert, F. Fallavollita[51], D. Fasanella, G. Franzoni, J. Fulcher, W. Funk, D. Gigi, A. Gilbert, K. Gill, F. Glege, M. Gruchala, M. Guilbaud, D. Gulhan, J. Hegeman, C. Heidegger, Y. Iiyama, V. Innocente, G. M. Innocenti, A. Jafari, P. Janot, O. Karacheban[22], J. Kieseler, A. Kornmayer, M. Krammer[1], C. Lange, P. Lecoq, C. Lourenço, L. Malgeri, M. Mannelli, A. Massironi, F. Meijers, J. A. Merlin, S. Mersi, E. Meschi, F. Moortgat, M. Mulders, J. Ngadiuba, S. Nourbakhsh, S. Orfanelli, L. Orsini, F. Pantaleo[19], L. Pape, E. Perez, M. Peruzzi, A. Petrilli, G. Petrucciani, A. Pfeiffer, M. Pierini, F. M. Pitters, D. Rabady, A. Racz, M. Rovere, H. Sakulin, C. Schäfer, C. Schwick, M. Selvaggi, A. Sharma, P. Silva, P. Sphicas[52], A. Stakia, J. Steggemann, V. R. Tavolaro, D. Treille, A. Tsirou, A. Vartak, M. Verzetti, W. D. Zeuner

Paul Scherrer Institut, Villigen, Switzerland
L. Caminada[53], K. Deiters, W. Erdmann, R. Horisberger, Q. Ingram, H. C. Kaestli, D. Kotlinski, U. Langenegger, T. Rohe, S. A. Wiederkehr

ETH Zurich-Institute for Particle Physics and Astrophysics (IPA), Zurich, Switzerland
M. Backhaus, P. Berger, N. Chernyavskaya, G. Dissertori, M. Dittmar, M. Donegà, C. Dorfer, T. A. Gómez Espinosa, C. Grab, D. Hits, T. Klijnsma, W. Lustermann, R. A. Manzoni, M. Marionneau, M. T. Meinhard, F. Micheli, P. Musella, F. Nessi-Tedaldi, F. Pauss, G. Perrin, L. Perrozzi, S. Pigazzini, M. Reichmann, C. Reissel, T. Reitenspiess, D. Ruini, D. A. Sanz Becerra, M. Schönenberger, L. Shchutska, K. Theofilatos, M. L. Vesterbacka Olsson, R. Wallny, D. H. Zhu

Universität Zürich, Zurich, Switzerland
T. K. Aarrestad, C. Amsler[54], D. Brzhechko, M. F. Canelli, A. De Cosa, R. Del Burgo, S. Donato, C. Galloni, T. Hreus, B. Kilminster, S. Leontsinis, V. M. Mikuni, I. Neutelings, G. Rauco, P. Robmann, D. Salerno, K. Schweiger, C. Seitz, Y. Takahashi, S. Wertz, A. Zucchetta

National Central University, Chung-Li, Taiwan
T. H. Doan, C. M. Kuo, W. Lin, S. S. Yu

National Taiwan University (NTU), Taipei, Taiwan
P. Chang, Y. Chao, K. F. Chen, P. H. Chen, W.-S. Hou, Y. F. Liu, R.-S. Lu, E. Paganis, A. Psallidas, A. Steen

Department of Physics, Faculty of Science, Chulalongkorn University, Bangkok, Thailand
B. Asavapibhop, N. Srimanobhas, N. Suwonjandee

Physics Department, Science and Art Faculty, Ukurova University, Adana, Turkey
A. Bat, F. Boran, S. Cerci[55], S. Damarseckin[56], Z. S. Demiroglu, F. Dolek, C. Dozen, I. Dumanoglu, G. Gokbulut, EmineGurpinar Guler[57], Y. Guler, I. Hos[58], C. Isik, E. E. Kangal[59], O. Kara, A. Kayis Topaksu, U. Kiminsu, M. Oglakci, G. Onengut, K. Ozdemir[60], S. Ozturk[61], D. Sunar Cerci[55], B. Tali[55], U. G. Tok, S. Turkcapar, I. S. Zorbakir, C. Zorbilmez

Middle East Technical University, Physics Department, Ankara, Turkey
B. Isildak[62], G. Karapinar[63], M. Yalvac, M. Zeyrek

Bogazici University, Istanbul, Turkey
I. O. Atakisi, E. Gülmez, M. Kaya[64], O. Kaya[65], B. Kaynak, Ö. Özçelik, S. Ozkorucuklu[66], S. Tekten, E. A. Yetkin[67]

Istanbul Technical University, Istanbul, Turkey
A. Cakir, K. Cankocak, Y. Komurcu, S. Sen[68]

Institute for Scintillation Materials of National Academy of Science of Ukraine, Kharkov, Ukraine
B. Grynyov

National Scientific Center, Kharkov Institute of Physics and Technology, Kharkov, Ukraine
L. Levchuk

University of Bristol, Bristol, UK
F. Ball, J. J. Brooke, D. Burns, E. Clement, D. Cussans, O. Davignon, H. Flacher, J. Goldstein, G. P. Heath, H. F. Heath, L. Kreczko, D. M. Newbold[69], S. Paramesvaran, B. Penning, T. Sakuma, D. Smith, V. J. Smith, J. Taylor, A. Titterton

Rutherford Appleton Laboratory, Didcot, UK
K. W. Bell, A. Belyaev[70], C. Brew, R. M. Brown, D. Cieri, D. J. A. Cockerill, J. A. Coughlan, K. Harder, S. Harper, J. Linacre, K. Manolopoulos, E. Olaiya, D. Petyt, T. Reis, T. Schuh, C. H. Shepherd-Themistocleous, A. Thea, I. R. Tomalin, T. Williams, W. J. Womersley

Imperial College, London, UK
R. Bainbridge, P. Bloch, J. Borg, S. Breeze, O. Buchmuller, A. Bundock, GurpreetSingh CHAHAL[71], D. Colling, P. Dauncey, G. Davies, M. Della Negra, R. Di Maria, P. Everaerts, G. Hall, G. Iles, T. James, M. Komm, C. Laner, L. Lyons, A.-M. Magnan, S. Malik, A. Martelli, V. Milosevic, J. Nash[72], A. Nikitenko[8], V. Palladino, M. Pesaresi, D. M. Raymond, A. Richards, A. Rose, E. Scott, C. Seez, A. Shtipliyski, M. Stoye, T. Strebler, S. Summers, A. Tapper, K. Uchida, T. Virdee[19], N. Wardle, D. Winterbottom, J. Wright, S. C. Zenz

Brunel University, Uxbridge, UK
J. E. Cole, P. R. Hobson, A. Khan, P. Kyberd, C. K. Mackay, A. Morton, I. D. Reid, L. Teodorescu, S. Zahid

Baylor University, Waco, USA
K. Call, J. Dittmann, K. Hatakeyama, C. Madrid, B. McMaster, N. Pastika, C. Smith

Catholic University of America, Washington, DC, USA
R. Bartek, A. Dominguez

The University of Alabama, Tuscaloosa, USA
A. Buccilli, O. Charaf, S. I. Cooper, C. Henderson, P. Rumerio, C. West

Boston University, Boston, USA
D. Arcaro, T. Bose, Z. Demiragli, D. Gastler, S. Girgis, D. Pinna, C. Richardson, J. Rohlf, D. Sperka, I. Suarez, L. Sulak, D. Zou

Brown University, Providence, USA
G. Benelli, B. Burkle, X. Coubez, D. Cutts, M. Hadley, J. Hakala, U. Heintz, J. M. Hogan[73], K. H. M. Kwok, E. Laird, G. Landsberg, J. Lee, Z. Mao, M. Narain, S. Sagir[74], R. Syarif, E. Usai, D. Yu

University of California, Davis, Davis, USA
R. Band, C. Brainerd, R. Breedon, D. Burns, M. Calderon De La Barca Sanchez, M. Chertok, J. Conway, R. Conway, P. T. Cox, R. Erbacher, C. Flores, G. Funk, W. Ko, O. Kukral, R. Lander, M. Mulhearn, D. Pellett, J. Pilot, M. Shi, D. Stolp, D. Taylor, K. Tos, M. Tripathi, Z. Wang, F. Zhang

University of California, Los Angeles, USA
M. Bachtis, C. Bravo, R. Cousins, A. Dasgupta, A. Florent, J. Hauser, M. Ignatenko, N. Mccoll, S. Regnard, D. Saltzberg, C. Schnaible, V. Valuev

University of California, Riverside, Riverside, USA
K. Burt, R. Clare, J. W. Gary, S. M. A. Ghiasi Shirazi, G. Hanson, G. Karapostoli, E. Kennedy, O. R. Long, M. Olmedo Negrete, M. I. Paneva, W. Si, L. Wang, H. Wei, S. Wimpenny, B. R. Yates

University of California, San Diego, La Jolla, USA
J. G. Branson, P. Chang, S. Cittolin, M. Derdzinski, R. Gerosa, D. Gilbert, B. Hashemi, A. Holzner, D. Klein, G. Kole, V. Krutelyov, J. Letts, M. Masciovecchio, S. May, D. Olivito, S. Padhi, M. Pieri, V. Sharma, M. Tadel, J. Wood, F. Würthwein, A. Yagil, G. Zevi Della Porta

University of California, Santa Barbara-Department of Physics, Santa Barbara, USA
N. Amin, R. Bhandari, C. Campagnari, M. Citron, V. Dutta, M. Franco Sevilla, L. Gouskos, J. Incandela, B. Marsh, H. Mei, A. Ovcharova, H. Qu, J. Richman, U. Sarica, D. Stuart, S. Wang, J. Yoo

California Institute of Technology, Pasadena, USA
D. Anderson, A. Bornheim, J. M. Lawhorn, N. Lu, H. B. Newman, T. Q. Nguyen, J. Pata, M. Spiropulu, J. R. Vlimant, R. Wilkinson, S. Xie, Z. Zhang, R. Y. Zhu

Carnegie Mellon University, Pittsburgh, USA
M. B. Andrews, T. Ferguson, T. Mudholkar, M. Paulini, M. Sun, I. Vorobiev, M. Weinberg

University of Colorado Boulder, Boulder, USA
J. P. Cumalat, W. T. Ford, F. Jensen, A. Johnson, E. MacDonald, T. Mulholland, R. Patel, A. P erloff, K. Stenson, K. A. Ulmer, S. R. Wagner

Cornell University, Ithaca, USA
J. Alexander, J. Chaves, Y. Cheng, J. Chu, A. Datta, A. Frankenthal, K. Mcdermott, N. Mirman, J. Monroy, J. R. Patterson, D. Quach, A. Rinkevicius, A. Ryd, L. Skinnari, L. Soffi, S. M. Tan, Z. Tao, J. Thom, J. Tucker, P. Wittich, M. Zientek

Fermi National Accelerator Laboratory, Batavia, USA
S. Abdullin, M. Albrow, M. Alyari, G. Apollinari, A. Apresyan, A. Apyan, S. Banerjee, L. A. T. Bauerdick, A. Beretvas, J. Berryhill, P. C. Bhat, K. Burkett, J. N. Butler, A. Canepa, G. B. Cerati, H. W. K. Cheung, F. Chlebana, M. Cremonesi, J. Duarte, V. D. Elvira, J. Freeman, Z. Gecse, E. Gottschalk, L. Gray, D. Green, S. Grünendahl, O. Gutsche, J. Hanlon, R. M. Harris, S. Hasegawa, R. Heller, J. Hirschauer, Z. Hu, B. Jayatilaka, S. Jindariani, M. Johnson, U. Joshi, B. Klima, M. J. Kortelainen, B. Kreis, S. Lammel, D. Lincoln, R. Lipton, M. Liu, T. Liu, J. Lykken, K. Maeshima, J. M. Marraffino, D. Mason, P. McBride, P. Merkel, S. Mrenna, S. Nahn, V. O'Dell, K. Pedro, C. Pena, O. Prokofyev, G. Rakness, F. Ravera, A. Reinsvold, L. Ristori, B. Schneider, E. Sexton-Kennedy, N. Smith, A. Soha, W. J. Spalding, L. Spiegel, S. Stoynev, J. Strait, N. Strobbe, L. Taylor, S. Tkaczyk, N. V. Tran, L. Uplegger, E. W. Vaandering, C. Vernieri, M. Verzocchi, R. Vidal, M. Wang, H. A. Weber

University of Florida, Gainesville, USA
D. Acosta, P. Avery, P. Bortignon, D. Bourilkov, A. Brinkerhoff, L. Cadamuro, A. Carnes, V. Cherepanov, D. Curry, R. D. Field, S. V. Gleyzer, B. M. Joshi, M. Kim, J. Konigsberg, A. Korytov, K. H. Lo, P. Ma, K. Matchev, N. Menendez, G. Mitselmakher, D. Rosenzweig, K. Shi, J. Wang, S. Wang, X. Zuo

Florida International University, Miami, USA
Y. R. Joshi, S. Linn

Florida State University, Tallahassee, USA
T. Adams, A. Askew, S. Hagopian, V. Hagopian, K. F. Johnson, R. Khurana, T. Kolberg, G. Martinez, T. Perry, H. Prosper, A. Saha, C. Schiber, R. Yohay

Florida Institute of Technology, Melbourne, USA
M. M. Baarmand, V. Bhopatkar, S. Colafranceschi, M. Hohlmann, D. Noonan, M. Rahmani, T. Roy, M. Saunders, F. Yumiceva

University of Illinois at Chicago (UIC), Chicago, USA
M. R. Adams, L. Apanasevich, D. Berry, R. R. Betts, R. Cavanaugh, X. Chen, S. Dittmer, O. Evdokimov, C. E. Gerber, D. A. Hangal, D. J. Hofman, K. Jung, C. Mills, M. B. Tonjes, N. Varelas, H. Wang, X. Wang, Z. Wu, J. Zhang

The University of Iowa, Iowa City, USA
M. Alhusseini, B. Bilki[57], W. Clarida, K. Dilsiz[75], S. Durgut, R. P. Gandrajula, M. Haytmyradov, V. Khristenko, O. K. Köseyan, J.-P. Merlo, A. Mestvirishvili, A. Moeller, J. Nachtman, H. Ogul[76], Y. Onel, F. Ozok[77], A. Penzo, C. Snyder, E. Tiras, J. Wetzel

Johns Hopkins University, Baltimore, USA
B. Blumenfeld, A. Cocoros, N. Eminizer, D. Fehling, L. Feng, A. V. Gritsan, W. T. Hung, P. Maksimovic, J. Roskes, M. Swartz, M. Xiao

The University of Kansas, Lawrence, USA
A. Al-bataineh, P. Baringer, A. Bean, S. Boren, J. Bowen, A. Bylinkin, J. Castle, S. Khalil, A. Kropivnitskaya, D. Majumder, W. Mcbrayer, M. Murray, C. Rogan, S. Sanders, E. Schmitz, J. D. Tapia Takaki, Q. Wang

Kansas State University, Manhattan, USA
S. Duric, A. Ivanov, K. Kaadze, D. Kim, Y. Maravin, D. R. Mendis, T. Mitchell, A. Modak, A. Mohammadi

Lawrence Livermore National Laboratory, Livermore, USA
F. Rebassoo, D. Wright

University of Maryland, College Park, USA
A. Baden, O. Baron, A. Belloni, S. C. Eno, Y. Feng, C. Ferraioli, N. J. Hadley, S. Jabeen, G. Y. Jeng, R. G. Kellogg, J. Kunkle, A. C. Mignerey, S. Nabili, F. Ricci-Tam, M. Seidel, Y. H. Shin, A. Skuja, S. C. Tonwar, K. Wong

Massachusetts Institute of Technology, Cambridge, USA
D. Abercrombie, B. Allen, V. Azzolini, A. Baty, R. Bi, S. Brandt, W. Busza, I. A. Cali, M. D'Alfonso, G. Gomez Ceballos, M. Goncharov, P. Harris, D. Hsu, M. Hu, M. Klute, D. Kovalskyi, Y.-J. Lee, P. D. Luckey, B. Maier, A. C. Marini, C. Mcginn, C. Mironov, S. Narayanan, X. Niu, C. Paus, D. Rankin, C. Roland, G. Roland, Z. Shi, G. S. F. Stephans, K. Sumorok, K. Tatar, D. Velicanu, J. Wang, T. W. Wang, B. Wyslouch

University of Minnesota, Minneapolis, USA
A. C. Benvenuti†, R. M. Chatterjee, A. Evans, P. Hansen, J. Hiltbrand, Sh. Jain, S. Kalafut, M. Krohn, Y. Kubota, Z. Lesko, J. Mans, R. Rusack, M. A. Wadud

University of Mississippi, Oxford, USA
J. G. Acosta, S. Oliveros

University of Nebraska-Lincoln, Lincoln, USA
E. Avdeeva, K. Bloom, D. R. Claes, C. Fangmeier, L. Finco, F. Golf, R. Gonzalez Suarez, R. Kamalieddin, I. Kravchenko, J. E. Siado, G. R. Snow, B. Stieger

State University of New York at Buffalo, Buffalo, USA
A. Godshalk, C. Harrington, I. Iashvili, A. Kharchilava, C. Mclean, D. Nguyen, A. Parker, S. Rappoccio, B. Roozbahani

Northeastern University, Boston, USA
G. Alverson, E. Barberis, C. Freer, Y. Haddad, A. Hortiangtham, G. Madigan, D. M. Morse, T. Orimoto, A. Tishelman-Charny, T. Wamorkar, B. Wang, A. Wisecarver, D. Wood

Northwestern University, Evanston, USA
S. Bhattacharya, J. Bueghly, T. Gunter, K. A. Hahn, N. Odell, M. H. Schmitt, K. Sung, M. Trovato, M. Velasco

University of Notre Dame, Notre Dame, USA
R. Bucci, N. Dev, R. Goldouzian, M. Hildreth, K. Hurtado Anampa, C. Jessop, D. J. Karmgard, K. Lannon, W. Li, N. Loukas, N. Marinelli, F. Meng, C. Mueller, Y. Musienko[42], M. Planer, R. Ruchti, P. Siddireddy, G. Smith, S. Taroni, M. Wayne, A. Wightman, M. Wolf, A. Woodard

The Ohio State University, Columbus, USA
J. Alimena, L. Antonelli, B. Bylsma, L. S. Durkin, S. Flowers, B. Francis, C. Hill, W. Ji, A. Lefeld, T. Y. Ling, W. Luo, B. L. Winer

Princeton University, Princeton, USA
S. Cooperstein, G. Dezoort, P. Elmer, J. Hardenbrook, N. Haubrich, S. Higginbotham, A. Kalogeropoulos, S. Kwan, D. Lange, M. T. Lucchini, J. Luo, D. Marlow, K. Mei, I. Ojalvo, J. Olsen, C. Palmer, P. Piroué, J. Salfeld-Nebgen, D. Stickland, C. Tully, Z. Wang

University of Puerto Rico, Mayaguez, USA
S. Malik, S. Norberg

Purdue University, West Lafayette, USA
A. Barker, V. E. Barnes, S. Das, L. Gutay, M. Jones, A. W. Jung, A. Khatiwada, B. Mahakud, D. H. Miller, G. Negro, N. Neumeister, C. C. Peng, S. Piperov, H. Qiu, J. F. Schulte, J. Sun, F. Wang, R. Xiao, W. Xie

Purdue University Northwest, Hammond, USA
T. Cheng, J. Dolen, N. Parashar

Rice University, Houston, USA
Z. Chen, K. M. Ecklund, S. Freed, F. J. M. Geurts, M. Kilpatrick, Arun Kumar, W. Li, B. P. Padley, J. Roberts, J. Rorie, W. Shi, A. G. Stahl Leiton, Z. Tu, A. Zhang

University of Rochester, Rochester, USA
A. Bodek, P. de Barbaro, R. Demina, Y. t. Duh, J. L. Dulemba, C. Fallon, T. Ferbel, M. Galanti, A. Garcia-Bellido, J. Han, O. Hindrichs, A. Khukhunaishvili, E. Ranken, P. Tan, R. Taus

Rutgers, The State University of New Jersey, Piscataway, USA
B. Chiarito, J. P. Chou, Y. Gershtein, E. Halkiadakis, A. Hart, M. Heindl, E. Hughes, S. Kaplan, S. Kyriacou, I. Laflotte, A. Lath, R. Montalvo, K. Nash, M. Osherson, H. Saka, S. Salur, S. Schnetzer, D. Sheffield, S. Somalwar, R. Stone, S. Thomas, P. Thomassen

University of Tennessee, Knoxville, USA
H. Acharya, A. G. Delannoy, J. Heideman, G. Riley, S. Spanier

Texas A&M University, College Station, USA
O. Bouhali[78], A. Celik, M. Dalchenko, M. De Mattia, A. Delgado, S. Dildick, R. Eusebi, J. Gilmore, T. Huang, T. Kamon[79], S. Luo, D. Marley, R. Mueller, D. Overton, L. Perniè, D. Rathjens, A. Safonov

Texas Tech University, Lubbock, USA
N. Akchurin, J. Damgov, F. De Guio, P. R. Dudero, S. Kunori, K. Lamichhane, S. W. Lee, T. Mengke, S. Muthumuni, T. Peltola, S. Undleeb, I. Volobouev, Z. Wang, A. Whitbeck

Vanderbilt University, Nashville, USA
S. Greene, A. Gurrola, R. Janjam, W. Johns, C. Maguire, A. Melo, H. Ni, K. Padeken, F. Romeo, P. Sheldon, S. Tuo, J. Velkovska, M. Verweij, Q. Xu

University of Virginia, Charlottesville, USA
M. W. Arenton, P. Barria, B. Cox, R. Hirosky, M. Joyce, A. Ledovskoy, H. Li, C. Neu, Y. Wang, E. Wolfe, F. Xia

Wayne State University, Detroit, USA
R. Harr, P. E. Karchin, N. Poudyal, J. Sturdy, P. Thapa, S. Zaleski

University of Wisconsin-Madison, Madison, WI, USA
J. Buchanan, C. Caillol, D. Carlsmith, S. Dasu, I. De Bruyn, L. Dodd, B. Gomber[80], M. Grothe, M. Herndon, A. Hervé, U. Hussain, P. Klabbers, A. Lanaro, K. Long, R. Loveless, T. Ruggles, A. Savin, V. Sharma, W. H. Smith, N. Woods

† **Deceased**

1: Also at Vienna University of Technology, Vienna, Austria
2: Also at Skobeltsyn Institute of Nuclear Physics, Lomonosov Moscow State University, Moscow, Russia
3: Also at IRFU, CEA, Université Paris-Saclay, Gif-sur-Yvette, France
4: Also at Universidade Estadual de Campinas, Campinas, Brazil
5: Also at Federal University of Rio Grande do Sul, Porto Alegre, Brazil
6: Also at Université Libre de Bruxelles, Bruxelles, Belgium
7: Also at University of Chinese Academy of Sciences, Beijing, China
8: Also at Institute for Theoretical and Experimental Physics named by A.I. Alikhanov of NRC 'Kurchatov Institute', Moscow, Russia
9: Also at Joint Institute for Nuclear Research, Dubna, Russia
10: Also at Helwan University, Cairo, Egypt
11: Now at Zewail City of Science and Technology, Zewail, Egypt
12: Now at Cairo University, Cairo, Egypt
13: Also at British University in Egypt, Cairo, Egypt
14: Now at Ain Shams University, Cairo, Egypt
15: Also at Purdue University, West Lafayette, USA
16: Also at Université de Haute Alsace, Mulhouse, France
17: Also at Tbilisi State University, Tbilisi, Georgia

18: Also at Ilia State University, Tbilisi, Georgia
19: Also at CERN, European Organization for Nuclear Research, Geneva, Switzerland
20: Also at RWTH Aachen University, III. Physikalisches Institut A, Aachen, Germany
21: Also at University of Hamburg, Hamburg, Germany
22: Also at Brandenburg University of Technology, Cottbus, Germany
23: Also at Institute of Physics, University of Debrecen, Debrecen, Hungary, Debrecen, Hungary
24: Also at Institute of Nuclear Research ATOMKI, Debrecen, Hungary
25: Also at MTA-ELTE Lendület CMS Particle and Nuclear Physics Group, Eötvös Loránd University, Budapest, Hungary, Budapest, Hungary
26: Also at IIT Bhubaneswar, Bhubaneswar, India, Bhubaneswar, India
27: Also at Institute of Physics, Bhubaneswar, India
28: Also at Shoolini University, Solan, India
29: Also at University of Visva-Bharati, Santiniketan, India
30: Also at Isfahan University of Technology, Isfahan, Iran
31: Also at Plasma Physics Research Center, Science and Research Branch, Islamic Azad University, Tehran, Iran
32: Also at Italian National Agency for New Technologies, Energy and Sustainable Economic Development, Bologna, Italy
33: Also at Centro Siciliano di Fisica Nucleare e di Struttura Della Materia, Catania, Italy
34: Also at Università degli Studi di Siena, Siena, Italy
35: Also at Scuola Normale e Sezione dell'INFN, Pisa, Italy
36: Also at Kyung Hee University, Department of Physics, Seoul, Korea
37: Also at Riga Technical University, Riga, Latvia, Riga, Latvia
38: Also at International Islamic University of Malaysia, Kuala Lumpur, Malaysia
39: Also at Malaysian Nuclear Agency, MOSTI, Kajang, Malaysia
40: Also at Consejo Nacional de Ciencia y Tecnología, Mexico, Mexico
41: Also at Warsaw University of Technology, Institute of Electronic Systems, Warsaw, Poland
42: Also at Institute for Nuclear Research, Moscow, Russia
43: Now at National Research Nuclear University 'Moscow Engineering Physics Institute' (MEPhI), Moscow, Russia
44: Also at St. Petersburg State Polytechnical University, St. Petersburg, Russia
45: Also at University of Florida, Gainesville, USA
46: Also at P.N. Lebedev Physical Institute, Moscow, Russia
47: Also at California Institute of Technology, Pasadena, USA
48: Also at Budker Institute of Nuclear Physics, Novosibirsk, Russia
49: Also at Faculty of Physics, University of Belgrade, Belgrade, Serbia
50: Also at University of Belgrade: Faculty of Physics and VINCA Institute of Nuclear Sciences, Belgrade, Serbia
51: Also at INFN Sezione di Pavia [a], Università di Pavia [b], Pavia, Italy, Pavia, Italy
52: Also at National and Kapodistrian University of Athens, Athens, Greece
53: Also at Universität Zürich, Zurich, Switzerland
54: Also at Stefan Meyer Institute for Subatomic Physics, Vienna, Austria, Vienna, Austria
55: Also at Adiyaman University, Adiyaman, Turkey
56: Also at Şırnak University, Sirnak, Turkey
57: Also at Beykent University, Istanbul, Turkey, Istanbul, Turkey
58: Also at Istanbul Aydin University, Istanbul, Turkey
59: Also at Mersin University, Mersin, Turkey
60: Also at Piri Reis University, Istanbul, Turkey
61: Also at Gaziosmanpasa University, Tokat, Turkey
62: Also at Ozyegin University, Istanbul, Turkey
63: Also at Izmir Institute of Technology, Izmir, Turkey
64: Also at Marmara University, Istanbul, Turkey
65: Also at Kafkas University, Kars, Turkey
66: Also at Istanbul University, Istanbul, Turkey
67: Also at Istanbul Bilgi University, Istanbul, Turkey
68: Also at Hacettepe University, Ankara, Turkey
69: Also at Rutherford Appleton Laboratory, Didcot, UK

70: Also at School of Physics and Astronomy, University of Southampton, Southampton, UK
71: Also at IPPP Durham University, Durham, UK
72: Also at Monash University, Faculty of Science, Clayton, Australia
73: Also at Bethel University, St. Paul, Minneapolis, USA, St. Paul, USA
74: Also at Karamanoğlu Mehmetbey University, Karaman, Turkey
75: Also at Bingol University, Bingol, Turkey
76: Also at Sinop University, Sinop, Turkey
77: Also at Mimar Sinan University, Istanbul, Istanbul, Turkey
78: Also at Texas A&M University at Qatar, Doha, Qatar
79: Also at Kyungpook National University, Taegu, Korea, Taegu, Korea
80: Also at University of Hyderabad, Hyderabad, India